Calcium hydroxide as antibacterial implant coating

Dissertation zur Erlangung des naturwissenschaftlichen Doktorgrades der
Julius-Maximilians-Universität Würzburg

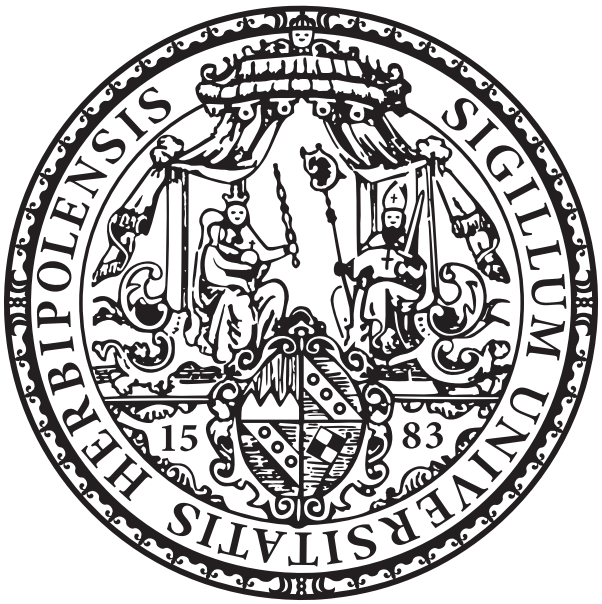

vorgelegt von
M. Sc. Markus Meininger
aus Würzburg

Würzburg, 2021

Eingereicht bei der Fakultät für Chemie und Pharmazie am

Gutachter der schriftlichen Arbeit

1. Gutachter: Prof. Dr. Jürgen Groll

2. Gutachter: Prof. Dr. Matthias Lehmann

Prüfer des öffentlichen Promotionskolloquiums

1. Prüfer: Prof. Dr. Jürgen Groll

2. Prüfer: Prof. Dr. Matthias Lehmann

3. Prüfer: Prof. Dr. Uwe Gbureck

Datum des öffentlichen Promotionskolloquiums

Doktorurkunde ausgehändigt am

Was Frau Wahrheit betrifft, so zeigt sie sich selbst ihren intimsten Verehrern nur in keuscher Umhüllung.

Wilhelm Busch

Summary

In modern medicine hip and knee joint replacement are common surgical procedures. However, about 11 % of hip implants and about 7 % of knee implants need re-operations. The comparison of implant registers revealed two major indications for re-operations: aseptic loosening and implant infections, that both severely impact the patients' health and are an economic burden for the health care system. To address these problems, a calcium hydroxide coating on titanium was investigated in this thesis. Calcium hydroxide is a well-known antibacterial agent and used with success in dentistry. The coatings were applied with electrochemically assisted deposition, a versatile tool that combines easiness of process with the ability to coat complex geometries homogeneously.

The pH-gradient during coating was investigated and showed the surface confinement of the coating process. Surface pre-treatment altered the surface morphology and chemistry of the titanium substrates and was shown to affect the morphology of the calcium hydroxide coatings. The influence of the coating parameters stirring speed and current pulsing were examined in various configurations and combinations and could also affect the surface morphology. A change in surface morphology results in a changed adhesion and behavior of cells and bacteria. Thus, the parameters surface pre-treatment, stirring speed and current pulsing presented a toolset for tailoring cellular response and antibacterial properties. Microbiological tests with *S. aureus* and *S. epidermidis* were performed to test the time-dependent antibacterial activity of the calcium hydroxide coatings. A reduction of both strains could be achieved for 13 h, which makes calcium hydroxide a promising antibacterial coating. To give insight into biofilm growth, a protocol for biofilm staining was investigated on titanium disks with *S. aureus* and *S. epidermidis*. Biofilm growth could be detected after 5 days of bacterial incubation, which was much earlier than the 3 weeks that are currently assumed in medical treatment. Thus, it should be considered to treat infections as if a biofilm were present from day 5 on. The ephemeral antibacterial properties of calcium hydroxide were further enhanced and prolonged with the addition of silver and copper ions. Both ionic modifications significantly enhanced the bactericidal potential. The copper modification showed higher antibacterial effects than the silver modification and had a higher cytocompatibility which was comparable to the pure calcium hydroxide coating. Thus, copper ions are an auspicious option to enhance the antibacterial properties.

Calcium hydroxide coatings presented in this thesis have promising antibacterial properties and can easily be applied to complex geometries, thus they are a step in fighting aseptic loosening and implant infections.

Zusammenfassung

Der Fortschritt in der modernen Medizin ist so weit, dass Hüft- und Kniegelenkersatz mit Implantaten heutzutage Standardoperationen sind. Allerdings kommt es in circa 11 % des Hüftgelenkersatzes und 7 % des Kniegelenkersatzes zu nicht zufriedenstellenden Ergebnissen und Revisionen sind nötig. Der Vergleich von Implantationsregistern zeigte zwei Hauptindikatoren für Revisionen: aseptische Lockerung und Implantatinfektionen, welche die Gesundheit der Patienten stark beeinträchtigen und eine wirtschaftliche Belastung für das Gesundheitssystem darstellen.

Um diese Probleme anzugehen, wurde Calciumhydroxid auf Titan als Beschichtung aufgebracht und in dieser Arbeit untersucht. Calciumhydroxid ist ein bekanntes antibakterielles Material und wird erfolgreich in der Zahnheilkunde eingesetzt. Die Beschichtungen wurden mit elektrochemisch gestützter Abscheidung aufgebracht, da diese Methode einen einfachen Prozess mit der Möglichkeit vereint, komplexe Geometrien homogen zu beschichten.

In dieser Arbeit wurde der pH-Gradient während der Beschichtung untersucht und zeigte die Beschränkung des Beschichtungsprozesses auf die direkte Oberfläche der Probe. Eine Vorbehandlung der Titansubstrate veränderte die Morphologie und die Chemie der Oberflächen und dadurch auch die Morphologie der Calciumhydroxidbeschichtung. Der Einfluss der Beschichtungsparameter Rührgeschwindigkeit und Pulsen des Stroms wurden in zahlreichen Konfigurationen und Kombinationen getestet und konnte ebenfalls die Oberflächenmorphologie verändern. Die Oberflächenmorphologie wiederum beeinflusst die Adhäsion und das Verhalten von Zellen und Bakterien. Deshalb sind die Parameter Oberflächenvorbehandlung, Rührgeschwindigkeit und Pulsen des Stroms ein Instrument für das Einstellen einer angepassten Zellantwort und der antibakteriellen Eigenschaften. Mikrobiologische Tests mit *S. aureus* und *S. epidermidis* wurden unternommen, um die Zeitabhängigkeit der antibakteriellen Aktivität auf Calciumhydroxidbeschichtungen zu bestimmen. Eine Reduktion beider Stämme konnte nach 13 h erreicht werden, was Calciumhydroxid zu einer erfolgversprechenden antibakteriellen Beschichtung macht.

Um einen Einblick in das Wachstum von Biofilmen zu geben, wurde ein Protokoll zur Biofilm-Färbung auf Titanplättchen mit *S. aureus* und *S. epidermidis* entwickelt. Biofilm-Wachstum konnte nach 5 Tagen Bakterien-Inkubation detektiert werden, was sehr viel früher war als die 3 Wochen, die aktuell bei der Behandlung von Implantatinfektionen angenommen werden. Folglich muss schon nach 5 Tagen darüber nachgedacht werden, Behandlungsmethoden gegen einen Biofilm anzuwenden.

Die kurzzeitigen antibakteriellen Eigenschaften von Calciumhydroxid konnten durch den Zusatz von Silber- und Kupferionen weiter verbessert und verlängert werden. Beide Ionen erhöhten die antibakterielle Wirkung signifikant. Die Kupfermodifikation zeigte dabei einen größeren antibakteriellen Effekt als die Silbermodifikation und war gleichzeitig besser zellverträglich. Die Zytokompatibilität der Kupfermodifikation lag auf dem Niveau der reinen Calciumhydroxidbeschichtungen. Deshalb sind Kupferionen eine vielversprechende Möglichkeit für eine weitere Verbesserung der antibakteriellen Eigenschaften.

Die in dieser Arbeit vorgestellten Calciumhydroxidbeschichtungen haben ein großes Potential als antibakterielle Oberflächen und können sehr leicht auch auf komplizierte Geometrien aufgebracht werden. Deshalb können sie ein entscheidender Baustein bei der Vermeidung von aseptischer Lockerung und Implantatinfektionen sein.

List of Publications

1. M. Meininger, T. Schmitz, T. Wagner, A. Ewald, U. Gbureck, J. Groll, C. Moseke, "Real-time measurement of protein adsorption on electrophoretically deposited hydroxyapatite coatings and magnetron sputtered metallic films using the surface acoustic wave technique", Mater. Sci. Eng. C. 2016, 61, 351–354

2. M. Meininger, C. Wolf-Brandstetter, J. Zerweck, F. Wenninger, U. Gbureck, J. Groll, C. Moseke, "Electrochemically Assisted Deposition of Strontium Modified Magnesium Phosphate on Titanium Surfaces", Mater. Sci. Eng. C. 2016, 67, 65–71

3. M. Meininger, S. Meininger, S., J. Groll, U. Gbureck, C. Moseke, "Silver and copper addition enhances the antimicrobial activity of calcium hydroxide coatings on titanium", Journal of Materials Science: Materials in Medicine 2018, 29, 61

4. T. Brückner, M. Meininger, J. Groll, A.C. Kübler, U. Gbureck, "Magnesium Phosphate Cement as Mineral Bone Adhesive", Materials 2019, 12, Number: 23, 3819

5. C. Moseke, K. Wimmer, M. Meininger, J. Zerweck, C. Wolf-Brandstetter, U. Gbureck, A. Ewald, "Osteoclast and osteoblast response to strontium-doped struvite coatings on titanium for improved bone integration", Biomedical Engineering / Biomedizinische Technik 2020, 65, 631–641

Parts of this thesis are published in paper 3., which also contains experiments from the author's Master Thesis (M. Meininger, "Modifikation elektrochemisch auf Titan aufgebrachter Calciumhydroxidschichten durch Silber- und Kupferionen", Julius-Maximilians-Universität Würzburg, 2011).

Contents

List of abbreviations

AFM	atomic force microscope.
AMP	antimicrobial peptides.
bcc	body centered cubic.
CFU	colony forming units.
ConA	concanavalin A.
CP-Ti	commercially pure titanium.
DMEM	Dulbecco's Modified Eagle Medium.
EBRA-FCA	Einzel-Bild-Röntgen-Analyse-femoral component analysis.
ECAD	electrochemically assisted deposition.
EDS	energy dispersive X-ray spectroscopy.
EPD	electrophoretic deposition.
EPS	extracellular polymeric substance.
FCS	fetal calf serum.
FISH	fluorescence in situ hybridization.
HA	hydroxyapatite.
hcp	hexagonal close packed.
hFOB	human fetal osteoblast cell line.
HMDS	hexamethyldisilazane.
ICP-MS	inductively coupled plasma mass spectrometry.
IMC	isothermal microcalorimetry.
LB agar plates	agar plates made with lysogeny-broth medium.
LB medium	lysogeny-broth medium.
MALDI-TOF	matrix-associated laser desorption/ionization time-of-flight.
MRSA	methicillin/multidrug resistant *S. aureus*.
MRSE	methicillin/multidrug resistant *S. epidermidis*.
MSCRAMMs	microbial surface components recognizing adhesive matrix molecules.
PBS	phosphate buffered saline.

PCR	polymerase chain reaction.
PEEK	polyetheretherketone.
PMMA	polymethylmethacrylate.
PS	polystyrene.
PS-HA	plasma sprayed hydroxyapatite.
PVD	physical vapor deposition.
PVL	panton-valentine-leukocidin.
qPCR	quantitative polymerase chain reaction.
ROS	reactive oxygen species.
RSA	Roentgen stereophotogrammetric analysis.
SBF	simulated body fluid.
SDD	silicon drift detector.
SEM	scanning electron microscope.
S. aureus	*Staphylococcus aureus*.
S. epidermidis	*Staphylococcus epidermidis*.
TTS	toxic shock syndrome.
UHMWPE	ultra-high molecular weight polyethylene.
WST	water soluble tetrazolium salt.
XRD	X-ray-diffraction.

List of symbols

A	surface area of the electrode.
C	mass concentration in the suspension.
D	diffusion coefficient.
ϵ_0	permittivity of vacuum.
EF	electric field strength.
E	applied potential.
ϵ_r	permittivity of the solvent.
η	viscosity of the solvent.
f	factor for electrophoretic deposition.
L	distance between electrodes.
μ	electrophoretic mobility.
Q	total electric charge.
t	time.
w	weight of the deposited particles.
z	number of electrons transferred per ion.
ζ	zeta-potential of the particles.

1. Introduction

Modern medicine has a big utility set to treat joint defects caused by wear, injuries or disease. While the joint can be preserved when little damage occurred, in many other cases the removal of the joint and implantation of a prosthesis is necessary. During the last decades replacement of hip and knee joints became a standard procedure and total numbers of implantations rose and further rising was predicted [1]. In order to track the outcome of joint replacement, joint registers were founded in many countries. Based on the collected data the number of revisions can be estimated at about 11 % for hip implants and about 7 % for knee implants. Moreover, two major indications causing implant re-operations could be identified: aseptic loosening and implant infection [2–6]. In the last years, the fraction of re-operation due to infection even rose [7]. Both have negative effects on the patient's health and prolong treatment, but of course an implant infection is more severe and can be life threatening. Studies show a one-year mortality rate after revision due to implant infection of about 8 % compared to a mortality rate of 5 % after revision due to aseptic loosening for total hip arthroplasties [8]. The mortality after 90 days was 2.6 %, which is higher than that after carotid endarterectomy, prostatectomy, or kidney transplant [9]. Even if the percentages of infections will stay the same, this will result in more afflicted patients, as the total volume of joint replacement increases steadily. This is because the population is getting older, in general healthier and wants to be agile until old age [10]. Moreover, a higher number of older and younger patients as before get implants, because of the good results obtained. Increasing obesity causes joint wear and again leads to more implantations of prostheses [11]. Additional to the personal problems of the patient, the economic burden of implant infections is high and will also increase in future [1, 12].

Even technical and organizational improvements could not eradicate all bacteria on surgical instruments and gloves of the personnel, thus a risk of a bacterial infection arises [13–16]. Many attempts were made to address implant infections and aseptic loosening with a large variety of implant coatings [17]. Calcium phosphate coatings are available systems to accelerate bone formation around implants and consequently improve the anchoring of the implants [18, 19]. This is important, because a fast and good implant fixation is the first step to circumvent aseptic loosening and infections [20, 21]. The most common calcium phosphate coating consists of hydroxyapatite (HA) because it has a similar composition as the mineral phase of natural bone [19, 22–24]. Plasma sprayed hydroxyapatite (PS-HA) was the first coating and gained importance due to faster and stronger fixation as well as increased bone formation around the implant [25]. Nevertheless, some drawbacks exist. A disadvantage of plasma spraying is,

that recrystallization and phase changes are unavoidable due to heating of the materials [26] leading to unwanted phases with different dissolution behavior. Thus, the biodegradation and bioresorption can be difficult to predict [27].

Due to these drawbacks, electrochemically assisted deposition (ECAD) was developed as alternative method [18, 28–31]. It utilizes electrical current for the electrolysis of water, which then leads to a lower pH-value at the cathode. As the solubility of calcium phosphates is pH dependent, at a lower pH-value calcium phosphates and many hydroxides are less soluble and deposit at the surface [32, 33]. The term assisted is assigned to an indirect use of the current via the electrolysis of water. ECAD operates at low temperatures, is not a line-of-sight technique and can thus be used to coat complex geometries homogeneously. A study showed that a HA coating amplified infections with *Staphylococcus aureus* (*S. aureus*) compared to the Ti-6Al-4V control, which is a common implant material [34]. Thus, a pure improvement of bone formation comes with the risk of a more severe implant infection. Here, a dual active coating, which enhances bone formation and has antibacterial properties, would be preferable.

In 2008 Drechsler et al. [35] firstly reported a calcium hydroxide coating produced by ECAD, which showed good cytocompatibility and antibacterial properties and the potential for enhanced bone formation. The aim of this work is to gain deeper insight into the dependencies of the calcium hydroxide coating formation during deposition and to further evaluate the antibacterial properties. At first this thesis had a look at the pH-value in the electrolyte during the coating process to clarify the dimensions of the deposition zone. The basic deposition zone around the samples during ECAD was visualized with Phenolphthalein. In a next step, the surface of the samples was altered before coating to increase wettability and roughness. This was hypothesized to lead to higher coating masses and more homogeneous coatings. The parameters of the coating process stirring and pulsing were also changed. Pulsing should result in more homogeneous coatings. The spikes of the coating would be dissolved during the phases of zero current flow, which would make the surface smoother. In the next phase of current flow further deposition would result in a more homogeneous coating. Moreover, stirring during coating was assumed to have the same effect. Clearly, a combination of the two parameters could also have a positive effect on the coating homogeneity and was investigated in detail. The vital parameter of the calcium hydroxide coatings is their antibacterial potential. Therefore, it was assessed with agar diffusion test, water soluble tetrazolium salt (WST)-test and a sonication assay. A reduced biofilm formation on calcium hydroxide coatings was assumed. Thus, the investigation of biofilms with concanavalin A (ConA), SYBR-Green and Hoechst staining as well as scanning electron microscope (SEM) imaging was established with biofilms on titanium samples. A decisive feature of antibacterial implant coatings is their cytocompatibility to enable an adequate implant ingrowth and new bone formation. The cytocompatibility of calcium hydroxide coatings was evaluated with human fetal osteoblast cell line (hFOB) over 10 days.

2. Theoretical background

The manifoldness of available arthroplasties has set the surgeon into position to treat a large variety of medical indications like joint failure, osteoarthritis, bone loss due to e. g. carcinoma, osteoporosis or infections of a joint or a primary implant. This chapter concentrates on the metallic part of the prostheses with a focus on titanium and its alloys. Furthermore, numbers for the outcome of implantations from different implant registers are summarized with special interest in numbers for aseptic loosening and implant infections. Implant infections require intensive treatment, that is described in the next section, including the role of biofilms. All this leads to the importance of preventive measures against aseptic loosening and implant infections. Consequently, coating techniques and implant coatings for enhanced osseointegration and antibacterial coatings are discussed with special focus on electrochemically assisted deposition (ECAD) and calcium hydroxide as antibacterial agent.

2.1. Implant materials

A material needs to fulfill certain requirements in order to be suitable for medical applications. First of all, biocompatibility is important, but also corrosion resistance, fatigue strength and Young's modulus are relevant properties. Processability and material costs must be also considered because they decide if industrial production of an implant is feasible.

2.1.1. Biological requirements

Biocompatibility is difficult to define in a positive way and listing the tasks and prerequisites an implant must fulfill is an endless job and differs depending on implant type and intended application. Therefore, the easiest definition is: The implant must not measurably harm the host neither by material nor design [36] and it should work in the same way as the natural item it replaces. Of course, nature will always be better, but the better nature is matched the better is the implant [37]. Corrosion resistance interplays with biocompatibility, because corroding implants release metal ions, which often lead to inflammation [38] or are even toxic [39–41]. In the course of time a corroding implant will sooner or later lose its mechanical stability and fail. The fatigue strength under the given conditions, surrounding medium and load, must be high enough to withstand cyclic loading over estimated 10^7 cycles within 20 years [36]. Young's modulus of the metallic implant should be in the range of the surrounding bone to prevent

stress shielding. Bone always adapts to the loading situation, which is essential for growth, maintenance and changes in behavior during life [42]. If the Young's modulus of an implant is much higher, the bone tries to adapt to the new loading situation. This results in bone loss at the unloaded side and more bone growth at the loaded side. Consequences can be mechanical loosening and total implant failure due to thin bone supporting area [43–47].

When it comes to the formation of bone around implants osteoinduction, osteoconduction and osseointegration play an important role [22]. Osteoinduction is the active stimulation of differentiation of pluripotent cells into bone-forming cells and thus the stimulation of new bone formation [22, 48]. Osteoconduction means that a material allows unhampered bone growth on the surface or into the (porous) material [22, 48]. Osseointegration describes the direct contact of the implant and living bone on a light microscopic level. A histological definition of "Dorland's Illustrated Medical Dictionary" is "direct anchorage of an implant by the formation of bony tissue around the implant without the growth of fibrous tissue at the bone-implant interface" [22]. A more practical definition is the rigid asymptomatic fixation of an implant in bone that is maintained during normal functional loading [22, 49].

2.1.2. Mechanical requirements

For load-bearing implants, metals are used mainly because of their superior mechanical performance compared to polymers and ceramics. A recently used polymeric implant material is polyetheretherketone (PEEK) that is implanted as cervical or lumbar interbody fusions [50]. Even though PEEK can reach the lowest levels of the Young's modulus of cortical bone [51] this is not sufficient for the use as hip or knee arthroplasty. Moreover, PEEK seems not to be integrated in bone as well as titanium [50] but possesses high potential for applications in the future after improvements of the material properties [52]. In acetabular hip cups ultra-high molecular weight polyethylene (UHMWPE) is used as liner because of its good wear-resistance and low friction coefficient [36].

Using ceramic materials, especially hydroxyapatite (HA) is obvious, because HA is the main mineral phase of bone [24, 53]. However, bone is not a pure ceramic, but composed of collagen fibrils and HA, cheap and lightweight materials, that make up about 95 % of the dry weight of bone [54]. The complex hierarchical structure results in the excellent fracture resistance that exceeds the values of the constituents and homogeneous mixtures of them by far. Involved are diverse deformation and toughening mechanisms at all length scales [42]. Molecular uncoiling and fibrillar sliding are intrinsic mechanisms at the smallest length scale that promote ductility of the bone [55, 56]. At the coarser length scales (10 µm to 100 µm) crack bridging and crack deflection/twist contribute to the resistance of bone [57, 58]. Especially the brittle interface of secondary osteons is most effective in crack deflection that diverts the crack path from the plane of maximum tensile stress, thus increasing the force needed for crack propagation. Moreover, bone has a large self-healing capacity, a feature where artificial materials lag far behind [42].

Nevertheless, artificial ceramics are used in special applications. While ceramics tend to fail when exposed to tensile or shear stress, they are excellent in pressure load situations e. g. in heads and liners of hip implants made of Al_2O_3 or ZrO_2 [36]. In addition, their low friction coefficients together with the UHMWPE liner and good wear-resistance makes them favorable for this application [36].

A benefit of metals is, that they allow the use of coating techniques where electrical conductivity is needed. The mostly used metals for implant and medical applications are stainless steel, CoCr alloys and titanium as well as titanium alloys [59]. The popular stainless steel 316L without surface treatment is today only used for short-term implants because it corrodes too fast in the body environment [36, 59–61]. But high nitrogen and nickel free stainless steels like Orthinox still have a high market-share in total hip replacements [36] but may suffer from fractures [62]. Cobalt-chromium-molybdenum alloys are used in orthopedics with good success, but the risk of metal ions is given. Cobalt and chromium are allergenic, and their release has caused huge problems in metal-on-metal bearings [36, 63, 64].

2.1.3. Titanium and its alloys as implant material

Titanium and its alloys have a relative low Young's modulus compared to other metals and high corrosion resistance as well as high strength and meet the requirements for biomedical applications better than stainless steel or CoCr-alloys [61, 65]. Therefore, this section provides a closer look at titanium and its diverse alloys. They have a broad range of application in nearly all technological fields ranging from lightweight automotive components over tubes for the chemical industry to medical applications as implants [65]. The original usage was in aerospace applications in airframes or aero-engines and in Soviet Alpha Class titanium hull submarines due to its high strength to density ratio [65]. Titanium is a transition metal and has two modifications. The α form is hexagonal close packed (hcp) and changes into a β form, a body centered cubic (bcc) at 882 °C. The phase diagrams for the addition of α- or β-stabilizers are given in figure 2.1.

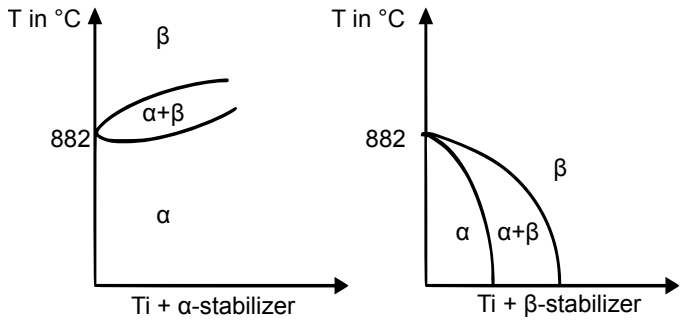

Figure 2.1: Phase diagrams of titanium with α- and β-stabilizer. Adapted from https://commons.wikimedia.org/wiki/File:Phasen-Titan.png, Luenibaer, public domain.

Oxygen diffusion limits the use of titanium to below 600 °C because at higher temperatures diffusion becomes too high and the oxygen layer starts to expand leading to a brittle surface that breaks and chips easily [65, p. 15]. Luckily, this limitation is far beyond the temperature range for medical applications. The high reactivity of titanium with oxygen is a double-edged sword. On the one hand, it causes a high price, because vacuum and inert gas atmospheres are needed during melting and milling. On the other hand, the TiO_2 oxide layer formed instantaneously when in contact with air is responsible for the high corrosion resistance and good biocompatibility [59]. Commercially pure titanium (CP-Ti), TiAl6V4 and TiAl6Nb7 are mainly used for biomedical applications [44] and are described in more detail below.

Commercially pure titanium

Commercially pure titanium is available in four grades that have different contents of iron and oxygen that are listed in table 2.1. Higher oxygen content is responsible for higher yield stress. CP-Ti is better formable than many titanium alloys and can therefore be used for more complex geometries and is very useful for craniofacial and maxillofacial implants [65, 66]. It is also highly biocompatible as CP-Ti has no toxic alloying elements and forms a stable TiO_2 surface.

Table 2.1: Iron (Fe) and oxygen (O) content in different grades of commercially pure titanium [65].

Grade	Fe in g/100g	O in g/100g
1	0.2	0.18
2	0.3	0.25
3	0.3	0.35
4	0.5	0.40

Titanium alloys

Three different alloy types exist, that have either a stabilized α, $\alpha + \beta$ or β phase. They vary in Young's modulus, yield strength and temperature stability. The Young's modulus of β alloys is generally lower than that of α and $\alpha + \beta$ alloys and lies in the range of 100 GPa to 105 GPa compared to 105 GPa for CP-Ti (α) and about 115 GPa for $\alpha + \beta$ alloys [65, p. 18]. The ideal Young's modulus to avoid stress shielding of an implant would be that of the surrounding natural bone, which is in the range of 15 GPa for cortical bone and 1 GPa for cancellous bone [67].

Ti-6Al-4V is always used when the strength of CP-Ti is not sufficient anymore. The elements Al, O, N and C are strong α stabilizers and Al is the most important of them. Aluminum increases the Young's modulus of the α phase and vanadium stabilizes the β-phase [68], thus Ti-6Al-4V is a $\alpha + \beta$-alloy. Ti-6Al-4V was used in a study with mini-implants for orthodontic

anchorage instead of CP-Ti because its higher yield strength enabled the low dimensions of the mini-implants. One drawback of Ti-6Al-4V was, that elevated vanadium levels were detected in the kidney, liver and lung of rabbits after 1, 4 and 12 weeks. The total amount remained below the toxic limit at its maximum after 4 weeks, but the results showed, that vanadium release from Ti-6Al-4V does occur and must be considered [69]. Consequently, new β titanium alloys with Nb, Ta, Zr and Mo were investigated, because they can have higher fatigue strength, a lower Young's modulus more similar to that of bone and enhanced biocompatibility due to the replacement of vanadium which is suspected to have a long-term negative toxic effect [65, p. 11]. TiAl6Nb7 was developed to evade vanadium. TiAl6Nb7 has even elevated biocompatibility compared to Ti-6Al-4V while maintaining similar mechanical properties [68, 70].

The neurotoxicity of aluminum and its connection to Alzheimer's disease is controversially discussed, but an impact on patient's health cannot be neglected [71–74]. Therefore, alloys without aluminum and vanadium were developed and investigated, for example the titanium zirconium alloy TiZr1317 [75]. Compared to CP-Ti it exhibited about equal osseointegration [75], equal biocompatibility, doubled hardness [76], a 40 % increased tensile strength and a 60 % higher yield strength [75].

CP-Ti and all titanium alloys have their special properties and are successfully used in medical applications. However, improvements are still desirable to minimize the number of aseptic loosening and implant infections.

2.2. Statistics about endoprostheses

With a rising number of implantations, the need for comparability and an overview over existing methods rose and led to the worldwide foundation of a variety of registries investigating and summarizing data of many clinics and patients as well as different implant types. From that data, aseptic loosening and implant infections were identified as the two major problems (compare table 2.2).

Aseptic loosening is defined as implant loosening without an infection. But about true causes for loosening many theories exist and it is most likely a multi-factorial process [43]. Loosening may be started by missing primary fixation and micro-motion within the first years and can have mechanical reasons. In addition, particles and endotoxins at their surface play a huge role and negatively affects the outcome through the induction of macrophages that synthesize cytokines. Cytokines from the macrophages can activate osteoclasts that lead to bone resorption and consequently amplify the beginning loosening. Interestingly, the origin of debris particles e. g., from the polyethylene liner, the cup, the stem or the cement and thus their material is less important than the size of the particles [43]. Stress shielding is another possible reason. The implantation of an artificial joint leads to an altered loading situation of the surrounding bone and thus to bone remodeling where more bone is growing in regions with higher load and

Table 2.2: Summary of numbers from four implant registers from England, USA, Sweden and Germany.

	England [2]	USA [3]	Sweden [4, 5]	Germany [6]
Time	2003-2015	2012-2015	see below	2015
Total cases	2 055 687	427 181		142.546
Hip			1979-2015	
- numbers	796 636	169 060	412 836	74 618
- revisions	88 822	17 180	44 579	8032
- cause of revision:				
— aseptic loosening	51.0 % *	39.3 % #	51.4 %	41.4 %
— implant infection	3.3 % *	8.4 %	14.5 %	15.6 %
Knee			2005-2014	
- numbers	871 472	258 121	112 708	56 884
- revisions	54 153	22 403	6127	5723
- cause of revision:				
— aseptic loosening	40.2 % *	26.9 % #	≈25 %	34.5 %
— implant infection	5.3 % *	9.3 %	≈25 %	19.3 %

*: Single stage

#: Sum of mechanical loosening of the prosthetic joint, instability related codes and articular bearing surface wear

bone is degraded in regions with lower load [43–47].

The 12th annual report of the National Joint Registry of England, Wales, Northern Ireland and the Isle of Man published in 2015 lists 1 636 048 linkable procedures for hips, knees, ankles, shoulders, and elbows in the years from 2003 to 2014 [77]. Causes of implant failure and revisions are listed for all implant types. From a total of 708 311 primary hip surgeries 17 916 had to be revised and aseptic loosening was most often indication (4276) followed by pain (3870), dislocation/subluxation (3027), particulate debris that led to adverse soft tissue reactions (3019) and infections (2443). Multiple answers were possible and especially pain was mentioned together with another reason. Additionally, the report lists all hip revision procedures, including the 17 916 for which a record for the primary procedure existed. Here a total of 79 859 revisions were investigated, which is divided in 69 655 single-stage revisions, 4664 stage one of two-stage revisions and 5540 stage two of two-stage revisions. Aseptic loosening was the foremost reason for a single-stage revision with 52 % and infections only accounted for 3.1 %. This is dramatically different when looking at two-stage revisions, where aseptic loosening is the reason for 14.3 % and infections accounts for as high as 79.7 %. Two-stage revisions are revisions, where the implant is replaced by an antibiotica loaded spacer as the first stage and then by a new, larger implant after the infection has been eradicated [78]. Infected prostheses are difficult to treat because bacteria can form a biofilm on the implant surface [79] and therefore late infections can nearly only be treated with two-stage revisions, whereas in early infections retaining of the prosthesis is desired [80]. The following 13th annual report published in 2016 showed 224 470 additional registered procedures, adding up to a total of 2 055 687 for 2012 to 2016.

The numbers of hip revisions sank from 9370 in 2014 to 8367 in 2015, while the rate of single- and two-stage revisions stayed about the same. The rate of single-stage revisions due to aseptic loosening changed from 52 % to 51 % and from 3.1 % to 3.3 % for infections. Two stage revisions were necessary for 13.7 % when aseptic loosening occurred and 80 % when an infection was the reason for revision. The ten-year risk of a re-revision after a first revision was 14.83 % which was about 3 times higher than the risk of revision after primary implantation. The number of first knee-revisions dropped from 5019 to 4711 from 2014 to 2015. A total of 871 472 knee replacements and 54 153 revisions were registered. The reason for a revision was in 40.2 % aseptic loosening and in 5.3 % an infection.

The Annual Report 2014 of the American Joint Replacement Registry [81] collected a total of 8257 revisions procedures of hip arthroplasties. From these 41.3 % failed due to aseptic mechanical reasons and 7.7 % due to infections. The reason for early revisions within the first three months was dislocation for 17.4 % (n = 117), followed closely by infection and inflammatory reaction that accounted for 17.0 % (n=114). Whereas early knee revisions were in 42.5 % (n=114) conducted due to infection and inflammatory reactions and below 10 % for mechanical reasons. Infection was the reason for 9.1 % of all 10 420 knee revisions and mechanical reasons accounted for about 45 %. Of all knee arthroplasties performed 8.1 % were revision procedures [81]. The total number of registered procedures nearly doubled in 2015 to 427 181 with 169 060 hip and 258 121 knee procedures. The overall revision burden was 10.2 % with 17 180 cases for hips and 8.7 % with 22 403 cases for knee implants. Infection as reason for a knee arthroplasty revision rose from 9.1 % to 9.3 % and for hip arthroplasties from 7.7 % to 8.4 % [3].

The Annual Report 2014 of the Swedish hip arthroplasty register [82] gives an overview over 51 617 revisions from 1979 to 2014. Here also the main reason with 52.4 % (n=27 037) was aseptic loosening and infections were second most with 13.9 % (n=7178). While chances for re-operations are higher within the first year the overall level has stabilized at about 12 % to 13 % of all performed hip replacements. In 2015 1860 revisions of hip arthroplasties were conducted and the sum beginning in 1979 rose to 44 579 revisions. This makes 82.2 % of all re-operations, indicating that for the rest the implant was left untouched, but here the risk of another re-operation/revision was much higher and survival rates were lower. The cause for re-operations were in 51.4 % aseptic loosening and in 14.5 % implant infections [4].

The German register for endoprostheses [6] published the first report in 2015 and assumed 400 000 implantations of hip and knee endoprostheses for Germany, but there were no unambiguous and reliable sources for this number at that time. Registered at the implant register were 202 125 operations for the time 2012 to 2015 with 142 546 surgeries registered in 2015. Again, loosening was the most frequent reason for revision and infections took the second place. Of an overall of 8032 hip revisions 41.4 % were conducted due to loosening and 15.6 % due to infections. Knee revisions showed the same trend: 34.5 % of 5723 were revised because of

loosening and 19.3 % because of infections. Reasons for revision surgery changed with the time after implantation. Within the first 180 days infection were the foremost reason, which was afterwards superseded by loosening. This was true for both, knee and hip revisions.

Taking the figures of all registers into account (compare table 2.2), about 11 % of hip implants and about 7 % of knee implants needed revision. Thereby, aseptic loosening and infections were major problems of arthroplasties of different kinds. Aseptic loosening had a higher prevalence and could be treated with single-stage revisions, whereas infections could either be treated without touching the implant but also more often needed two-stage revisions that are more expensive and lead to more severe impacts on the patient. Infections are more likely to occur earlier, that is within the first year, after implantation than aseptic loosening, which reaches a maximum beyond five years [2]. Thus, antibacterial agents are especially needed directly after implantation.

Studies showed that bacteria within a biofilm or inside osteoblasts were easily overlooked, because no bacteria were detected with standard microbiological techniques and no clinical signs of an infection were present. Of course, they could be the actual reason for loosening [83–85]. Consequently, the number of infections is higher than diagnosed and, additionally, the numbers of infections reported to the registers seems to be lower than the real numbers [86, 87]. All this indicates the need for antibacterial implant coatings that integrate well into bone to avoid aseptic loosening and implant infections, because treatment of both can be difficult.

2.3. Treatment of aseptic loosening and implant infections

Aseptic loosening and implant infections are the two most common failure modes of implants but need different treatment. Both can require the replacement of the joint and filling of missing bone [88], but infections need additional antimicrobial treatment. However, it can still be difficult to decide which form of failure is present. Bacteria within a biofilm are not easily detectable with standard microbiological approaches, leading to an infection wrongly being treated as aseptic loosening [79, 84, 85, 89]. Of course, it is favorable to detect aseptic loosening or implant infections as soon as possible to identify poor-performing implants early in the case of aseptic loosening [90] and to prevent the spreading of the infection in the case of an implant infection.

The gold standard for the detection of aseptic loosening is Roentgen stereophotogrammetric analysis (RSA) because of its accuracy and the ability to perform 3D measurements of the migration, but it needs the placement of tantalum markers during implantation. Einzel-Bild-Röntgen-Analyse-femoral component analysis (EBRA-FCA) operates without markers and can be used on already recorded standard radiographs and is also accurate enough to detect the migration of the stem [90]. Detection of early migration within the first 24 months is related to higher risks of aseptic loosening within the first or the early second decade after surgery [90].

Many molecular targets in bone and inflammatory process often involved in aseptic loosening are investigated, but unfortunately effective drugs are rare, and replacement of the implant becomes necessary until now [91–93].

For all patients getting an implant, preoperative antibiotic treatment is recommended and is effective in preventing implant infections, as a comparison between patients who got antibiotic treatment following the guideline and patients without it revealed [94].

Renz et al. [87] and Gehrke et al. [78] describe the treatment of infected knee implants but the procedure is similar for other infected joint implants [95, 96]. First of all, it is vital to decide, if the infection is acute or chronic. In order to do this, knowing the origin of the germs and the course of disease is important. Three different origins were listed: colonization of the implant during operation, hematogenous infection and direct (per continuitatem) contact with the surrounding or a neighboring infection. The risk of hematogenous infections persists lifelong but is highest within the first two years after implantation. Bacteria from nearly any other infection that spread through the blood can adhere to the implant and cause an infection. About two thirds of the infections start during operation (perioperative), can be acute and show within the first four weeks after implantation. These infections are caused by highly virulent germs like *Staphylococcus aureus* (*S. aureus*), streptococci or enterococci. They can also be delayed and manifest between 3 and 36 months after surgery. In the latter case low virulent germs like coagulase negative staphylococci or *Propionibacterium acnes* are present.

In the case that the infection is acute (manifestation within 4 weeks if perioperative, symptoms for less than 3 weeks for hematogenous and per continuitatem infections) the early biofilm, that is not fully built up, can be eradicated by aggressive debridement, the removal of all infected non-bleeding soft or osseous tissue, and only modular parts of the implant must be changed [78, 97]. In all other cases chronic infections with a mature biofilm are assumed and the complete change of the implant is advised.

Implant infections are not easy to detect and are sometimes polymicrobial (10 % to 30 %), that is more than one germ is involved in the infection. Common laboratory tests include the analysis of the joint fluid including leucocyte esterase, white cell count, neutrophil percentage and fluid culture [78]. Typical microbiological methods have shortcomings when bacteria are embedded in biofilms, not culturable or a previous or ongoing therapy with antibiotics took place. Therefore, different approaches and culture independent methods are necessary and under investigation. Tissue culture after arthroscopy or removal of the implant and sonication of removed parts with subsequent microbiological evaluation of the sonication fluid improves the diagnostic and helps to find the proper therapy. Additional long cultivation times for up to 14 days improve the detection of anaerobic species [87]. However, these diagnostic methods are time consuming. Molecular detection techniques are promising alternatives that can be completed within hours and are even beneficial in detecting non-culturable microbes, dormant and metabolically inactive organisms and distinguish the different species of bacteria [79, 98].

All this is hardly possible with standard microbiological cultures. Culture independent techniques are quantitative polymerase chain reaction (qPCR), pyrosequencing, matrix-associated laser desorption/ionization time-of-flight (MALDI-TOF) mass spectrometry, fluorescence in situ hybridization (FISH) and DNA microarrays. They are under intense investigation and have their own sets of benefits and disadvantages, but show promising results, especially when used in combination [79].

If removal of the implant is unavoidable, the replacement with a new one can be done in one, two or three stages. A one-stage revision (implant change) is possible if no fistula and no problematic germ are present and if it is not a re-revision. Moreover, neurovascular bundles must not be involved in infections as this makes radical debridement impossible. Otherwise, more-stage revisions are indicated. Two-stage revisions can be done with a long or short intermediate period with the option of the implantation of an antibiotic impregnated spacer or special antibiotic treatment. Sometimes a tree-stage revision with the renewal of the spacer before placing the new implant is beneficial. The whole procedure takes between 2 and 12 weeks, but optimal time points for the stages and route of antibiotic administration are not robustly evidenced, especially if resistant bacteria are involved [78, 87, 99].

Antibiotic therapy for all infections of joint implants is advised for 12 weeks and depends on the resistance profile of the bacteria as well as the patient. Antibiotics are vital in the fight against bacterial infections but need to be used cautiously to prevent further formation of resistances. Until now Rifampicin is the only known antibiotic that is effective against biofilms of staphylococci. If it is lost, biofilms on protheses cannot be prevented and fought anymore. Some staphylococcus strains are already resistant to Rifampicin, and for other difficult-to-treat germs, Chinolon - (Ciprofloxacin)-resistant Gram-negative bacteria as well as fungi (Candida species), no biofilm-active antibiotic exists. Suppression of bacteria is the last chance in these cases. It does not eradicate the bacteria but tries to hold bacterial counts below a critical value. The infection can reoccur anytime without prior notice. Moreover, antibiotic therapy has always side effects. Some antibiotics can cause severe problems like renal insufficiency, irreversible neuropathy (damage of nerves e. g., nervus opticus of the eyes) or ototoxicity (damage of hearing) [78, 87]. Therefore, the impact of an implant infection on the patient as well as the health care system in terms of high costs is severe and the need for preventive measures is immense.

2.4. Bacteria in implant infections and biofilm formation

Staphylococci cause most of the implant infections and especially *S. aureus* and *Staphylococcus epidermidis* (*S. epidermidis*) are the two predominant species with more than 50 % of the infections [80, 100, 101]. Staphylococci belong to the cocci. Coccus ($\kappa o \kappa \kappa o \varsigma$) is the old Greek word for "berry" and stands for spherical bacteria. Staphylo, also derived from old Greek ($\sigma \tau \alpha \Phi \nu \lambda \eta$ "staphyle"), means grape and is assigned to Staphylococci because they arrange grape-like. The arrangement has its origin in the cell division where the cells are not completely separated but stick together. Thus, Staphylococcus describes round and grape-like arranged bacteria colonies. They are Gram-positive and can be distinguished from Gram-negative bacteria through Gram-staining. Gram-staining utilizes the differences in the cell membrane to stain positive bacteria in dark-violet and negative in red. Gram-positive bacteria have a thicker cell wall without the normal outer membrane, but developed other surface structures like capsular polysaccharides, S-layer proteins and mycolic acids. The cell wall of Gram-positive bacteria is highly variable for the different strains, but all have cell wall glycopolymers in common, to which the teichoic acids belong. However, the diversity and function are still not fully known [102, 103]. These differences are an important factor in the susceptibility to antibiotics and the host immune system.

Staphylococcus aureus originates from the Latin word aureus, which means golden, because its colonies are yellow to golden. *S. aureus* is facultative anaerobe and can grow with as well as without oxygen. In both states it can survive in many environmental niches and produce different virulence factors [104]. Virulence factors like cell-wall-anchored proteins, capsular polysaccharides and microbial surface components recognizing adhesive matrix molecules (MSCRAMMs) promote evasion of immune response to biofilm formation, adhesion and invasion of host cells and tissue, minimize phagocytosis by neutrophils and supply the bacteria with nutrients [105]. Superantigens encoded on pathogenic islands cause non-specific activation of T-cells followed by massive cytokine release that can cause life-threatening symptoms like shock and multi organ failure [104–107]. The prototype and most known toxic shock syndrome (TTS) toxin 1 is associated with tampons (menstrual TTS) or skin and soft tissue infections (non-menstrual TTS) [105]. Moreover, exoenzymes and cytotoxins actively destroy immune cells, host cells and tissue, but also human host cell play an important role and contribute to the cytotoxicity of *S. aureus* [105, 108]. Some strains can host lysogenic bacteriophages with genes for panton-valentine-leukocidin (PVL), that has a high affinity for human leukocytes and destroys them. These strains were associated with severe skin infections and necrotizing pneumonia in young people [107, 109, 110].

S. aureus produces catalase that converts H_2O_2 to water and oxygen and is used to distinguish staphylococci from enterococci and streptococci. The coagulase test is a test to differentiate between *S. aureus* and coagulase negative staphylococci, but not all strains of *S. aureus* are

coagulase positive, thus other methods like polymerase chain reaction (PCR) are necessary [111, 112].

Resistance against antibiotics occurred in hospitals when methicillin was used, consequently resistant strains were called methicillin resistant *S. aureus* (MRSA). Unfortunately, resistance against new antibiotics developed fast in *S. aureus* and therefore MRSA nowadays is an acronym for methicillin/multidrug resistant *S. aureus* (MRSA) [107]. Even more endangering is that resistant *S. aureus* are found not only in hospitals, but in the community (community associated MRSA (CA-MRSA)) or in animals (livestock-associated MRSA), where other resistances and virulence traits may form and then spread [113]. Mathematical models try to determine the minimal time needed by bacteria to react to environmental changes and can improve the investigation of the development of resistances [114–116]. The permanent increase and change in *S. aureus* virulence and resistance will remain an ongoing challenge for scientists and health care [105, 117]. While *S. aureus* is a high virulent bacteria *S. epidermidis* is lower virulent, thus infections with *S. aureus* occur earlier than with *S. epidermidis*.

Staphylococcus epidermidis commonly lives on the skin (epidermis) of nearly every human and is normally unproblematic and not involved in severe infections. In contrast to *S. aureus*, it is coagulase negative and does not produce coagulase. This difference is usually used in diagnosis to distinguish between the two bacterial species. However, care has to be taken because some strains of *S. aureus* are also coagulase negative and methods like PCR become necessary [111, 112]. *S. epidermidis* is more widespread but less virulent than *S. aureus*. However, it easily gets in contact with catheters that are inserted through the skin and can form biofilms, especially on polymeric devices [112]. Staphylococci use the *agr* system for quorum sensing, a signaling cascade related to population density. Interestingly, studies showed that *S. epidermidis* inhibited most of the quorum sensing of *S. aureus* and could therefore be in favor, but the *in vivo* impact of this is still unclear [112]. On the skin *S. epidermidis* is nearly only confronted with antimicrobial peptides (AMP) produced by the innate host immune system but has also developed mechanisms to evade the acquired host defense system. Resistances against antibiotics are also rising and in fighting methicillin/multidrug resistant *S. epidermidis* (MRSE) even highest hygienic standards failed, because new MRSE strains arose within a year [112, 118]. However, *S. epidermidis*'s most effective defense and the predominant virulence factor is the formation of biofilms [119].

Other bacteria that are less frequent, but commonly found in implant infections are other Gram-positive germs (Streptococci and Enterococci) as well as Gram-negative bacteria like *Escherichia coli* and the anaerobic *Propionibacterium acnes* [87, 120]. Even if Enterococci are less frequent, they are associated with a nearly 3 times higher mortality risk than *S. aureus* [8].

Biofilms are defined by the IUPAC as "Aggregate of microorganisms in which cells that are frequently embedded within a self-produced matrix of extracellular polymeric substance (EPS) adhere to each other and/or to a surface.
Note 1: A biofilm is a fixed system that can be adapted internally to environmental conditions by its inhabitants.
Note 2: The self-produced matrix of EPS, which is also referred to as slime, is a polymeric conglomeration generally composed of extracellular biopolymers in various structural forms" [121]. With this matrix biofilms serve as water and nutrient storage and prevent the bacteria from desiccation [101, 122–124]. Moreover, they protect the inhabiting bacteria from biological, physical and chemical attacks [122, 124] and are present in up to 80 % of bacterial infections in humans [79]. Interestingly, bacteria change their morphology and phenotype and reduce transcription, translation and cell division [125] within a biofilm, making them difficult to access by antibacterial agents [124, 126]. In order to be effective against bacteria embedded in a biofilm the minimal inhibition concentration of antibiotics needs to be 1000fold higher than that for planktonic bacteria [123]. Thus, the biofilm is an optimized defense not only against the host immune system, but also drugs.

S. aureus and *S. epidermidis* can be biofilm forming or not, depending on the ability to produce polysaccharide intercellular adhesin, that is encoded by the genes *ica*A and *ica*D. The expression of both genes is important for full slime production [127]. Interestingly, the presence of this genes is not the only factor dominating biofilm formation, at least in *S. aureus*, because some strains that had the genes were found not to produce biofilm [128, 129]. Biofilm formation is controlled by several mechanisms (compare figure 2.2). Due to the complexity of these

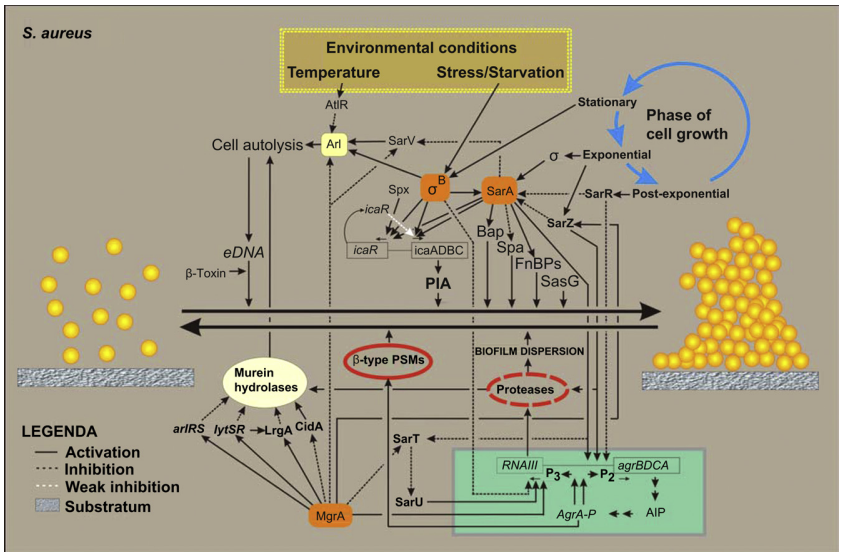

Figure 2.2: Biofilm formation and adaption are very complex, and some details are still not fully understood. Reprinted from [130] with permission from Elsevier.

mechanisms they are still under investigation, mainly derived from *in vitro* experiments, and

could therefore turn out to be different in *in vivo* implant infections [122, 130]. The formation of biofilms can be divided in four steps (compare figure 2.3) [130]. The first step is the adhesion

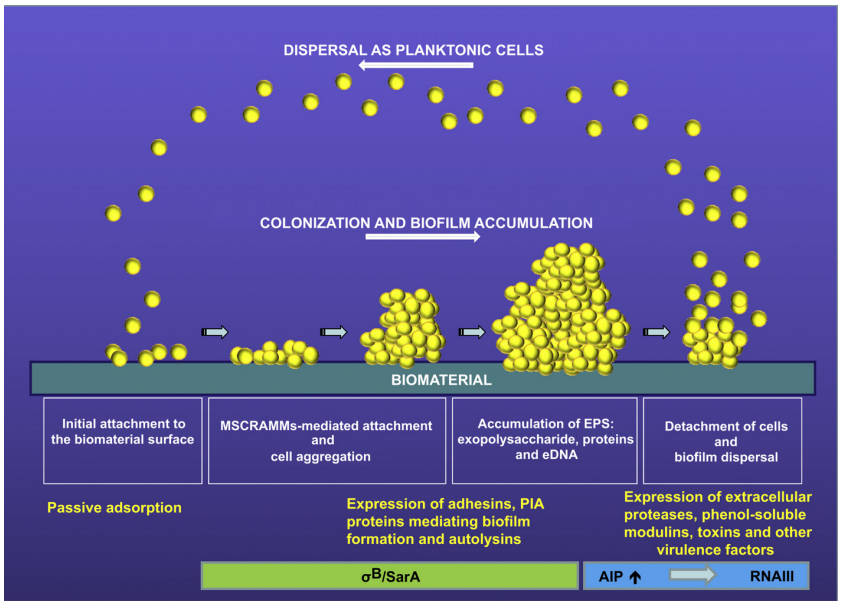

Figure 2.3: The circle of biofilm. After an initial attachment phase the biofilm ripens and grows. Detachment and spreading of cells are the last step, followed by biofilm growth at another place. Reprinted from [130] with permission from Elsevier.

of bacteria to a synthetic or biologic surface covered with extracellular proteins, where a lot of adhesins are involved [131]. Second, the bacteria adhere to one another and form multiple layers through MSCRAMMs mediation. After that, the biofilm matures and shows the characteristics for the respective bacterial species [130]. A mature biofilm can also be inhabited by different bacterial species that form an even more complex matrix [124]. The last step is the detachment of the biofilm that can either happen through a bacterial program for mobilization of a subset of bacteria or by physical shear forces. Both lead to planktonic bacteria that colonize other places and form new biofilms [126].

An environmental condition causing stress and thus influencing biofilm formation is the pH-value of the surrounding. Zmantar et al. [128] showed, that at pH 3 all strains were biofilm negative, whereas at pH 12 most strains were biofilm negative except for two who showed increased biofilm formation compared to pH 7. However, pH dependency of the biofilm formation is controversial. This is also discussed in [128].

All in all, biofilms are an ever changing and adapting fortress that effectively defend their inhabiting bacteria and render treatment nearly impossible.

2.5. Coating Techniques

Different modifications of the implant surface try to address the problems of aseptic loosening and implant infections. Strategies to achieve this are for example to modify the design and the surface morphology of the implant or to coat the implant. Therefore, various techniques can be employed to form these coatings on implants.

2.5.1. Plasma spraying

Plasma spraying is a special section of thermal spraying and utilizes plasma to melt the material to be deposited, the feedstock, that can be applied as powder, wire or liquid and spray it towards the substrate [25]. The easiest method is atmospheric spraying at atmosphere pressure, but also low pressure or vacuum plasma spraying are available. Typically, argon and mixtures of argon with He, H_2, N_2 or O_2 are used as plasma gas and ignited with a strong direct current arc or radio frequency [132, 133]. Particles within the plasma are rapidly heated to temperatures of up to 20 000 K and accelerated but cool down as rapidly when they leave the plasma. Control of particle speed and heating rate are key factors of plasma spraying, as particles should ideally reach the substrate completely molten at high velocities [132]. At the substrate, the particle flattens and freezes. Because of the high cooling rate, the particles freeze on their own, resulting in a lamellar structure built up of layered flattened particles [133]. The cooling rate also influences the residual stress distribution in coatings, thus substrate preheating and/or cooling can have a big influence on coating adhesion [134]. Plasma spraying is a versatile tool for the application of nearly all materials on many substrates. The quality of the coating depends on the feedstock powders, spray parameters and the substrate material [25]. For example, local recrystallization conditions depend on the substrate material and can lead to structural heterogeneity of HA coatings prepared with plasma spraying [135]. Since concerns arose about implant loosening caused by fast degrading coatings, high crystalline HA coatings are favored. However, these coatings still incorporate unmelted or partially melted particles that could lead to particle debris and lower bonging strength [25]. Mismatch in the thermal expansion coefficient of HA and titanium is considered to be at least one reason for the low bonding strength [136]. A thickness of about 50 µm is considered optimal to avoid fatigue failure, which commonly occurs in coatings above 100 µm [25]. Therefore, the coatings of commercial orthopedic implants are in the range of 50 µm to 70 µm [25].

2.5.2. Physical vapor deposition

Physical vapor deposition (PVD) is a coating technique that is used to produce films with a thickness of nanometers to about 75 µm [137, 138]. During PVD coating material is vaporized and subsequently condensates onto the substrate and forms a coating. Different methods can be used to vaporize the material, for example ion sputtering, arc evaporation or vacuum

evaporation [139]. For PVD low pressures of about 10^{-3} Pa to 10^{-6} Pa are necessary to have long mean free paths for the target ions and to avoid collisions with gas atoms [140]. Collisions could lead to loss of energy or reactions with the gas atoms [140]. The latter can be used for reactive sputtering to produce for example titanium dioxide or titanium nitride coatings with a titanium target and O_2 and N_2, respectively [141, 142]. With this methods metals, semiconductors and ceramics as well as polymers can be deposited on nearly every substrate [138, 143–147]. Ever improving techniques allow the control of phases, micro-structure, defect density and composition of the growing film [137]. However, it is mainly a line-of-sight technique and coating of complex geometries is still challenging [148, 149]. Multicomponent coatings can be prepared for example with magnetron sputtering either with multiple or modular targets [150]. Additionally, multilayer and gradient coatings are possible [151, 152]. In biomedical applications PVD coatings are for example prepared of tantalum, niobium or HA [138, 153, 154].

2.5.3. Electrophoretic deposition

Electrophoretic deposition (EPD) can be applied to a broad field of materials and substrates [155]. The only prerequisites are that the coating material is available as fine powder or can form a colloidal suspension [155] and that the substrate is conductive. This has the big advantage that the particles can thoroughly be analyzed before deposition and deposited "as are", without changing the physical state. EPD uses the electrical field between anode and cathode to move charged particles to the differently charged electrode. Positively charged particles are drawn towards the cathode and negatively charged ones to the anode, where they collect and form a powder compact [155]. The rate of EPD is independent from the target material if no chemical or physical reaction takes place [156, 157]. The electrolyte consists of the particles for deposition suspended in water or organic liquids. While water is cheaper and non-toxic, the electrolysis of water can occur and lead to bubble formation and entrapment of bubbles in the deposit, leading to lower coating quality. Moreover, the process deviates from the linear Hamaker growth, which makes the control of the process more difficult [156]. The Hamaker equation (see equation 2.1) is an estimation for the weight of the deposited particles w and therefore the thickness of the film:

$$w = \int_{t_1}^{t_2} f \cdot \mu \cdot EF \cdot A \cdot C \cdot dt \tag{2.1}$$

with the deposition time t, the factor f considering that not all powder that moved to the electrode really deposited, the electrophoretic mobility μ, the electric field strength EF, the surface area of the electrode A and the mass concentration in the suspension C [155, 156]. Another equation (see equation 2.2) for ideal electrophoretic conditions was investigated [158–160]. It is valid for the initial period, ignores the charge carried by free ions and sometimes

referred to as Henry's equation:

$$w = \frac{2}{3} C \cdot \epsilon_0 \cdot \epsilon_r \cdot \zeta \cdot \frac{1}{\eta} \cdot \frac{E}{L} \cdot t \tag{2.2}$$

with the permittivity of vacuum ϵ_0, the relative permittivity of the solvent ϵ_r, the zeta-potential of the particles ζ, the viscosity of the solvent η, the applied potential E and the distance between the electrodes L as well as the deposition time t [158–160]. Since the particles, the solvent and the apparatus do not change for a given system, the only variables for the coating thickness are the particle concentration C, the potential E and the deposition time t [158–160]. Among these parameters the zeta-potential is dependent on the pH-value, adding another influence to the complex system. Therefore, statistical methods like the design of experiment can help to find the best parameter set [161].

During EPD the electric filed strength changes due to the resistance of the depositing film and a possible change in the resistance of the suspension. Moreover, the applied potential is consumed by potential drops on both electrodes. Therefore, calculating the electric field strength by dividing the applied potential through the distance of the electrodes is only a rough estimation for the initial state [160]. Measuring the electric field strength during deposition is a better solution to accurately control the process [155].

Aqueous solutions are widely used because they are non-toxic. However, organic liquids are mostly superior, but flammability has to be considered, especially as higher voltages must be used for deposition. Typical solvents for EPD are ethanol, isopropanol or acetone, but many others are used, depending on the application.

An approach for using water without the disadvantage of water electrolysis are unbalanced alternating current fields. During one half cycle the particles can travel longer distances due to the non-linear dependency of the velocity to the strength of the electrical field. Therefore, they travel in one direction during the whole period [162]. Since most of the current flows through the double layer capacitance of the electrode-electrode interface, there is only low current left for water decomposition and thus bubble formation is suppressed [162, 163]. Despite all research and the well investigated process of electrophoresis, the process of deposition during EPD is still not well understood [157] and further theoretic and modelling investigation is needed to connect the different theories with the actual EPD process [164].

With EPD a wide range of biomaterials like HA, bio-active glasses and glass ceramics as well as composite materials could be deposited on implant substrates in a single step [165–167].

2.5.4. Electrochemically assisted deposition

The ECAD is sometimes also referred to as electrolytical deposition [168], electroprecipitation [169], electrodeposition [170] or electrocrystallization [19]. It utilizes the electrolysis of water to increase the pH-value around the sample connected as cathode. Thus, it enables the deposition

of coatings that have lower solubility at elevated pH-values, for example calcium or magnesium phosphates [32, 171, 172].

The electrolysis of water is described by reaction equations 2.3 to 2.6. At the anode water is split into oxygen, that leaves the electrolyte and H_3O^+ that lowers the pH-value:

$$6\,H_2O \longrightarrow O_2\uparrow + 4\,e^- + 4\,H_3O^+ \tag{2.3}$$

At the same time OH^- are created at the cathode, leading to an elevated pH-value there:

$$2\,H_3O^+ + 2\,e^- \longrightarrow H_2\uparrow + 2\,H_2O \qquad \text{(acidic)} \tag{2.4}$$

$$2\,H_2O + 2\,e^- \longrightarrow H_2\uparrow + 2\,OH^- \qquad \text{(basic)} \tag{2.5}$$

The overall reaction shows that the pH-value at anode and cathode change locally but the bulk electrolyte is not affected:

$$2\,H_2O \longrightarrow 2\,H_2\uparrow + O_2\uparrow \tag{2.6}$$

At increasing cathodic potential, the surface of the titanium samples showed an increase in hydrogen content, as detected with secondary ion mass spectrometry [31]. This can be explained by the partial reduction of titanium dioxide:

$$TiO_2 + 2\,H_2O + e^- \longrightarrow Ti(OH)_3 + OH^- \tag{2.7}$$

Rössler et al. [31] estimated a complete titanium hydroxylation as described in equation 2.7 after 5 s at $-1\,\mathrm{mA\,cm^{-2}}$ of a sample with 10 mm diameter and a height of 2 mm to 3 mm. Following this estimation, the samples coated here (diameter 15.5 mm, height 1 mm) at $-56\,\mathrm{mA\,cm^{-2}}$ should be covered within the first second. Thus, this layer determines the initial precipitation of a coating. The elevated pH-value leads to supersaturation of the desired coating and precipitation starts. Following equation 2.5 one electron ($z = 1$) is needed for the production of one OH^-. Faraday's law of electrolysis allows the estimation of the produced amount of OH^- $n(OH^-)$ from the total electric charge Q

$$n(OH^-) = \frac{Q}{z \cdot F} \tag{2.8}$$

with the Faraday constant $F = 96\,485\,\mathrm{A\,s\,mol^{-1}}$. Because a static current I is used, Q can be calculated by $Q = I \cdot t$ with the time t the current was applied. Therefore, equation 2.8 can be written as:

$$n = \frac{I \cdot t}{z \cdot F} \tag{2.9}$$

In the case of calcium hydroxide coatings OH^- and Ca^{2+} ions are consumed at the surface of the cathode. Calcium ions are refilled through diffusion and electrophoretic forces, because of their positive charge and OH^- through their generation at the cathode. During a deposition time of 900 s at a current of −961 mA a maximum of $n(OH^-) = 8.96\,\text{mmol}$ are produced, if all electrons are consumed by this process.

Assuming that Ca^{2+} are always available at the cathode and all produced OH^- precipitate as $Ca(OH)_2$, $n(Ca(OH)_2) = 4.48\,\text{mmol}$. The maximal mass of $Ca(OH)_2$ ($m(Ca(OH)_2)$) can be calculated with the molar mass $M(Ca(OH)_2) = 74.093\,\text{g mol}^{-1}$ with $m = M \cdot n$ to $m(Ca(OH)_2) = 332\,\text{mg}$.

Liu and Walcarius [173] calculated the concentration of OH^- (C_{OH^-}) at a static direct current and also took the diffusion into account. They started describing the diffusion of OH^- during ECAD following Fick's second law:

$$\frac{\partial C_{OH^-}}{\partial t} = D_{OH^-} \frac{\partial^2 C_{OH^-}}{\partial x^2} \tag{2.10}$$

with the diffusion coefficient of OH^- in solution D_{OH^-}. For the solution of equation 2.10 they considered three boundary conditions for C_{OH^-}. At the timepoint $t = 0$ no OH^- was produced, therefore, C_{OH^-} at every position x is the bulk concentration of OH^- $C_{OH^-}*$:

$$C_{OH^-}(x, 0) = C_{OH^-}* . \tag{2.11}$$

This is also valid for infinite distance from the cathode:

$$C_{OH^-}(\infty, t) = C_{OH^-}* . \tag{2.12}$$

The third boundary condition is given by Fick's first law. The 'diffusion flux' (stream of particles from/through an area) is proportional to the concentration gradient with the diffusion coefficient as constant:

$$D_{OH^-} \frac{\partial C_{OH^-}}{\partial x} = -\frac{I}{zFA} \tag{2.13}$$

with the number of electrons required for forming one OH^- z and the area of the electrode A.

With these boundary conditions they calculated the solution of equation 2.10

$$\begin{aligned} C_{OH^-}(x,t) = C_{OH^-}* + \frac{I_F}{nFAD_{OH^-}} \Bigg[& 2\sqrt{\frac{D_{OH^-} \cdot t}{\pi}} \\ & \cdot \exp\left(-\frac{x^2}{4D_{OH^-} \cdot t}\right) - x\,\text{erfc}\left(\frac{x}{2\sqrt{D_{OH^-} \cdot t}}\right)\Bigg] \end{aligned} \tag{2.14}$$

with the complementary error function erfc. The solution can be simplified for the assumption

that the concentration of OH^- in the bulk solution is negligible ($C_{OH^-}* = 0$), which is a good estimation for acidic solutions:

$$C_{OH^-}(x,t) = \frac{I_F}{nFAD_{OH^-}}\left[2\sqrt{\frac{D_{OH^-}\cdot t}{\pi}} \cdot \exp\left(-\frac{x^2}{4D_{OH^-}\cdot t}\right) - x\,\mathrm{erfc}\left(\frac{x}{2\sqrt{D_{OH^-}\cdot t}}\right)\right] \tag{2.15}$$

However, equation 2.15 is only valid, if D_{OH^-} is the same in solution and in the forming coating [173], which requires a coating highly permeable to OH^-.

During the electrolysis hydrogen bubbles form at the cathode (compare equation 2.5) and may have a negative effect on the surface homogeneity, but also increase the porosity of coatings which can be positive for bone ingrowth.

A big advantage of ECAD, over, for example PVD, is, that it is a non-line-of-sight technique and complex geometries and sponges with interconnecting pores can be coated. ECAD coatings form directly at the surface and are usually thinner than plasma sprayed coatings, which seems favorable for bone formation [174]. For example, typical thicknesses of plasma sprayed hydroxyapatite (PS-HA) are 50 µm to 200 µm and ECAD-HA is only 5 µm thick [174]. Other advantages of ECAD are the low process temperature and environmental pressure as working pressure. Neither the titanium substrate nor the coating material is exposed to high temperatures that may alter their properties. Moreover, it enables the incorporation of drugs and of thermolabile proteins that maintain their structure, a vital parameter for their biological activity [175–177]. Electrolytes for ECAD consist only of water and fully dissolved components, thus preparation of the electrolyte is easy and at most longer stirring times are needed for complete dissolution. This is an advantage over EPD, where first particles must be synthesized and then stabilized in a suspension.

All in all, ECAD is a non-line-of-sight technique and combines this with the easiness of electrolyte preparation and instrumental setup.

2.6. Calcium and magnesium phosphate coatings

Osseointegration of an implant in bone is the best form of fixation, because bone is directly connected to the implant and no fibrous capsule impairs the mechanically firm integration [22]. With the techniques described above many different coatings like magnesium phosphate, calcium phosphate or partially hybrid coatings with organic and inorganic components as well as drug loaded coatings can be produced [178–183]. Many studies about calcium phosphates and calcium phosphate coatings exist [23, 182, 184, 185]. A further classification is not possible in many cases, because the coatings are a mixture of different calcium phosphates [182, 186].

Therefore, such coatings are just declared as "calcium phosphate coatings". Octacalcium phosphate [187] and brushite ($CaHPO_4 \cdot 2\,H_2O$)[19, 188, 189] were investigated as coatings, but the vast majority were made of HA [190]. According to ISO 13779-4:2002(E) HA has the chemical formula $Ca_5(PO_4)_3OH$ and is characterized by the powder diffraction file PDF 9-432 in X-ray-diffraction (XRD). Most important, HA, to be more precise nano-crystalline apatite where calcium can be replaced by magnesium or strontium and HPO_4^- can be replaced by carbonate, is the main component of the mineral phase of bone [53]. Magnesium phosphate coatings are less frequently investigated, mostly consist of struvite ($MgNH_4PO_4 \cdot 6\,H_2O$) and/or newberyite ($MgHPO_4 \cdot 3\,H_2O$) and show promising results for their use in clinical applications [191–195].

2.6.1. Comparison of electrochemically assisted deposition and other techniques

ECAD can be used for many different coatings, but other methods are mostly limited to HA. Therefore, ECAD is compared with other techniques based on HA-coatings.

One *in vivo* study investigated the influence of surface preparation methods on the bone formation around the implants put into the muscles of rabbits after 6 and 12 weeks [174]. The different surface preparations included: 1) porous titanium coating, 2) porous titanium coating and Bonemaster and 3) porous titanium coating with PS-HA. Bonemaster (Biomet Deutschland GmbH, Berlin, Germany) is a thin HA coating produced via ECAD (ECAD-HA) [31] that was about 5 µm and thus 10 times thinner than PS-HA with around 50 µm. They found bone around 5 of the 12 implants with a porous titanium coating and around 1 of 12 ECAD coated samples, but no bone was observed around titanium coatings with PS-HA. From this they concluded that HA coatings reduced the bone formation compared to uncoated porous titanium [174]. This study had a very small number of samples and convertibility from rabbits to humans is doubtful. Another study revealed that rabbits and dogs show quite different results concerning osteogenesis around calcium phosphates in muscles or subcutaneous [196]. So, a difference between rabbits and humans is likely, especially as studies for calcium phosphate integration into bone showed comparable results for dogs and humans [197].

Daugaard et al. [198] compared plasma sprayed titanium alloy, PS-HA coatings with ECAD-HA and a combination of ECAD-HA with collagen in the proximal humerus of American Hound Dogs. The titanium alloy was partially surrounded by a fibrous capsule and, consequently, showed low mechanical fixation. Also, the addition of collagen to the HA coating resulted in low fixation. Both HA coatings led to a better mechanical fixation, but there was no difference within the group. The histomorphometric bone volume in the gap was higher for all HA coatings but was only statistically significantly higher for ECAD-HA.

Wang et al. [168, 199] investigated the proliferation and differentiation of osteoblast-like MC3T3-E1 cells on three different calcium phosphate surfaces. Biomimetic coatings were prepared by soaking in five times concentrated simulated body fluid (SBF) with crystal

growth inhibitors followed by five times concentrated SBF with less $Mg_2{}^+$ and $HCO_3{}^-$ for 24 h. Octacalcium phosphate coatings were precipitated by replacing the second SBF with TRIS-buffered supersaturated calcium phosphate solution at pH 7.4 and soaking for 48 h. The ECAD coating was prepared from the same supersaturated calcium phosphate solution but set to pH 7.0 with $-2.5\,\mathrm{mA\,cm^{-2}}$ at 52 °C for 8 h. They found big differences in crystal size with the biggest ones on octacalcium phosphate coatings, then on ECAD coating and smallest crystals on biomimetic coatings. They suggested the difference in crystal size could be the reason for the different cell response. The cells proliferated and differentiated best on biomimetic coatings followed by octacalcium phosphate coatings and then ECAD coating. The big advantage of ECAD coating was their comparably fast production with 8 h compared to 24 h or even 48 h. Unfortunately, they showed lowest cell proliferation and differentiation. However, the ECAD coating coatings were two-layered with a layer of crystals on the surface similar to that on octacalcium phosphate and a layer of amorphous calcium phosphate globes below that. This lower layer was more similar to the biomimetic coating. If the coating process for ECAD coating had been stopped earlier, the crystalline top layer would not have formed and the results for cell proliferation and cell differentiation could have been more similar to that of the biomimetic coating. In addition, the coating time would be even shorter, increasing this advantage of ECAD coating.

Wang et al. [200] found big differences in the morphology of the coatings. ECAD-HA showed single crystals whereas PS-HA exhibited large molten smooth globules. The implantation of uncoated and coated Ti-6Al-4V into canine trabecular bone for 7 and 14 days revealed differences in the bone formation. The time point 6 h was too early for a meaningful evaluation. After 7 days the bone apposition ratio was highest for PS-HA, but after 14 days ECAD-HA and PS-HA had both similar and much higher ratios than uncoated Ti-6Al-4V. Moreover, they state that initial protein adsorption and deposition of calcium phosphates of other calcium/phosphate ratios than HA seemed more important at an early stage.

The difference of ECAD-HA and PS-HA as coating of hip T stems was investigated with 50 patients (55 hips) postoperatively and after 3, 6, 12 and 24 months [201] as well as after 5 years (60 month) [202]. They conducted radiostereometric analysis to determine the fixation and dual-energy X-ray absorptiometry for bone mineral density as well as conventional radiography. Harris hip score and Oxford hip score were used for clinical evaluation. After two years the bone loss in Gruen zone 1, the proximal lateral part (upper part at the outside) of the stem [203], was significantly lower in the ECAD-HA group. For all other Gruen zones no differences were found. Considering bone mineral density, ECAD-HA seemed to be beneficial for bone ingrowth. The stems showed movement for the first 3 month postoperatively and then stabilized. After two years there was no difference in migration and retroversion of the stem. Additionally, the two clinical hip scores showed no significant differences. As expected, after 5 years they found no significant differences to the 2-year results at all and concluded that ECAD-HA is as save in

use as PS-HA.

As shown, HA coatings can improve the implant fixation, and better implant fixation is associated with a lower infection risk [20, 204]. However, some studies showed that implants or sutures can intensify an infection and less bacteria were necessary to produce an implant infection [205, 206]. Vogely et al. [34] showed that HA implant coatings amplified an infection of *S. aureus* compared to the uncoated Ti-6Al-4V control in the tibiae of New Zealand White rabbits. The rabbits were inoculated with 0.1 mL bacteria suspension with 10^2 to 1×10^5 colony forming units (CFU) and after four weeks bacteriological and histological examinations were performed. The bacterial count was significantly elevated for HA coatings as was the histological score of infection. Another study compared micro-PS-HA coated and uncoated Ti-6Al-4V with respect to their osseointegration and bacterial affinity [207]. The implants were placed in the humerus of 12 black Bengal goats and analyzed after 42, 90 and 180 days. The coated PS-HA implants showed higher push out forces in the push out test and micro-tomography, histology and scanning electron microscope (SEM) revealed higher bone contact as well as better and faster integration. Though, bacterial tests indicated higher risks for infections on HA coated implants [207]. Also, calcium phosphates with other calcium to phosphate ratios than HA were colonized by more *S. aureus* than pure metallic implants [208]. In an infection model with *S. epidermidis* in sheep HA coated, uncoated stainless steel, and polymethylmethacrylate (PMMA) were compared [209]. On HA coated implants as well as PMMA bacteria grew on 6 out of 6 interposition tissue and bone cultures, whereas this was the case only for 2 out of 6 cultures of the uncoated stainless steel.

In addition, pins with HA coating or uncoated for the external fixation at the wrist were investigated in patients [210]. HA coating showed no clinical advantage, but only a slight tendency to better anchorage and also increased risk of minor pin-track infections.

These findings emphasize the need for coatings that combine enhanced bone ingrowth with antimicrobial activity.

2.7. Antimicrobial activity of coatings

Antimicrobial activity is most important to prevent severe implant infections. Generally, two design strategies are possible: repelling or killing. Repelling can either be realized through steric or electrostatic repulsion as well as low surface energy. Microbes can be killed either by released biocide or a contact active biocide. Of course, these effects can be combined to create multifunctional antimicrobial surfaces [211].

Killing microbes with a contact active biocide is also referred to as contact killing and means that a microbe is killed solely by the contact with the surface and no other mechanism e.g. release is involved. It is controversially discussed in literature, especially for metallic surfaces, if contact killing is a valid mechanism and how it could work [212–216]. First of all, it is complicated to experimentally determine contact killing. In most cases, killing of microbes without the measurable presence of antimicrobial agents is taken as contact killing, but the concentration may only be below the detection limit in the medium whereas it is high enough to kill bacteria at the surface. Experiments that include multiple washing steps over a longer time period and control of the concentration within washing solution and coating would help to get a better understanding, but still is no prove for contact killing [211]. Two theories for contact killing are predominant for polymeric coatings: polymeric spacer effect and phospholipid sponge effect [211]. The polymeric spacer effect tries to explain the antibacterial activity of biocides attached to the surface via a spacer. The spacer allows the biocide to penetrate the cell wall of adherend bacterial cells and reach the phospholipid cytoplasmic membrane, which is subsequently destroyed. Interestingly, the surface coating can be more active than the polymer in solution [217]. This concept seems to be valid [211] for surface grafted quaternary polyethyleneimine [218], single walled carbon nanotubes [219] and surface grafted N-hexylated poly(4-vinylpiridine) [217] as well as antimicrobial peptides [220].

The phospholipid sponge effect theory says that the phospholipid layer of bacteria is destroyed by the ability of the coating to adsorb phospholipids [221], which might travel through the cell wall in liposomes [211]. This mechanism is supposed to explain the antibacterial activity of polymeric coatings that are modified with the same biocidal functional groups but not at the end of spacer-like polymers [222].

When it comes to contact killing on metal surfaces the role of the surface itself, metal ion dissolution and the generation of reactive oxygen species (ROS) are widely discussed, but all agree that it is a multi-factorial effect.

Metals like silver and copper are used since ages as antimicrobial surfaces for general hygiene and medical applications [212, 223]. After antibiotics were discovered and developed, metals were nearly forgotten, but widespread resistance to antibiotics revived the interest in metals [212, 223]. Metals can be divided in essential and non-essential ones. Essential metals like Na, Mg, K, Ca, V, Cr, Mn, Fe, Co, Ni, Cu, Zn, Se and Mo are necessary for the normal physiological function of organisms in certain concentrations and are mostly found in proteins [223–225].

However, they are toxic in higher concentrations, whereas non-essential metals like silver are toxic in very low concentrations, especially for most bacteria and microbes [223, 226, 227]. Some metals are even able to kill multidrug-resistant bacteria [228–230] or disrupt antibiotic resistant biofilms [226, 228, 231].

Within a cell, essential metals exist only in very limited chemical forms and are always guided to their specific enzymes and structural or storage proteins [232]. On the one hand, some biomolecules exhibit a high level of discrimination and bind their wanted metal cofactor with orders of magnitude greater affinity [233]. On the other hand, other biomolecules bind metal ions or metal complexes that have similar structure like the cofactor (ionic or molecular mimicry) and lose their biological function [234, 235]. The redox potential of metals enables the transfer of electrons and is vital for respiration and photosynthesis, but it is also related to the toxicity of many redox-active metal ions [236, 237].

As first step of poisoning the uptake and accumulation of metals is presumed [223]. Much effort has been put into studying the uptake and efflux, and its role in microbial heavy-metal resistance [227, 238]. However, the route highly toxic metals, like silver, take, is still unknown, but some sorts of transporters are most likely involved [223]. Inside a bacterium different mechanisms of toxicity interplay with each other. The metal mediated generation of ROS, like $O_2^{\bullet -}$, H_2O_2 and $OH^{\bullet}$, leads to an upregulation of genes involved in ROS elimination [239–241] and damaged DNA and inhibited enzyme activities were found [242]. Thus, ROS and metal catalyzed oxidation reactions are likely to be involved in metal toxicity. Another target for metal toxicity is the cell membrane. Possible mechanisms are the disruption of the cell membrane by lipid peroxidation shown for Cu(II) and hypothesized to be the mode of action of copper and copper alloy surfaces [212], the disturbance of the bacterial electron transport chain found for silver [243–245] or the dissipation of the chemiosmotic potential causing membrane leakage [246]. Chernousova and Epple [247] give an excellent overview over the effect of silver concentrations and different forms of applications, mainly nanoparticles, on bacteria, fungi and algae as well as eukaryotic cells and even multicellular organisms *in vivo*.

Warnes and Keevil [215] inhibited the action of copper ions on copper surfaces by chelators, quenched the ROS and found that less bacteria were killed. However, quenching hydroxyl radicals and decomposition of hydrogen peroxide did not influence the killing rate. From these findings they concluded that ROS were not generated via Fenton chemistry, but play an important role in the antibacterial activity of the surface together with metal ions.

From their experiments Luo et al. [216] concluded that oxidation must take place under ambient conditions and that metal ions must be released, of which the bactericidal activity is dependent on their soft hard-soft acid-base character according to Pearson/high thiophilicity. Due to these findings, they suggested that copper and cadmium are the most antibacterial metals.

Mathews et al. [213] compared the rate of bacterial killing on pure copper surfaces and copper

surfaces covered with an inert polymer grid, which prevented the direct contact of the bacteria with the surface. The copper ion release of both surfaces was about the same, but bacteria were only effectively killed when they were in direct contact with the surface. Hence, ion release is supported by another antibacterial effect. Here, they hypothesized that damage of the cell envelope could be involved, which facilitated the entrance of ions.

2.7.1. Biocide releasing antibacterial coatings

Antibiotics are usually given systemically or mixed into the bone cement [87] but can also be used as coating [248]. Antibiotics like minocycline, rifampin [248], doxyclicline [249], ciprofloxacin [250], vancomycin [251], norvancomycin [252] and gentamicin [177, 253] were investigated. Hickok and Shapiro [254] wrote a review about the use of antibiotics for prevention of implant infections and especially about immobilizing them on surfaces, which is suggested for reading.

Silver is by far the most studied antimicrobial metal [255–257] and showed higher antibacterial activity than copper and zinc, two metallic candidates used as antibacterial agents [258, 259].

Tîlmaciu et al. [260] used self-assembled monolayers of mercaptododecylphosphonic acid post-treated with $AgNO_3$ as coating for titanium. An *in vitro* study with MC3T3-E1 cells showed that attachment, proliferation and osteogenic differentiation were not negatively influenced, but the adhesion as well as biofilm formation of *S. epidermidis* and *Escherichia coli* was successfully inhibited. The coatings showed similar *in vivo* biocompatibility as uncoated titanium disks for 4 days in DBA1 mice. In addition, *in vivo* tests for the antibacterial activity were performed by adding 50 µL PBS with $1{\times}10^4$ CFU *S. epidermidis* to the subcutaneously implanted samples. In comparison with uncoated titanium disks a 500-fold reduction in viable adherent bacteria was found. Since the silver thiolate bonds and phosphonate monolayers are limited in stability in biological environments, this coating could be beneficial for the first days after implantation and prevent infections of germs that entered the wound during surgery.

To investigate the relationship between composition and structure of silver and titanium, a silver-titanium oxide gradient sputter-deposited in a reactive oxygen environment was used [261]. While the silver content varied from 35 % to 62 % the release was dominated by porosity and crystallinity of the surface and not the total amount of silver. The higher release on the silver-rich side of the gradient lead to a reduction of *S. aureus* of 99 %, whereas 17 % were measured for the titanium-rich side. The silver-rich side showed irregular clusters up to 1 µm with voids in the structure and a contact angel of 9°. In the middle section silver was mostly present as smaller particles on a porous titanium surface. A denser columnar structure with silver nanoparticles was found on the titanium-rich side with a higher contact angle of 49°. In addition, the structural properties influenced the HA forming ability. After immersion in SBF more HA precipitation could be detected on the silver-rich side.

For a prolonged release kinetic, silver was incorporated in bioactive glass and extracellular matrix hydrogels [257]. It showed long-lasting antibacterial effects against *E. coli* and *E. faecalis*.

Moreover, no cytotoxicity against dental pulp cells, but indications for enhanced bioactive behavior were found. Application as injectable composite for tooth defect areas is conceivable.

In an *in vivo* study with New Zealand white rabbits, megaprostheses coated with silver showed an antibacterial effect against *S. aureus* [262]. In order to enable the release of silver ions, a gold coating was applied before the silver coating. Gold is a more noble metal and can serve as cathode while silver is the anode and then able to release silver ions. The silver coated megaprostheses significantly reduced pus and the bacterial count of *S. aureus* compared with uncoated titanium-vanadium megaprostheses. All implants were well integrated into bone without pathological findings, despite elevated silver concentrations around the implant. Silver concentrations were significantly elevated in blood, liver and spleen, but the functional parameters and histology were normal. The same coating was also tested in a clinical trial with 20 patients and revealed no systemic or local toxic side effects [263]. In addition, 51 patients with bone sarcoma were treated with this silver coated megaprostheses and showed substantially reduced infection rates of 5.9 % compared to 17.6 % in the group with uncoated implants [264]. Moreover, the coated prostheses prevented amputation and allowed less aggressive treatment of infections. Nevertheless, the time of infection was the same in both groups and they state that silver will not be able to fight the infection alone. Silver was only present very close to the implant surface and could not reach infected tissue elsewhere. It could also be depleted after a while, allowing suppressed infections to become clinically apparent, therefore, antibiotic treatment was still necessary. Implants coated with silver with another technique reduced the infection, too, even after two-stage revisions [265]. A review published in 2017 [266] about silver coated megaprostheses stated that benefits of silver in infection prevention could not be confirmed, because the lack of studies with large numbers of patients, but that many retrospective studies suggested a decreased rate of infections. The stable integration of silver coated implants in bone was seen as problematic, but three studies suggest that it is possible. However, further investigations are needed [267–269].

An often-neglected problem of silver is that despite restricted use of silver containing products the resistance of bacteria against silver rose [270]. This endangers the efficacy of these products and could lead to the same situation as with many antibiotics.

In a study [39] the antibacterial activities of silver, zinc, copper, mercury, cobalt and aluminum ions were tested against *S. aureus* and *S. epidermidis*. Moreover, the cytotoxicity against embryo calvaria mouse osteoblast-like cells (MC3T3- E1) and mouse fibroblasts L929 was compared. $Co_2{}^+$ killed the cells immediately and Ag^+, $Zn_2{}^+$, $Hg_2{}^+$ were extremely cytotoxic, even at low concentrations, but relatively high concentrations of $Cu_2{}^+$ and $Al_3{}^+$ were tolerated by the cells. $Cu_2{}^+$ combined good cell compatibility with the highest antibacterial activity (reduction rate of $2.5{\times}10^4$) at a LD50 of $2.3{\times}10^{-1}\,\mathrm{mmol\,L^{-1}}$ for L929 cells, while Ag^+ only showed a reduction rate of 0.93 at LD50 of $2.5{\times}10^{-3}\,\mathrm{mmol\,L^{-1}}$. Even higher concentrations of $Cu_2{}^+$ only reduced the cell count and activity to the level of the Ti-6Al-4V control. Scanning

electron microscopy images showed some injured cells and cells with rounded morphology, but the majority of cells was well spread and attached. Therefore, copper has the favor of lower cytotoxicity compared to silver [258]. Moreover, copper in a concentration of $0.1\,\mathrm{mmol\,L^{-1}}$ could stimulate the proliferation of mesenchymal stem cells and enhance the differentiation in osteogenic differentiation medium [271]. The antibacterial effect was seen for $3\,\mathrm{mmol\,L^{-1}}$ and $5\,\mathrm{mmol\,L^{-1}}$ against *S. aureus*. The conclusion was that copper could be an antibacterial agent directly at the implant surface and stimulate the mesenchymal stem cells in further distance or later at the surface, when the concentration became appropriate [271].

As an alternative to silver and copper bismuth was investigated by Lin et al. [272]. Bismuth nitrate showed a larger inhibition zone in agar diffusion test compared to silver nitrate against *A. actinomycetemcomitans*, *S. mutans* and MRSA. Therefore, they created bismuth-modified titanium dioxide layers with anodic oxidation and could show that also the layers showed better antibacterial properties against *A. actinomycetemcomitans* and MRSA. At the same time osteoblast-like MG63 cells on bismuth-modified titanium layers had similar ALP-activity and cell viability (MTT) than on silver-modified ones. These findings make bismuth a promising alternative to silver.

Iodine coatings were successfully tested on megaprostheses in patients with malignant bone tumor, infection or pyogenic arthritis [273]. No adverse systemic or local effects nor loosening could be detected. In 1 out of 20 patients an infection occurred, that could be treated by antibiotics without removal of the implant, which was a good outcome for a tumor patient. Thyroid function was monitored after implantation and showed normal activity. Therefore, iodine coatings seem save to use and effective in the prevention and treatment of infections for large bone defects.

Another alternative for antibacterial coatings is fluoridated HA [274]. Amorphous fluoridated HA was deposited via ECAD and crystallinity increased by heat treatment for 3 h at 600 °C. Antibacterial activity was determined by reduction of CFU of *S. aureus*, *E. coli* and *P. gingivalis* on titanium, HA and fluoridated HA. With respect to titanium, HA and fluoridated HA showed a significant effect. Structural analysis revealed that F^- replaced OH^- in the HA lattice ($Ca_5(PO_4)_3OH$), whereas roughness parameter in the micrometer scale were similar. As a result, they stated that surface morphology had no influence, but the effect came from the incorporated fluoride. Differences in surface morphology in the sub-micrometer range seen in SEM images were not considered and may not be represented by the surface roughness parameters in the micrometer scale. Therefore, an influence of the surface morphology may be present, but it is very difficult to isolate the effects of surface morphology and fluoride. Let it be for the surface morphology, the fluoride or a combination of both. For sure, the different surface morphology is caused by fluoride addition to HA and the so produced coating had antibacterial activity.

Chlorhexidine is a cationic antibacterial agent used in dentistry against infections and has a

broad range of antibacterial properties. Its solubility is pH-dependent and makes ECAD the method of choice for the co-deposition with calcium phosphates, namely amorphous calcium phosphate and HA. Chlorhexidine contents between $150\,\mathrm{ng\,cm^{-2}}$ to $65\,\mathrm{mg\,cm^{-2}}$ could be realized, allowing adaption to the implant site [275].

2.8. Calcium hydroxide coatings

Calcium hydroxide is a well-known antibacterial agent and therefore the idea arose to use it as antibacterial implant coating. This section will have a closer look at the antibacterial properties and the work on coatings done before this thesis.

2.8.1. Calcium hydroxide as antibacterial agent

Calcium hydroxide is commonly used in dentistry for root-channel disinfection [276] and pulp capping [277] with good results.

Calcium hydroxide's way of action is the rising of the pH-value in the surrounding. Thus, it can be counted as biocide releasing. In water saturated calcium hydroxide elevated the pH-value to about 12.5 to 12.8, while the increase is limited by natural buffer systems to about 10 within the dentine [278]. Calcium hydroxide is effectively used as root-channel dressing and exhibits satisfying results in most cases [276]. However, a pH-value of 10 can be survived by *Enterococcus faecalis* and *Candida albicans* [279] and also other bacterial species can survive calcium hydroxide therapy [21, 276]. Nevertheless, a significant reduction of *E. faecalis* and *C. albicans* could be found *in vivo* after 7 days of calcium hydroxide treatment, which was as effective as antimicrobial photodynamic therapy [280]. Weiger et al. [281] could not detect a significant difference between one-visit without the use of calcium hydroxide and two-visit root-channel treatments with the use of calcium hydroxide as root-channel dressing between the two visits. On the contrary, it was tested to be more effective than camphorated phenol or camphorated paramonochlorophenol [282]. Moreover, calcium hydroxide can degenerate bacterial lipopolysaccharides that are involved in bone resorption during pulpal infections and therefore preserve bone that is important for implant fixation [283, 284].

Interestingly, not only OH^- ions but also Ca^{2+} could be effective against *S. aureus* [285]. Dye-leakage tests were performed with model membranes and showed a disruption of the membrane for a concentration of Ca^{2+} greater than $10\,\mathrm{mmol\,L^{-1}}$. This gave a hint for antibacterial activity, which was then tested on stationary phase *S. aureus*. A statistically significant viability loss of about 60 % was detectable for $40\,\mathrm{mmol\,L^{-1}}$ Ca^{2+} as far as *S. aureus* was concerned. The same concentrations tested with *E. coli* and *B. subtilis* did not result in any notable change in viability, which they ascribe to the higher cardiolipin content in *S. aureus* membranes. Moreover, calcium hydroxide has shown to enhance mineralization in hard tissues due to activation of alkaline phosphatase, which in turn results in phosphate release that can form new bone mineral

together with calcium [286, 287]. Better fixation of the implant in bone and higher intrabacterial ROS generation caused by CaO coatings resulted in dramatically reduced infections of MRSA in *in vivo* studies [288]. In the same study the expression of osteocalcin, osteopontin, alkaline phosphatase and bone morphogenic protein 2 was up-regulated in bone marrow stem cells after 7 and 14 days of incubation, indicating enhanced osteoblastic differentiation [288]. Additional to the presence of Ca^{2+}, the elevated pH-value plays a role, because bone formation has its optimum between pH 8 and pH 8.5 [289]. Even the immune system is positively influenced by Ca^{2+} and releases calprotectin to inhibit bacterial superoxide defense and to kill bacteria [290–292].

All these findings show that calcium hydroxide is a highly promising antibacterial agent with additional bone healing capacity combining the dual action of OH^- and Ca^{2+}.

2.9. History of calcium hydroxide coatings

Calcium hydroxide coatings deposited via ECAD were firstly described in [30, 35, 293]. They investigated different electrolyte compositions (compare table 2.3) with concentrations of $Ca(NO_3)_2$ of $42\,mmol\,L^{-1}$ or $84\,mmol\,L^{-1}$, $(NH_4)H_2PO_4$ with $0\,mmol\,L^{-1}$, $25\,mmol\,L^{-1}$ and $50\,mmol\,L^{-1}$ and a citric acid concentration of $50\,mmol\,L^{-1}$ and found the optimal conditions with $84\,mmol\,L^{-1}$ $Ca(NO_3)_2$, $25\,mmol\,L^{-1}$ $(NH_4)H_2PO_4$ and $50\,mmol\,L^{-1}$ citric acid at $100\,mA\,cm^{-2}$.

Table 2.3: Tested electrolyte compositions for the deposition of calcium hydroxide. Reprinted from [30] with permission, Copyright © 2009 WILEY-VCH Verlag GmbH & Co. KGaA, Weinheim

	Conc. $Ca(NO_3)_2$ in mmol/l	Conc. $(NH_4)H_2PO_4$ in mmol/l	Conc. citric acid in mmol/l	T in °C	Current density in mA/cm^2	Coating quality
1	42	0	50	70	ca 120*	-
2	42	25	50	70	ca 120*	+
3	42	5	50	70	ca 120*	+
4	84	25	50	70	ca 120*	++
5	84	25	50	50	ca 120*	++
6	84	25	50	20	ca 120*	+-
7	84	25	50	50	83 #	+
8	84	25	50	50	100 #	+++
9	84	25	50	50	133 #	+

*: Voltage = constant, #: Current = constant

Another important factor for the use as implant coating is the ability to sterilize the coating without any changes in the composition. Autoclaving and disinfection with ethanol were tested and did not change the X-ray diffraction patterns of the coating, thus the coatings were stable and both methods can be used without altering the composition.

Moseke et al. [30] also showed that longer deposition times lead to thicker coatings and reached a coating thickness of about 20 µm after 30 min. In a scratch test with a 0.2 mm Rockwell indenter the calcium hydroxide coatings withstood 5 N and 7 N and were thus comparable to commercially available brushite/HA coatings. Autobiocompatibilization, that is the conversion to HA in contact with a medium, was found for SBF, DMEM and FCS after 3 to 17 days and could help in the fixation of a coated implant in bone. Unpublished histological investigations of an *in vivo* study revealed higher bone formation around coated implants compared to titanium.

The antibacterial activity against *S. epidermidis* and *Klebsiella pneumoniae* were determined in comparison with uncoated titanium samples. The samples were dehydrated with an ethanol series and then stained with SYBR®-green. Thereafter, the bacterial count was quantified by a fluorescence measurement [294]. Compared to the reference, the bacterial growth of *S. epidermidis* was reduced to about 50 % and that of *K. pneumoniae* to about 20 %.

Growth of human osteoblasts (cell line MG 63) cells was evaluated for 5, 7 and 10 days on titanium, HA and calcium hydroxide coated surfaces. At the beginning the cell number and cell activity was decreased on calcium hydroxide but reached the same level as HA on day 10.

Braissant et al. [295] used isothermal microcalorimetry (IMC) to compare the antibacterial activity of calcium hydroxide coatings and silver doped HA coatings against *S. epidermidis*. IMC uses the heat dissipated by the metabolism of the bacteria to monitor their growth. One big advantages of IMC is the quantification of bacterial growth over time, because common assays that use staining can only determine the state at the end point. Moreover, the process is independent of the sample geometry. Bacteria within a porous sample or coating can be analyzed and no complicated, often not quantitative, detachment steps are necessary. They found, that *S. epidermidis* on 6 out of 12 calcium hydroxide coatings showed a significantly increased lag phase and a decreased growth rate. Moreover, for the remaining 6 samples no growth at all could be detected during the whole experiment that lasted about 5 days. From this they calculated the proportion of *S. epidermidis* that was killed and found 100 % for no growth at all and 99.999 % when late growth was observed. Thus, this coating had a high efficacy.

The influence of incorporated metal ions on calcium hydroxide coatings were also investigated [296]. Strontium, magnesium, zinc and silver ions were added to the electrolyte and co-deposited with calcium hydroxide. Calcium hydroxide could be deposited with all additions except for zinc, where only zinc and an amorphous most likely calcium containing coating could be detected with XRD. After immersion in SBF all coatings converted to HA.

All these results make calcium hydroxide a promising antibacterial and osteointegrative surface coating. This study steps back and investigates the influences of production parameter and thoroughly characterizes the antibacterial activity.

3. Material and methods

3.1. Standard coating procedure

The last paragraph was already published in [297]. Reprinted with permission from Springer Nature, Copyright © 2018

Disks made of commercially pure grade 2 titanium with a diameter of 15.5 mm and a height of 1 mm, were sandblasted with 50 µm, or 100 µm for biological experiments, aluminium oxide (Korox 50 and Korox 110, respectively, BEGO, Bremen, Germany) for 10 s at a distance of 2 cm with a pressure of 3 bar in a sandblasting device (Basic Quattro, Renfert GmbH, Hilzingen, Germany). The disks were cleaned in an ultrasonic bath (Sonorex Type RK 102 H, Bandelin electronic, Berlin, Germany) once with 5 % (5 mL/100 mL) Extran MA 05 (Merck, Schwalbach, Germany) and twice with ultra-pure water (resistance 18.2 MΩ) for 10 min per washing step. The electrolyte for the deposition of calcium hydroxide consisted of 84 mmol L^{-1} $Ca(NO_3)_2 \cdot 4\,H_2O$ (Merck, Darmstadt, Germany), 50 mmol L^{-1} citric acid monohydrate (Sigma Aldrich, Munich, Germany) and 25 mmol L^{-1} $(NH_4)_2HPO_4$ (Merck, Darmstadt, Germany). ECAD was carried out with four titanium disks screwed to a four-fold sample holder and connected as cathode to the galvanostat HP96 (Bank Elektronik – Intelligent Controls GmbH, Pohlheim, Germany) controlled by the appropriate software (CPCDA:Potentiostat Version 6f.7.2004/supplemented 9.04). A platinized net served as anode and the current was set to -961 mA(~ -56 mA cm^{-2}). During deposition, the current was monitored with a multimeter (Keithley Multimeter 2700, Tektronix GmbH, Cologne, Germany). The electrolyte was kept at (50±1) °C in a double-walled electrochemical cell by means of a heating system with a thermostat (Thermo Haake C10 Typ 003-5009, Thermo Fisher Scientific, Karlsruhe) and, if not stated otherwise, stirred at 200 rpm with a magnetic stirrer (IKA-Combimag RET, Janke & Kunkel GmbH u. Co KG IKA-Werk, Staufen, Germany or MR Hei-Tec, Heidolph, Schwabach, Germany). The coating was conducted for 900 s, if not stated otherwise, and after that the coated titanium disks were dipped in ultra-pure water for 30 s in order to remove excess electrolyte. Then the coated titanium disks were air-dried. Coating masses were determined through weighing the samples before and after coating.

For the modification of the coatings with metal ions the electrolyte was prepared as described above and 0.84 mmol L^{-1} $AgNO_3$ respectively $CuSO_4 \cdot 5\,H_2O$ (Merck, Darmstadt, Germany) were added. The coatings were deposited at 200 rpm with a current in the range of -70 mA cm^{-2} to -80 mA cm^{-2} for Ag-$Ca(OH)_2$ and -80 mA cm^{-2} to -90 mA cm^{-2} for Cu-$Ca(OH)_2$ [297].

3.2. pH-value measurement

The pH-value of the as-prepared electrolyte was measured with an electronic pH meter (pH level 1, inoLab, WTW, Electrode: pH 0...14 Sentix 61). This pH meter was also used for a measurement during ECAD, but electric fields and current negatively influenced results. Therefore, 10 mL of electrolyte were collected from the vicinity of the cathode with a syringe during about one minute and then measured with the pH meter. After that pH indicator solutions with different pH ranges were used in the required concentration of 3 drops per 5 mL: pH 0 - 5 (109177 Merck), pH 4 - 10 (109175 Merck) and pH 9 - 13 (109176 Merck). The successfully used indicator was phenolphthalein, which changes from colorless to pink in a pH range from 8.0 to 9.6 and stays pink until pH 11. Above pH 11 phenolphthalein is colorless again [298, p. 254 - 257]. Here 10 mL of a 0.1 g mL^{-1} phenolphthalein solution in 50 % ethanol were added to 100 mL electrolyte.

3.3. Surface pretreatment

Surface properties before coating can have a big influence on the coating quality, thus, different surface pretreatments were tested.

Polishing of titanium disks was done with silicon carbide abrasive paper with P 1200 grit followed by P 2400 grit and finalized to near mirror-polished with a MD Chem polishing disk and OP-S suspension (both from Struers, Ballerup, Denmark) on a MetaServ 3000 (Buehler, Esslingen, Germany).

Sandblasting was conducted with aluminum oxide (Korox 50/Korox 110/Korox 250, BEGO, Bremen, Germany) for 10 s at a distance of 2 cm with a pressure of 3 bar in a sandblasting device (Basic Quattro, Renfert GmbH, Hilzingen, Germany).

For sodium hydroxide treatment titanium disks were stored in 5 mol/L NaOH at 60 °C for 24 h, air-dried and then heated to 600 °C with a heating rate of 5 °C per minute and stabilized for 1 h before cooling [299, 300].

Before acid etching the samples were ground with P 2400 grit silicon carbide abrasive paper at 100 rpm for 30 s to get comparable surface roughness. Acid etching was performed in a mixture of nitric acid and hydrofluoric acid (100 mL of mixture contained 81 mL distilled water, 12 mL 65 % HNO_3 and 7 mL 40 % HF) for 30 s followed by washing twice in water and air-drying (compare [301]).

3.4. Measurement of contact angle

The contact angle was determined with a contact angle measuring device OCA20 Data Physics Instruments controlled by the software version V.5.4.3 build 1053 (DataPhysics Instruments GmbH, Filderstadt, Germany) with a 3 µl drop of ultra-pure water.

3.5. Surface roughness

Smooth samples were measured with atomic force microscope (AFM), FlexAFM with a C3000 controller (Nanosurf, Liestal, Switzerland) in tapping mode (intermittent contact mode) in air. The silicon cantilever (BudgetSensors, Wetzlar, Germany) had a thickness of 3 µm, a resonance frequency of 190 Hz and a spring constant of 48 $\mathrm{N\,m^{-1}}$. Each AFM image contains 512-1024 lines for each direction. The scan speed was proportional to the scan size and the scan frequency was between 0.5 Hz and 2.3 Hz. After recording, images were filtered and analyzed using the open-source software Gwyddion 2.47 (available from: http://gwyddion.net). The roughness of rougher samples could not be measured with AFM and thus a roughness testing machine Mitutoyo SJ201 was calibrated to 3 µm (DIN roughness standard) and used with the following parameter: 5 measurements with a cut-off length of 0.8 mm at a speed of 0.5 $\mathrm{mm\,s^{-1}}$ filtered with the Pc50 filter.

3.6. Influence of stirring speed and pulsing in various combinations

Stirring was conducted during the whole deposition and stirring speed was varied between 0 rpm and 900 rpm in steps of 100 rpm. A magnetic stirrer (IKA-Combimag RET, Janke & Kunkel GmbH u. Co KG IKA-Werk, Staufen, Germany or MR Hei-Tec, Heidolph, Schwabach, Germany) was employed with a stirring bar of 3 cm and a diameter of 6 mm.

For current pulsing, a rectangular signal with 5 s of current flow followed by a period of 1 s with zero current was generated by a custom-made relay setup triggered with an Arduino UNO microcontroller (Arduino.cc, Italy). Used pulsing patterns are explained in figure 3.1. Stirring was conducted during the whole deposition and stirring speed was varied between 200 rpm and 500 rpm. In addition, pulsing was applied after $t_{precoat}$ until 900 s deposition time were reached ($t_{precoat} + t_{pulse} = 900\,s$) or until the time the current flowed was 900 s ($t_{precoat} + \sum t_{on} = 900\,s$). Both are explained in figure 3.1.

Instead of pulsing the current was kept constant and stirring was applied after $t_{precoat}$ until 900 s deposition time were reached. As Stirring speeds 200 rpm and 500 rpm were chosen, it is $t_{precoat} + t_{200\,rpm} = 900\,s$ and $t_{precoat} + t_{500\,rpm} = 900\,s$, respectively.

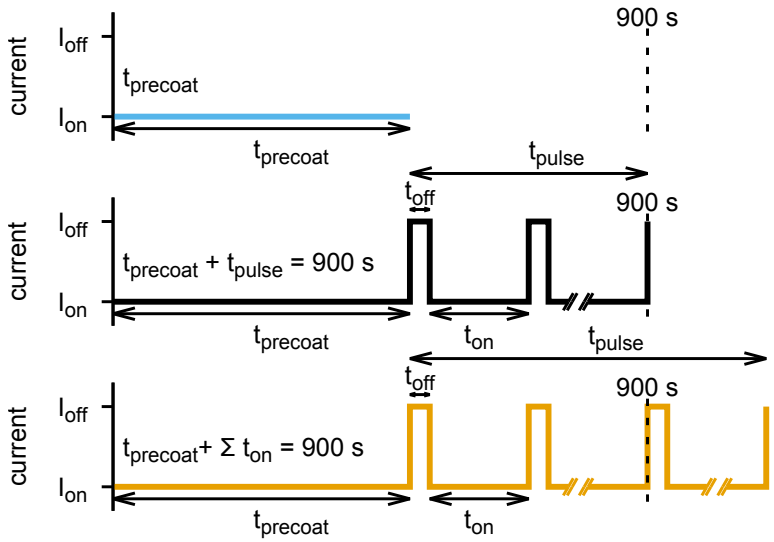

Figure 3.1: Schematic illustration of different pulsing patterns applied during coating.

3.7. Dissolution of calcium hydroxide coatings

In order to study the dissolution behavior in the electrolyte dry calcium hydroxide coated titanium samples were fixed to the four-fold holder and put into the electrolyte at 50 °C for 1 s, 5 s, 10 s, 20 s and 40 s, respectively. Dissolution was studied without stirring as well as with stirring at 500 rpm. In order to determine the dissolved mass, all samples were weight before and after dissolution.

3.8. Adhesion

Tape testing was performed with Tesa®-Tape pressed onto the surface and removed by hand.

For testing the adhesion during ultrasonication a Sonorex RK100H ultrasonic bath from Bandelin (Berlin, Germany) was used with a high-frequency power of 80 W at a frequency of 35 kHz. The samples were put into ultra-pure water and treated with ultrasound for 30 s. After that they were dried in a gentle airstream and photographic pictures were taken to visually analyze delamination.

Scratch-Test was performed with a hardness testing machine type 3212001 (Zwick, Ulm, Germany) with a Rockwell indenter 3627 and an electronic stage ITL09 (micro controle, Beaune-la-Rolande, France). Coated titanium disks were screwed to the sample holder and tested with 0.2 kg, 0.3 kg, 0.4 kg, 0.7 kg, 1 kg, 1.5 kg and 2 kg at a speed of 1 mm min^{-1}. Scratches were investigated with SEM and energy dispersive X-ray spectroscopy (EDS).

3.9. SEM and EDS

Investigations of the surface morphology were conducted with a field emission SEM Crossbeam 340 (Zeiss, Oberkochen, Germany) and EDS was used for element mapping with an INCA Energy 350 AzTec Advanced system using a silicon drift detector (SDD) (Oxford Instruments, Abingdon, UK). Some samples were sputtered with 4 nm platinum. EDS was performed at 20 kV with an aperture of 60 µm for 10 frames at a resolution of 512 with a process time of 4 and a pixel dwell time of 100 µs.

Biological samples need special treatment before they can be examined in SEM. Titanium disks seeded with *S. aureus* were washed two times with PBS and then fixated with 6 % glutaraldehyde for 15 min on ice. After that, the disks were washed twice with 2 mL phosphate buffered saline (PBS) on ice and dried with an ethanol row. Each concentration (70 %, 90 % and 100 %) was used twice for 10 min each at room temperature. Finally, the disks were dried with hexamethyldisilazane (HMDS) (Lot# SHBF6076 V, Sigma Aldrich, Munich, Germany) for two times 15 min and then air-dried in a fume hood.

3.10. XRD

XRD patterns were recorded in a 2θ range of 10° to 60° with a step size of 0.02° and a dwell time of 1 s/step in Bragg-Brentano geometry with Cu-K_α radiation ($\lambda = 0.1541$ nm) using a Siemens D5005 X-ray diffractometer (Bruker AXS, Karlsruhe, Germany) operated with a tube voltage of 40 kV and tube current of 40 mA. The resulting diffraction patterns for $Ca(OH)_2$ (04-0733), corundum (46-1212), titanium (01-1197) and silver (01-1167) were assigned using the JCPDS database with the given PDF numbers.

3.11. Inductively coupled plasma mass spectrometry

This section was already published in [297]. Reprinted with permission from Springer Nature, Copyright © 2018

Inductively coupled plasma mass spectrometry (ICP-MS) (Varian/Bruker Daltonik GmbH, Bremen, Germany) was used to determine the total amount of silver and copper in Ag-$Ca(OH)_2$ and Cu-$Ca(OH)_2$ coatings. The samples were dissolved in 1.5 mL HNO_3 (65 %, Suprapur®, Merck) and diluted to 1:100 and 1:1000 for measurement of Cu and Ag, respectively.

The release of $Cu_2{}^+$ and Ag^+ was investigated in SBF (Na^+ 142.0 mmol L^{-1}, K^+ 5.0 mmol L^{-1}, Mg^{2+} 1.5 mmol L^{-1}, Ca^{2+} 2.5 mmol L^{-1}, Cl^- 148.8 mmol L^{-1}, $HCO_3{}^-$ 4.2 mmol L^{-1}, $HPO_4{}^{2-}$ 1.0 mmol L^{-1}, $SO_4{}^{2-}$ 0.5 mmol L^{-1}). The samples were immersed in 10 mL at 37 °C and SBF was changed after 1 h, 3 h, 5 h and 7 h and then daily for 14 days. Total silver and copper content in the coatings was measured with ICP-MS calibrated with 50 ppb and 100 ppb standard solutions [297].

3.12. Microbiology

All titanium disks for biological experiments were sandblasted with Korox 110 and used as controls or coated with the standard procedure as described in the beginning of this section. Samples and controls were disinfected two times with 70 % ethanol in 24 well-plates and then air dried under a biological safety cabinet. An overnight culture of 20 µL *S. aureus* (strain RN4220) or *S. epidermidis* (strain RP62A) in 10 mL lysogeny-broth medium (LB medium) was shaken with 250 rpm at 37 °C. The overnight culture was diluted to 10×10^{-6}, 10×10^{-7}, 10×10^{-8} and 10×10^{-9} and 100 µL were plated on agar plate to control the number of bacteria. The solution aiming for 445 CFU/mL was used directly and diluted to 10×10^{-1}, 10×10^{-2} and 10×10^{-3} and 100 µL were plated on agar plates made with lysogeny-broth medium (LB agar plates).

3.12.1. Agar diffusion test

An overnight culture was prepared from 10 mL LB medium and 20 µL of thawed *S. aureus* culture and cultivated at 37 °C and 250 rpm in a thermoshaker (Unimax 1010 with Inkubator 1000 (Heidolph Instruments GmbH & Co. KG, Schwabach)). LB agar plates were seeded with 100 µL of the overnight culture with about 8.5×10^{8} CFU/mL and calcium hydroxide coated titanium samples were placed onto them with the calcium hydroxide coating facing downwards. Uncoated titanium samples served as control.

3.12.2. Bactericidity test

This section was already published in [297]. Reprinted with permission from Springer Nature, Copyright © 2018

To evaluate the antimicrobial properties, as-deposited Ag-$Ca(OH)_2$ and Cu-$Ca(OH)_2$ coatings were tested with *S. epidermidis*. LB medium was employed to cultivate the bacteria in a shaker (Unimax 1010 with incubator 1000, Heidolph Instruments GmbH & Co. KG, Schwabach, Germany) at 250 rpm for 4.5 h. The cultivation was done in 10 mL and stored at 37 °C. Subsequently, one half of the suspension was further cultivated in 40 mL LB medium for another 2 h at 37 °C. Beside Ag-$Ca(OH)_2$ and Cu-$Ca(OH)_2$ coatings, control surfaces of polystyrene, sandblasted titanium and calcium hydroxide coatings without silver or copper were investigated (n=3). Ag-$Ca(OH)_2$ (n=9) and Cu-$Ca(OH)_2$ (n=9) as well as control surfaces were cultivated in 24-well plates, immersed in 1 mL of bacteria suspension. After incubation at 37 °C for 24 h the supernatant was removed. 500 µL of a 1:10 water soluble tetrazolium salt (WST)-solution (Roche Diagnostics, Mannheim, Germany) in PBS was given to each sample and incubated for 20 min at 37 °C. WST-supernatant was centrifuged at 50 000 rpm for 5 min. Analysis was performed with an ELISA-Reader (Tecan, Crailsheim, Germany) and the associated software Magellan 3 (Tecan, Crailsheim, Germany). Therefore, two times 200 µL of the WST-solution

were analyzed in a 96-well-plate. Statistical evaluation (ANOVA with planed contrasts) was performed with SPSS 18.0 (IBM Germany, Ehningen, Germany) [297].

3.12.3. Bacterial growth over time

After disinfection, the samples were seeded with 445 CFU *S. aureus* or *S. epidermidis* in 1 mL 1:500 LB medium. The dilution of LB medium to 1:500 for this test was in accordance with ISO 22196/2011-08 and was chosen, because antibacterial effects could be more pronounced, as previous tests showed (unpublished data). For determination of bacteria at the surface of the samples the same protocol was applied as was during animal studies for the cylindrical implants. The bacterial suspension was removed from the samples and they were transferred to a well filled with 1 mL PBS for washing. After washing the samples were transferred to a 50 mL centrifuge tube each filled with 1 mL 0.9 % NaCl solution and put 10 times for 30 s in an ultrasonic bath (Bandelin Sonorex Typ RK 512 H , Bandelin electronic, Berlin, Germany) with 15 s pause between sonication. In addition, they were vortexed 4 times (Vortex Genie 2, Scientific Industries, New York, USA) for 15 s at level 9 with 45 s pause. Then 100 µL of serial 10-fold dilutions of the solution were plated on LB agar plates. Formed colonies were counted after 24 h or 48 h incubation at 37 °C. In order to investigate the timeline of the bacterial growth, the experiment was conducted for 1 h, 3 h, 5 h and 7 h as well as 7 h, 9 h, 11 h and 13 h and 1, 2 and 3 days.

3.12.4. Biofilm

During all experiments, *S. aureus* was cultivated in LB medium, and the medium was changed every 1 or 2 days.

Straining of biofilm with concanavalin A

Samples were placed on hooks and gently washed twice in 150 mL PBS; every washing was performed like this if not stated otherwise. Thereafter, they were placed in a wet chamber and incubated with 100 µL 2 % (2 g/100 mL) paraformaldehyde (PFA) in PBS for 5 min, followed by two times washing and incubation with 100 µL 0.2 % (0.2 mL/100 mL) Triton X in PBS for 5 min and again two times washing. Then the samples were stained with 100 µL of a 0.1 µg mL^{-1} solution of FITC-labeled concanavalin A (Sigma-Aldrich, Munich, Lot-# 026K7039V) in PBS for 50 min and after 40 min of the 50 min two drops of Hoechst 33342-solution (5 µg mL^{-1}) were added. Afterwards, they were washed thrice for 5 min, once standing still and twice at 50 rpm on a shaker (Heidolph Unimax 1010). The samples were incubated with ethanol for 1 min, air-dried and then the fluorescence was measured together with SYBR-green. For microscopy, all samples were embedded in Mowiol (3 g/40 mL PBS) (Hoechst, Frankfurt, Germany).

Based on the experience from the first two runs the protocol was changed. Washing was

no longer performed on hooks, but samples were washed with 1.5 mL in their wells. Due to surface tension, a meniscus build up between the walls of the wells and 100 µL were not enough anymore to have a full coverage of the sample surface in the wells. The amount of all substances was increased to 200 µL.

Staining of bacteria with SYBR-green

Samples in a 24-well-plate were washed twice with 1.5 mL PBS per well and then fixated with 1.5 mL 3.7 % formaldehyde solution in PBS for 20 min. The samples were washed twice with 1.5 mL PBS and dehydrated with a series of 1.5 mL ethanol: 50 %, 80 %, 99 % and 99 % for 5 min, each. Then the samples were air-dried and stained with 1.5 mL of a 100 000-fold dilution of SYBR-green in TRIS-buffer for 15 min in the dark. Surplus dye was removed by extensive washing with TRIS-buffer. After drying the fluorescence of SYBR green was evaluated in a Spectrafluor Plus or SPARK 20M (Tecan, Crailsheim, Germany) with Megellan software (Tecan, Crailsheim, Germany). Microscopic pictures were taken with an Axio Imager M1 (Zeiss, Oberkochen, Germany) with an HBO 100 lamp for fluorescence excitation and appropriate filter sets for blue (353 nm/465 nm), green (495 nm/519 nm) and red (558 nm/575 nm).

LIVE/DEAD staining

Bacteria were stained with the LIVE/DEAD© *Bac*Light™ Bacterial Viability Kit L7012 from Molecular Probes (Leiden, Netherlands). The calibration curve was calculated and evaluated following DIN 32654 using the R programs "Kalib_ersten_Grades.R Version 0.9 (28.12.2015)" and "Analyse_ersten_Grades.R Version 0.5 (28.12.2015)" made by Prof. Dr. Karl Molt, down-loadable under https://bscw.uni-due.de/pub/bscw.cgi/12944089 and discussed in [302].

3.13. Cytocompatibility testing

This section was already published in [297]. Reprinted with permission from Springer Nature, Copyright © 2018

The metal-ion containing modifications Ag-$Ca(OH)_2$ and Cu-$Ca(OH)_2$ were tested with human fetal osteoblast cell line (hFOB) 1.19 (LGC Standards, Wesel, Germany) in passage 9. Four samples each were placed in the wells of a 24-well plate and polystyrene (PS), sandblasted titanium and pure $Ca(OH)_2$ served as control. The wells were seeded with 5×10^4 hFOB cells in 1 mL DMEM, supplemented with 1 % penicillin and streptomycin, 0.3 mg mL^{-1} geneticin (G-418 sulfate), and 10 % fetal calf serum (FCS) (all from Invitrogen Life Technologies, Karlsruhe, Germany). Incubation at 34 °C and with 5 % CO_2 followed.

The cell activity and cell number were accessed at days 1, 3, 7 and 10. For evaluation of the cell activity, cells were incubated with a 1:10 mixture of WST-1 with cell culture medium at

34 °C and with 5 % CO_2 for 30 min. After that the supernatant was transferred in duplicate into a 96-well-plate and measured with an ELISA-Reader and the Magellan 3 Software (both Tecan, Crailsheim, Germany). Thereafter the samples were washed three times with PBS. The cells were lifted with Accutase® and counted with a Cellometer Auto T4 cell counter (Nexcelcom Bioscience, Lawrence, Massachusetts USA).

3.14. Software

Image arrangement and annotation of microscopic and SEM pictures was done with FIJI/ImageJ [303] with the help of ScientiFig [304] and the bio formats plugin [305]. For statistical calculations R Version 3.3.2 (https://www.r-project.org/) was used.

4. Results and Discussion

4.1. pH gradient during coating

The elevation of pH-value near the cathode caused by the electrolysis of water is the driving force for the deposition of calcium hydroxide. Therefore, it is very important to measure the pH-gradient from the surface of the titanium substrate into the bulk electrolyte.

Using an electrical pH-meter with a glass electrode seems to be the easiest method on the first sight. The pH-meter showed a pH-value for the bulk electrolyte of 2.65±0.05 before the coating experiment was started with the 4-fold holder and the cylindrical anode setup. Directly after starting the pH-meter reached the measuring limit and reported an overflow, meaning a pH higher than 15, when measuring directly next to the cathode and between cathode and anode. At the anode, a pH of about 14 was measured. The experiment was ended after 900 s and the pH immediately fell to 2.65±0.05, the bulk pH-value measured before starting. The pH-value at the anode should be below the pH-value of the bulk, because at the anode oxygen is released and the concentration of H^+ ions increases:

$$6\,H_2O \longrightarrow O_2\uparrow + 4\,e^- + 4\,H_3O^+ \tag{4.1}$$

At the same time OH^- are created at the cathode

$$2\,H_3O^+ + 2\,e^- \longrightarrow H_2\uparrow + 2\,H_2O \qquad \text{(acidic)} \tag{4.2}$$

$$2\,H_2O + 2\,e^- \longrightarrow H_2\uparrow + 2\,OH^- \qquad \text{(basic)} \tag{4.3}$$

leading to an overall unchanged pH-value in the electrolyte.

$$2\,H_2O \longrightarrow 2\,H_2\uparrow + O_2 \tag{4.4}$$

Thus, an overall rise of the pH-value is not possible when only electrolysis of water occurs. And a nearly unchanged pH-value was found after the current was turned off. Consequently, the electrical field interfered with the glass electrode making meaningful measurements impossible.

As a next step, different pH-indicator solutions were used in order to visualize the pH-gradient. A pH-value indicator made for measuring pH-values between 4 and 10 changed the color from red to yellow during the coating process (compare 4.1 A and B). This would indicate a change

of pH from below 4 to about 6. But again, the whole electrolyte changed color, which is illogical for above-described reasons. Thus, two samples of the yellow solution were taken and NaOH (left glass on figure 4.1 C) and citric acid (right glass on figure 4.1 C), respectively, were added. The addition of NaOH should have led to a color change to purple, but the color changed to pink. Moreover, the yellow color did not change to red after citric acid addition. Hence, the dye did not work properly anymore, which could be explained by the destruction of the dye during the coating process.

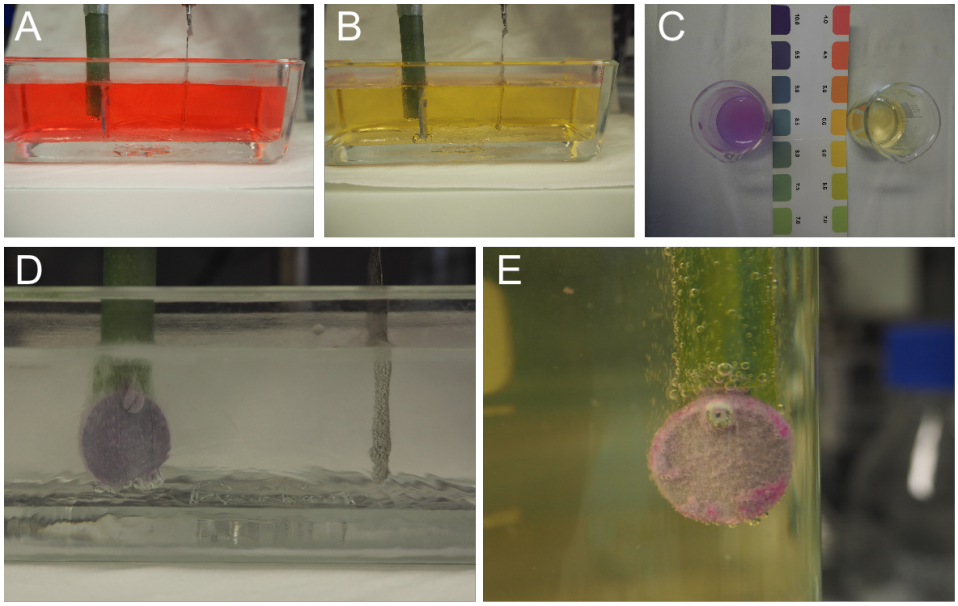

Figure 4.1: Determination of pH-gradient during coating. A-C: indicator for pH 4-10. A: at the beginning, B: at the end of the coating procedure. The color changed from red to yellow. C: NaOH was added to the left glass and citric acid was added to the right glass. The colors did not match the colors on the color card and the pH measured with a pH-meter. This means the color change was due to destruction of the dye. D: Phenolphthalein indicator during the coating procedure. Directly at the cathode the color changes to pink, indicating an elevated pH-value. E: Same experiment as in D, but with another set-up.

Another suitable pH-indicator is phenolphthalein because it changes from colorless to pink in a pH range from 8.0 to 9.6 and stays pink until pH 11, where it turns colorless again [298, p. 254 - 257]. When the ECAD-process was started, the hydrogen bubbles sparkled from the surface of the cathode and shortly after that the layer below the bubbles turned pink and stayed pink until the end (compare figure 4.1 D and E). A short calculation will bring some understanding of the processes and the time frame. The assumptions to make are that there is no diffusion, all electrons are producing OH^- and the volume is restricted to 1 mm around the implant. Within this volume of 0.867 mL, all H_3O^+ from the starting pH-value of 2.65 are depleted after less than 0.2 s and the pH-value rises to about 14. In the experiment diffusion and a not 100 % effective OH^- production from the electrons limits the rise of the pH to the

measured value of about 11. Phenolphthalein was also used as indicator for electrodeposition and showed a similar pH-change [306].

These experiments showed that measuring the pH-value in an electrical field with an electronic pH-meter can lead to wrong results and misinterpretation. Phenolphthalein turned out to be favorable, because of its color change between colorless and pink. Using phenolphthalein, the pH-value at the cathode could be determined to lay between 8 and 11 during the ECAD-process. This surface confined pH elevation from 2.6 to above 8 leads to the deposition of calcium hydroxide.

4.2. Influence of surface pretreatment

Contact angle and roughness parameter were determined for all prepared surfaces, because wettability and surface roughness are key parameter for good integration of the coating into the substrate surface. The results can be found in table 4.1. While polished and acid etched surfaces had high contact angles, the contact angle of NaOH-treated surfaces was not measurable, because the drop spread immediately when it reached the surface. Thus NaOH-treatment led to a good wettability, that should be favorable for coating.

Table 4.1: Static contact angles and surface roughness parameter of differently pretreated titanium samples.

surface	contact angle in °	Ra-mean in nm	Ry-max in nm	Rz-max in nm	Rq-mean in nm
machined	51.7±2.4	730 ±270	24 490	6910	1180 ±530
polished*	52.4±11.1	4.6±4.7	–	–	6.9±7.4
acid etched*	68.6±45.0	13.1±11.1	–	–	18.1±15.4
NaOH	#	470 ±36	3540	3060	580 ±40
Korox 50	9.2±1.9	910 ±70	8450	7300	1170 ±70
Korox 110	44.5±2.5	1440 ±130	14 160	11 420	1870 ±150
Korox 250	21.0±5.6	3033 ±258	31 000	25 000	3970 ±399

*: roughness measured with atomic force microscopy
#: drop immediately sank in, no static contact angle measurable

Surface roughness will influence the ability of the coating to interlock with the surface of the titanium substrate. Thus, it has an influence of the bonding strength of the coating [307]. The surface roughness parameters were either measured with AFM for the smooth surfaces or with a profilometer. Scanning electron images of all surfaces showed the differences in surface roughness clearly and verified the measurements (compare figure 4.2).

Polished titanium samples showed nearly no surface roughness except of single scratches and rare grainy spots. These spots were identified by EDS (see figure 4.3) as silicon carbide implanted into the surface originating from the abrasive paper or the OP-S suspension used for polishing. Due to the low surface roughness the interlocking of the calcium hydroxide coating

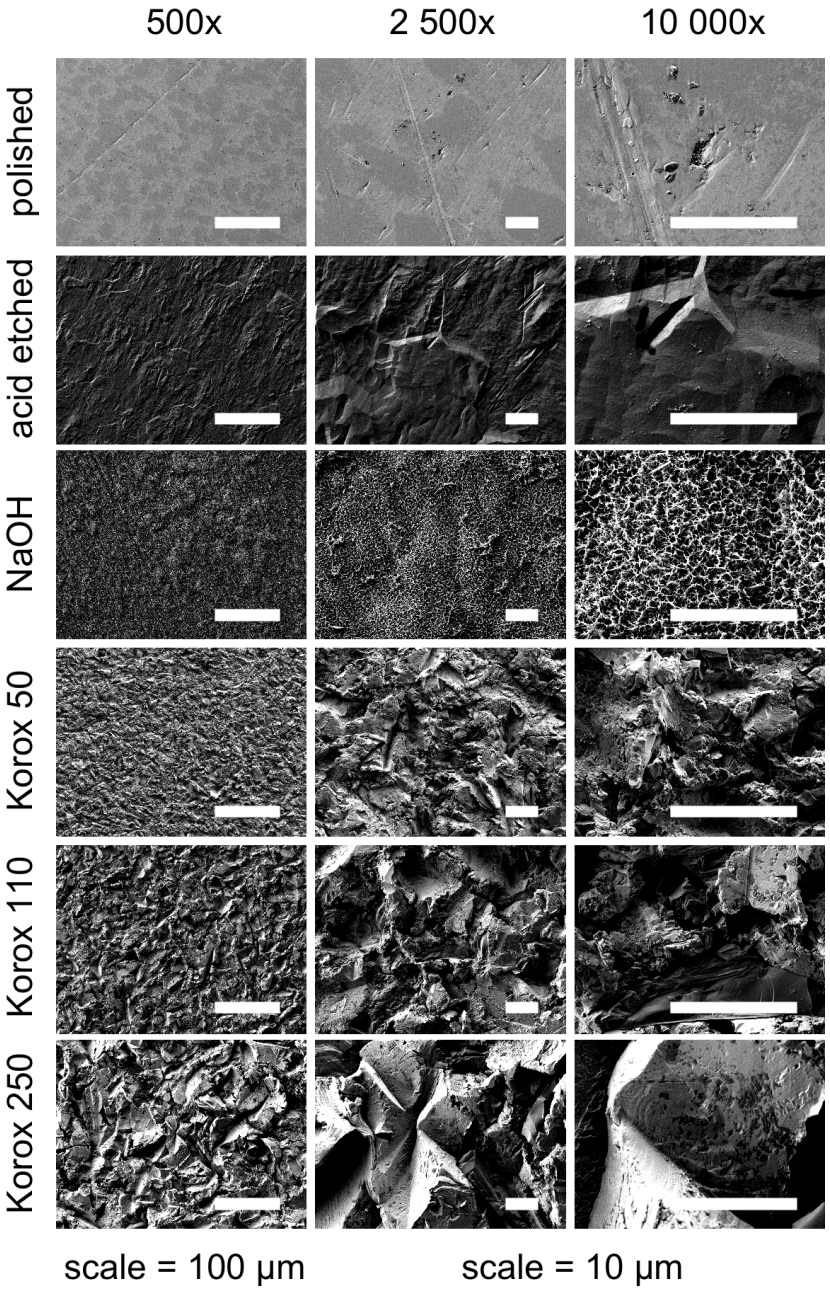

Figure 4.2: Scanning electron microscopy images of the differently pretreated surfaces before coating. Polished surfaces are smoothest. Acid etched and NaOH-treated surfaces show low homogeneity at lower magnifications (500x) but at higher magnifications a homogeneous microstructure is clearly visible. Thus, both have a different macro and micro surface morphology. With increased size of the sandblasting particles (Korox 50 - Korox 250) the surface appears rougher and shows bigger structures.

was not good and only little was deposited (compare figure 4.5 A). Therefore, nearly no peaks for calcium hydroxide could be detected with XRD (compare figure 4.5 B) and hardly any coating on SEM images (compare figure 4.4).

Acid etching predominantly changed the micro- and nanostructure (compare figure 4.2). Scratches of the abrasive paper used before etching were still visible but were partially removed. Most notable were the wave-like structures on top of the microstructure that could be seen at higher magnifications (10 000x). This greatly increased the surface area and presented small nucleation sites for calcium hydroxide. This could be an explanation why thin and high peaks were visible in the diffraction pattern (compare figure 4.5 B), while the coating mass was hardly more than on a polished surface (see figure 4.5 A). Only titanium was visible with EDS and no impurities could be found on the surface (compare figure 4.3). SEM images (see figure 4.4) showed a surface completely coated with calcium hydroxide that had no crater-like structures and therefore seemed thin. Typical cracks were also visible.

Titanium samples treated with NaOH for 24 h and heated at 600 °C revealed an even more complex surface micro-structure than acid etched samples (compare figure 4.2). Tiny struts were three-dimensionally connected and formed a highly porous surface. This structure looked like the one in the literature, the surface pretreatment was taken from [300], indicating a successful pretreatment. Additional to titanium, sodium was detected in the surface by EDS (compare figure 4.3) that could be bound in the form of amorphous sodium-titanate as was described in literature [299]. Since it was amorphous it was not visible in XRD (compare figure 4.5 B), but XRD revealed another change in the surface composition. Rutile peaks occurred, indicating an increased TiO_2 layer, which is also in accordance with literature [299]. The coating was dense, exhibited craters and was similar to the coatings on Korox blasted surfaces (figure 4.4). The perfect wettability and the high surface led to a higher coating mass than on polished or acid etched samples, but all Korox sandblasted samples could be coated with higher masses (see figure 4.5 A).

During sandblasting Korox (Al_2O_3) was implanted into the surface (compare figure 4.3 with a Korox 250 image), thus they were chemically identical, but the scale of their surface morphology was different (compare figure 4.2). Their contact angles were all below that of polished or acid etched surfaces but differed strongly. The surface sandblasted with Korox 50 showed the lowest contact angle of the three, followed by Korox 250- and Korox 110-treated surfaces. Therefore, Korox 50 had the best wettability and coating masses would be expected to be highest for Korox 50-, then Korox 250- and lowest for Korox 110-blasted surfaces. Interestingly, the deposited coating mass was increasing in the order: Korox 50, Korox 110 and Korox 250 blasted surfaces (compare figure 4.5 A). This is most likely because the surface roughness is higher (see table 4.1 and figure 4.2) and consequently the surface area as well. However, the X-ray diffraction pattern in figure 4.5 B shows decreasing peaks with increasing coating mass, thus indicates lower crystalline coatings. A look at the coatings with the SEM (figure 4.4) revealed that the

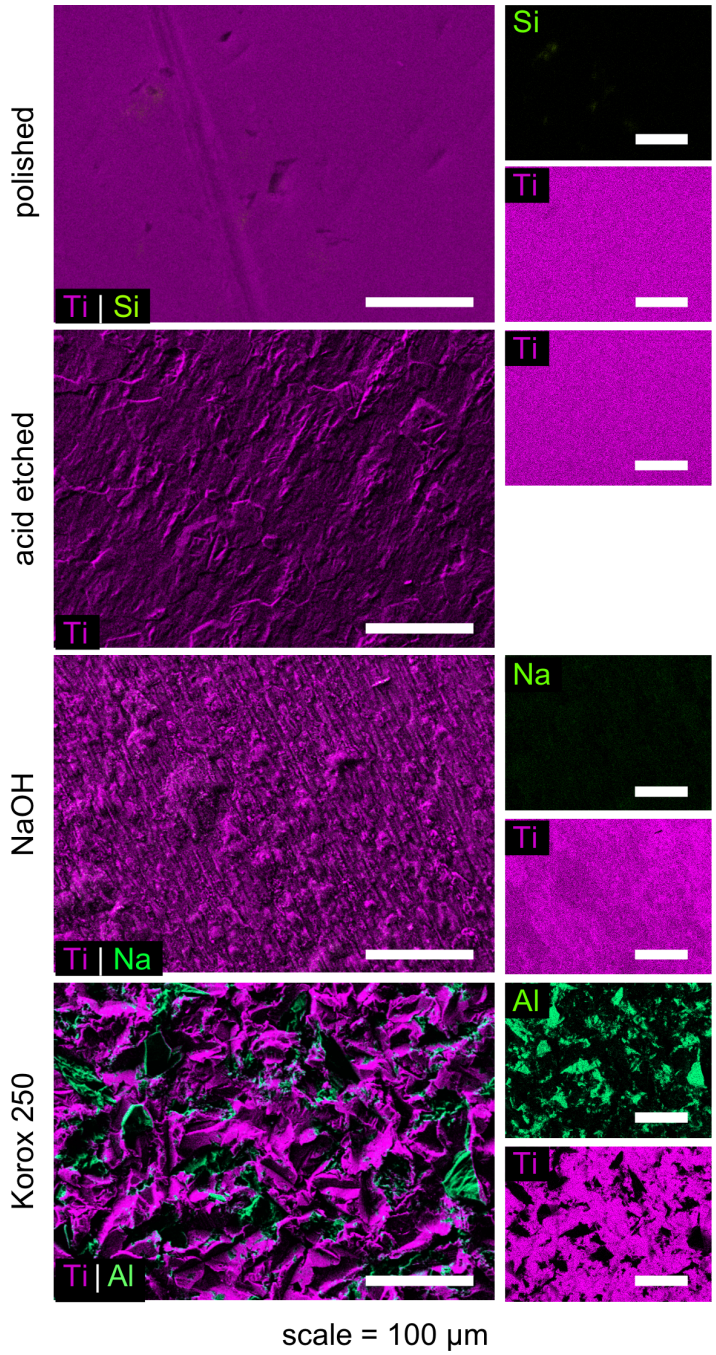

Figure 4.3: Energy dispersive X-ray spectroscopy of differently pretreated surfaces before coating. All surface pretreatments retain titanium as the main surface component but can introduce new elements. The polished surface shows small silicon leftovers from the silicon carbide grinding paper. Acid etching left no elements. Traces of sodium can be detected on NaOH-treated surfaces. Sandblasting with Korox 250 implanted Al_2O_3 into the surface, clearly visible as spots with high Al and no Ti content.

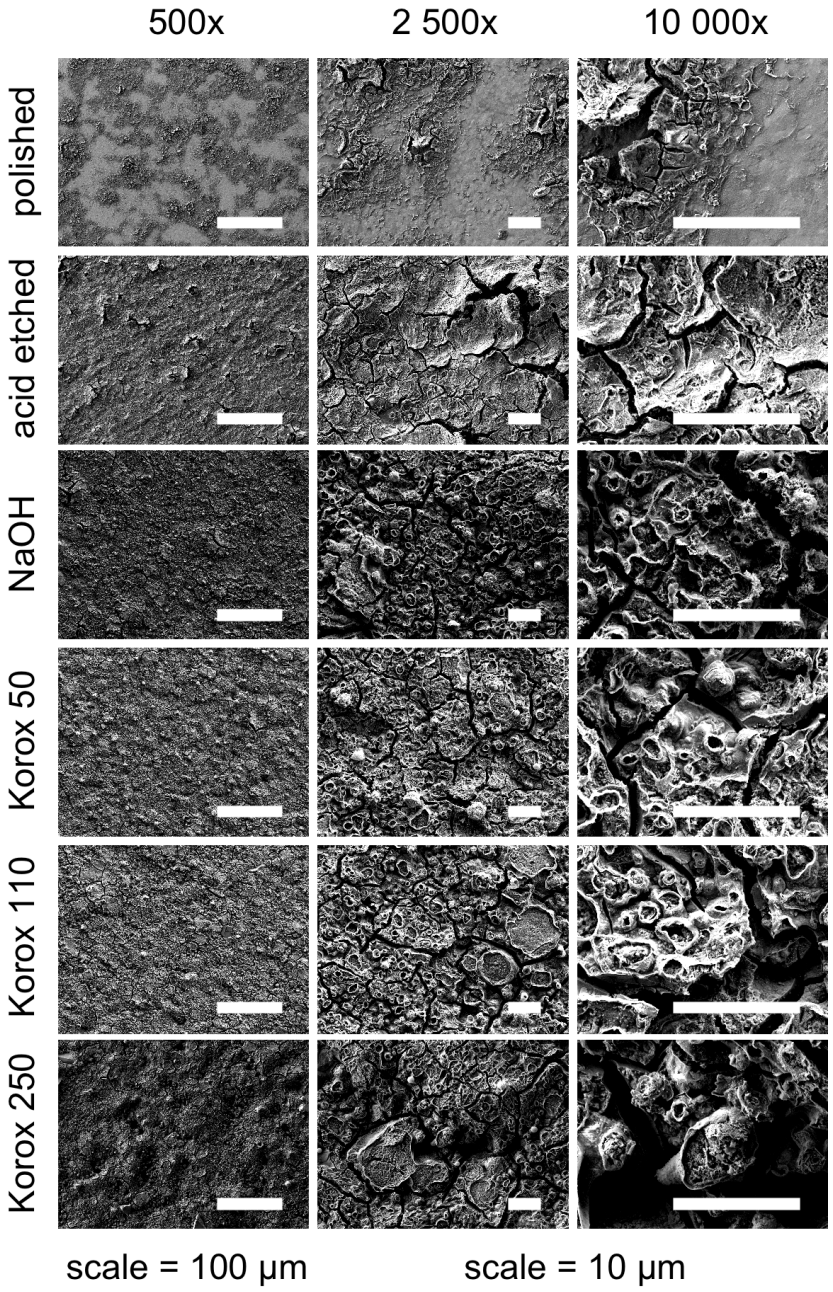

Figure 4.4: SEM images of differently pretreated surfaces after coating. The clear differences found before coating are more subtle but can still be found. Polished surfaces are hardly coated. Acid etched surfaces show a homogeneous coating as do the NaOH-treated. The unevenness of the coating increases with the size of blasting sand, inheriting the roughness of the underlying substrate.

surface morphology is inherited from the surface pre-treatment. Coatings on Korox 50-blasted titanium where smoothest, followed by Korox 110-basted and then Korox 250-blasted.

All in all, the surface roughness seemed to have a bigger influence on coating mass than the contact angle/wettability of the surface. The influence of contact angle, surface roughness and morphology are broadly discussed concerning adhesion strength of the coating, bone-implant contact, antibacterial properties and spreading of osteoblasts [308–312]. The wettability of the surface plays an important role, as the hydrophilic character and thus the surface energy of implants was found to affect differentiation and maturation of bone cells and osseointegration [309]. For example, highly hydrophilic HA exhibited enhanced bioactivity [313].

The influence of the surface roughness and contact angles of Ti-6Al-4V and Ti-6Al-4V structured with nanotubes on osteoblast and *S. aureus* adhesion were investigated by Izquierdo-Barba et al. [310]. Ti-6Al-4V had a root mean square roughness on an 2 µm x 2 µm area of 3 nm and a contact angle of 56°, while the nano-tube surface exhibited a roughness of 57 nm and a contact angle of 102°. However, the AFM tip was not able to fully penetrate the tubes, leading to an underestimation of the roughness. Despite these differences osteoblasts showed similar adhesion and proliferation on both surfaces. Interestingly, *S. aureus* was influenced and adhered significantly less on the nano-tube surface. The authors concluded that osteoblasts saw the nano-tube surface as smooth, because they are much larger and could adapt to the surface due to their flexible cell membrane. Since *S. aureus* is much smaller and possesses a more rigid cell wall, it cannot adhere well to the nano-tube surfaces. Thus, the effect of roughness is dependent on the size of the cells and bacteria and can vary widely.

The hypothesis that polished surfaces can minimize bacterial adhesion due to their lower surface roughness is controversial. Harris et al. [314] showed that the adhesion of one *S. aureus* strain was equal on stainless steel, standard microrough CP-titanium, electropolished titanium and electropolished Ti-6Al-7Nb but more on standard microrough Ti-6Al-7Nb. Therefore, reducing the roughness (Ra) of CP-titanium from (0.900±0.027) µm to (0.190±0.030) µm via electropolishing did not influence the *S. aureus* adhesion, but electropolishing Ti-6Al-7Nb from (0.770±0.076) µm down to (0.180±0.037) µm reduced the *S. aureus* amount significantly. The authors explain it with the different morphology of the surfaces. Standard microrough Ti-6Al-7Nb showed micro-protrusions of niobium enriched β-phase titanium, which were removed by electropolishing. On CP-titanium similar micro-protrusions were never present. Hence, the general micro-roughness did not influence the adhesion of *S. aureus*, but the presence of micro-protrusions enhanced the adhesion. An earlier publication of the same authors [315] also showed no direct dependency of surface roughness and bacterial adhesion. Polished surfaces with lower surface roughness had higher bacterial adhesion than the standard material and special surface coatings with similar roughness had different bacterial adhesion depending on the surface chemistry. Interestingly, there were also huge differences between medical implant quality anodized titanium surfaces bought from two different manufacturers that should have

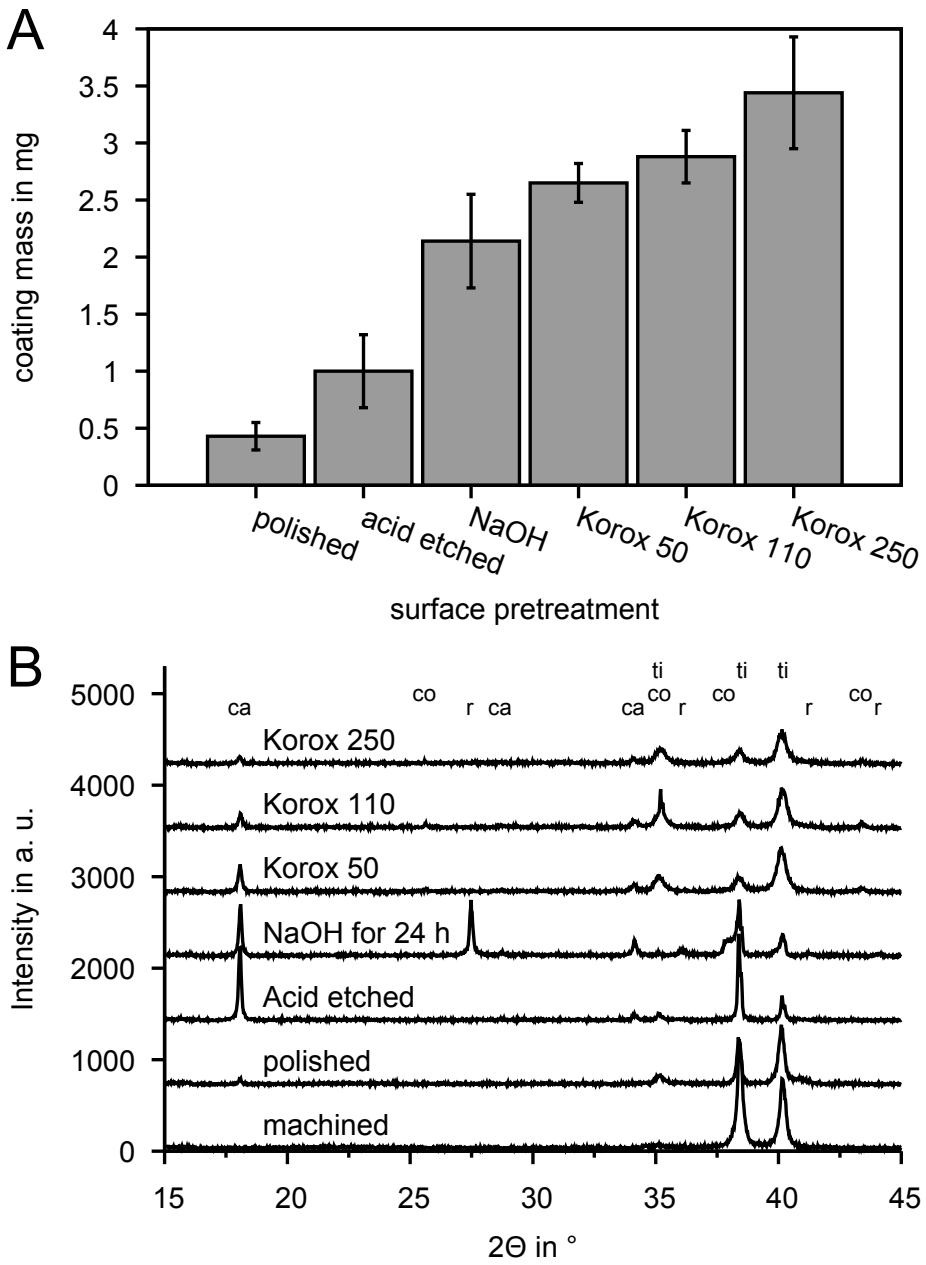

Figure 4.5: A) Calcium hydroxide mass deposited on differently pre-treated titanium surfaces produced under the same coating conditions. Coated surface area $\sim 17.2\,\mathrm{cm}^2$. Surfaces vary in surface chemistry, morphology, roughness and/or contact angle. B) X-ray diffraction patterns of calcium hydroxide coatings on differently pretreated surfaces. The XRD of the machined surface is given as reference for the untreated titanium and was not coated. Acid etched and NaOH-treated surfaces showed high peaks for calcium hydroxide and NaOH-treatment also led to a visible rutile peak. The polished surface was too smooth and barely any $Ca(OH)_2$ could interlock with the surface. Thus, the calcium hydroxide peak is barely visible. Of the three Korox pre-treatments Korox 50 showed the highest $Ca(OH)_2$-peak. Peak positions were determined from their PDF-numbers (calcium hydroxide (ca) 04-0733, rutile (r) 21-1276, corundum (co) 46-1212, titanium (ti) 01-1197

similar surface roughness and chemistry.

In general, bone retention is influenced by the surface roughness. Rønold et al. [311] prepared coin-shaped implants of 6.25 mm diameter and 1.95 mm height made of grade 2 titanium with differently sandblasted surfaces. Titanium dioxide particles with sizes between 22 µm to 28 µm (group 1) and 180 µm to 220 µm (group 2) and were used as blasting sand solely or one after the other (group 3). The surface roughness parameter S_a describing the arithmetic mean deviation of the surface and S_t standing for the maximum peak to valley height of the surface were measured. Group 1 reached S_a(1.12±0.27) µm and S_t (28.07±3.65) µm, group 2 S_a (3.79±1.07) µm and S_t (59.74±17.73) µm and group 3 S_a = (2.05±0.20) µm and S_t=(38.51±7.36) µm. Implants were fixed in the tibia of twelve 8-month-old New Zealand White adult female rabbits and analyzed after 8 weeks. They measured the bone retention with a tensile test procedure [316] and found the highest force of (25.28±14.33) N for group 2, the roughest surfaces. They concluded that bone bonding was not the reason for higher forces, but mechanical retention at the present undercuts, that could only be detected for the roughest surfaces.

The surface pretreatment with Korox 50 combined a low contact angle and thus good spreading of electrolyte with simplicity of treatment. Most important, the deposited calcium hydroxide coating masses were higher than on polished, acid etched, and NaOH-treated surfaces and the coating was more homogeneous and smoother than the coatings on surfaces sandblasted with Korox 110 or Korox 250. Consequently, sandblasting with Korox 50 was chosen as standard surface pretreatment.

4.3. Influence of stirring and pulsing on the coating

Stirring of the electrolyte or deposition with pulsed current can have an influence on the deposition of the coating, because they may change the equilibrium and the pH-gradient at the surface and hence alter diffusion processes. The following experiments explore the effects of stirring and pulsing as separate parameters as well as in various combination.

4.3.1. Stirring speed

There was a noticeable influence of stirring speed on the deposited masses (see figure 4.6). The higher the stirring speed was, the lower was the resulting coating mass. Higher stirring speeds led to higher flow at the surface, which mainly added to the following two effects. First, loosely bound coating particles could be washed away without the ability to aggregate with the more solidly bound coating. Second, the pH-gradient could change, since the flow could transport produced hydroxide ions away and lead to a lower pH-value at the surface, which is less favorable for coating deposition. Stirring not only had a big influence on the deposited masses, but also on the surface morphology of the resulting coatings (see figure 4.8). All coatings produced without stirring and stirring speeds of 100 rpm and 200 rpm showed the typical crater-like structure

and were crazed with cracks. From 300 rpm on, flower-like structures could be detected in 10 000x magnification. Between 300 rpm and 700 rpm flower-like structures could be seen more frequently on some samples but were not visible on other samples. All inspected samples produced with 800 rpm showed a mixture between crater and flower-like structures. Samples produced with 900 rpm were completely covered with flower-like structures. It is important that these findings are only valid for the central surface. At the edge of the samples voltage spikes occur, change the situation and can alter the morphology. X-ray diffraction patterns showed lower diffraction peaks for calcium hydroxide when stirring speed increased (see figure 4.7). These were most likely caused by a combination of lower coating mass and a changed crystallinity resulting from the change in surface morphology. Thus, different stirring speeds can be used to alter the mass and morphology of calcium hydroxide coatings.

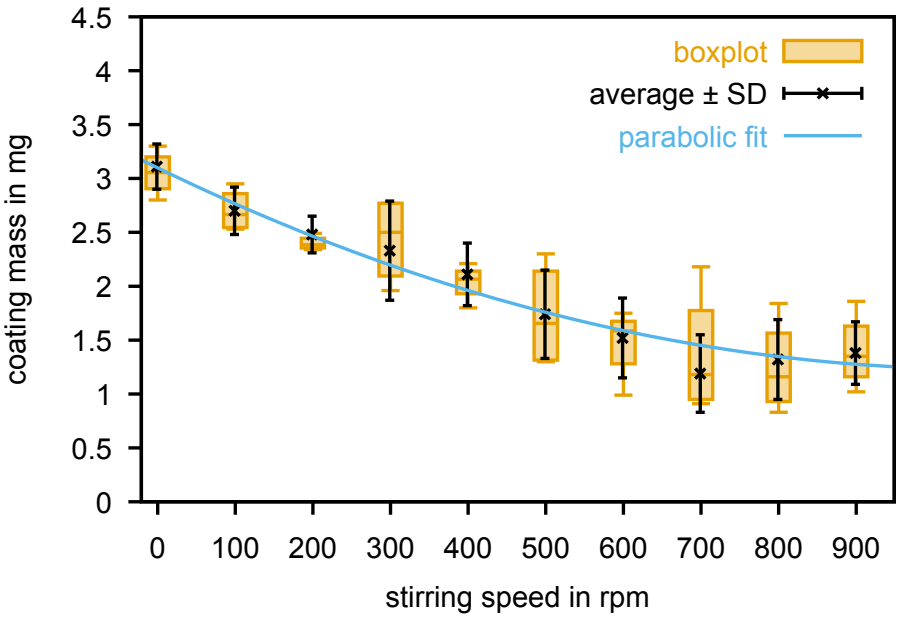

Figure 4.6: Influence of the stirring speed on the deposited coating masses. The faster the electrolyte was stirred, the lower masses deposited.

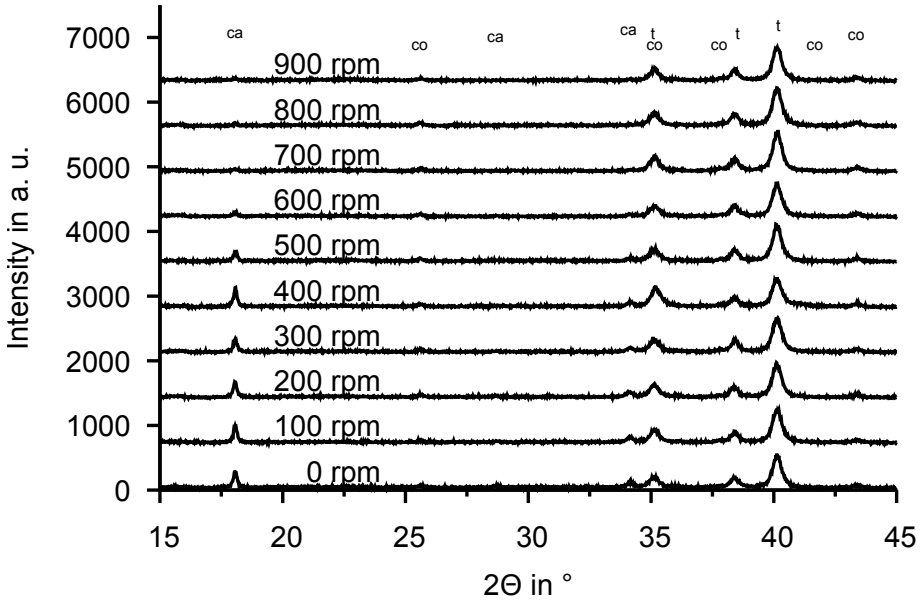

Figure 4.7: X-ray diffraction patterns of coatings produced with different stirring speeds during deposition. Higher stirring speeds led to lower calcium hydroxide (ca) diffraction peaks, but no additional peaks appear. Corundum (co) diffraction peaks result from implantation of Al_2O_3 during sandblasting into the titanium (t) surface.

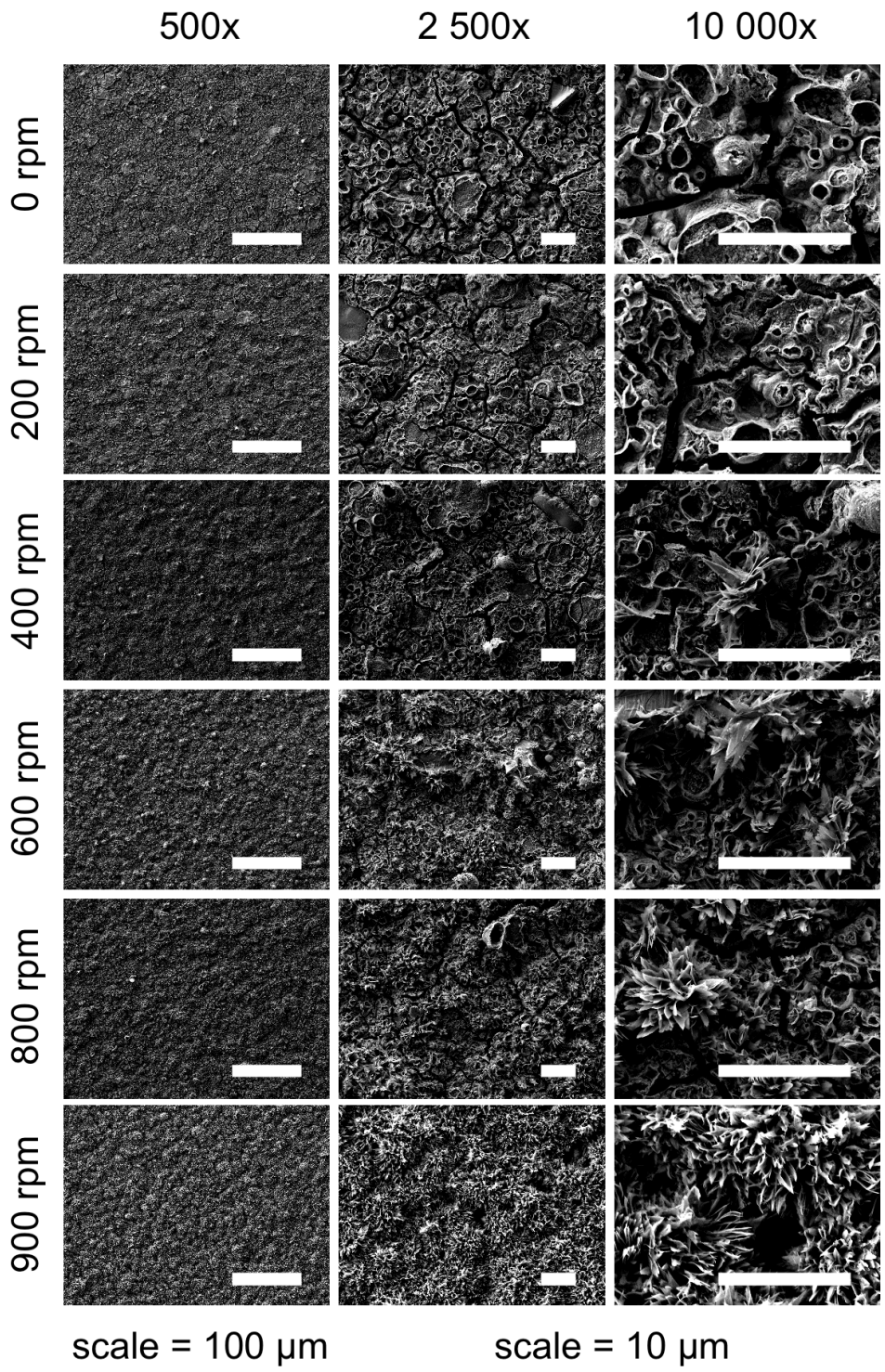

Figure 4.8: Scanning electron microscopy images of calcium hydroxide coatings produced with different stirring speeds. With increasing stirring speed, the morphology of the coating changed from crater to flower-like.

4.3.2. Influences of pulsing

In order to investigate the influence of current pulsing on deposition of calcium hydroxide, experiments using the same current density but three different time patterns for coating were conducted: one with only static current as reference ($t_{precoat}$) and two with precoating and pulsing ($t_{precoat} + t_{pulse} = 900\,s$ and $t_{precoat} + \Sigma\ t_{on} = 900\,s$). The static current was applied for 480 s, 540 s, 600 s, 660 s, 720 s, 780 s, 840 s and 900 s to allow the calcium hydroxide to precipitate as a precoating. The next setup added pulsing to the precoating step. Precoating was done exactly as in the setup before, but then pulsing with the pulsing pattern $t_{off} = 1\,s$ and $t_{on} = 5\,s$ was applied until the total coating time t_{total} reached 900 s. This set of experiments is referred to as $t_{precoat} + t_{pulse} = 900\,s$ (compare figure 4.9 B). Because these both setups worked with the same t_{total}, but different amounts of charge used for the coating process a third setup was arranged that used the same amount of charge for each coating process. The amount of charge Q can be calculated by the multiplication of time (t) and current (I) ($Q = t \cdot I$). Since the current was kept constant, the time, the current was flowing, i. e., the sum of $t_{precoat}$ and all t_{on}, was adjusted to 900 s for each coating. Precoating and pulsing patterns were not changed in respect to the setups before. Only t_{pulse} was longer to get a total time of flowing current ($t_{precoat} + \Sigma\ t_{on} = 900\,s$) of 900 s. Consequently, t_{total} was also longer.

For $t_{precoat}$ set to 900 s all time patterns were the same, because $t_{precoat} + t_{pulse} = 900\,s$ and $t_{precoat} + \Sigma\ t_{on} = 900\,s$. Consequently, all graphs meet there at a coating mass of about 3 mg (figure 4.9 B). They had also in common that longer $t_{precoat}$ led to a trend of increasing coating masses for every of the three different time patterns. As soon as pulsing was involved, this trend got bigger. In addition, samples coated with $t_{precoat} + t_{pulse} = 900\,s$ seemed to have a slightly higher coating mass than that coated with $t_{precoat} + \Sigma\ t_{on} = 900\,s$, but this difference was only statistically significant for 540 s and 720 s. Between the coating masses of coatings produced with $t_{precoat} + t_{pulse} = 900\,s$ and $t_{precoat} + \Sigma\ t_{on} = 900\,s$ and the coating masses of the samples coated only with $t_{precoat}$ there was a statistically significant difference ($p < 0.01$) until $t_{precoat} \leqslant 780\,s$. However, coating masses of $t_{precoat} + t_{pulse} = 900\,s$ and $t_{precoat} + \Sigma\ t_{on} = 900\,s$ differed significantly at 540 s and 720 s. Interestingly, pulsing ($t_{precoat} + t_{pulse} = 900\,s$ and $t_{precoat} + \Sigma\ t_{on} = 900\,s$) led to lower coating masses than coating only with $t_{precoat}$. This sounds contradictory at the first thought, because pulsing after $t_{precoat}$ means that the current was flowing for a longer time. Thus, the amount of charge became higher, which should result in higher coating masses. But when pulsing was applied a higher amount of charge was not the only change that occurred, but also periods with no current flow (t_{off}) were introduced. During t_{off}, no electrolysis of water took place, and hence the pH-value started to fall. Since the coating masses were lower as soon as pulsing was applied, the pH dropped enough to dissolve already deposited coating. Therefore, dissolution of the coating due to a lower pH-value during t_{off} is the dominating effect over an overall higher amount of charge.

The influence of coating time on X-ray diffraction patterns was exemplarily investigated

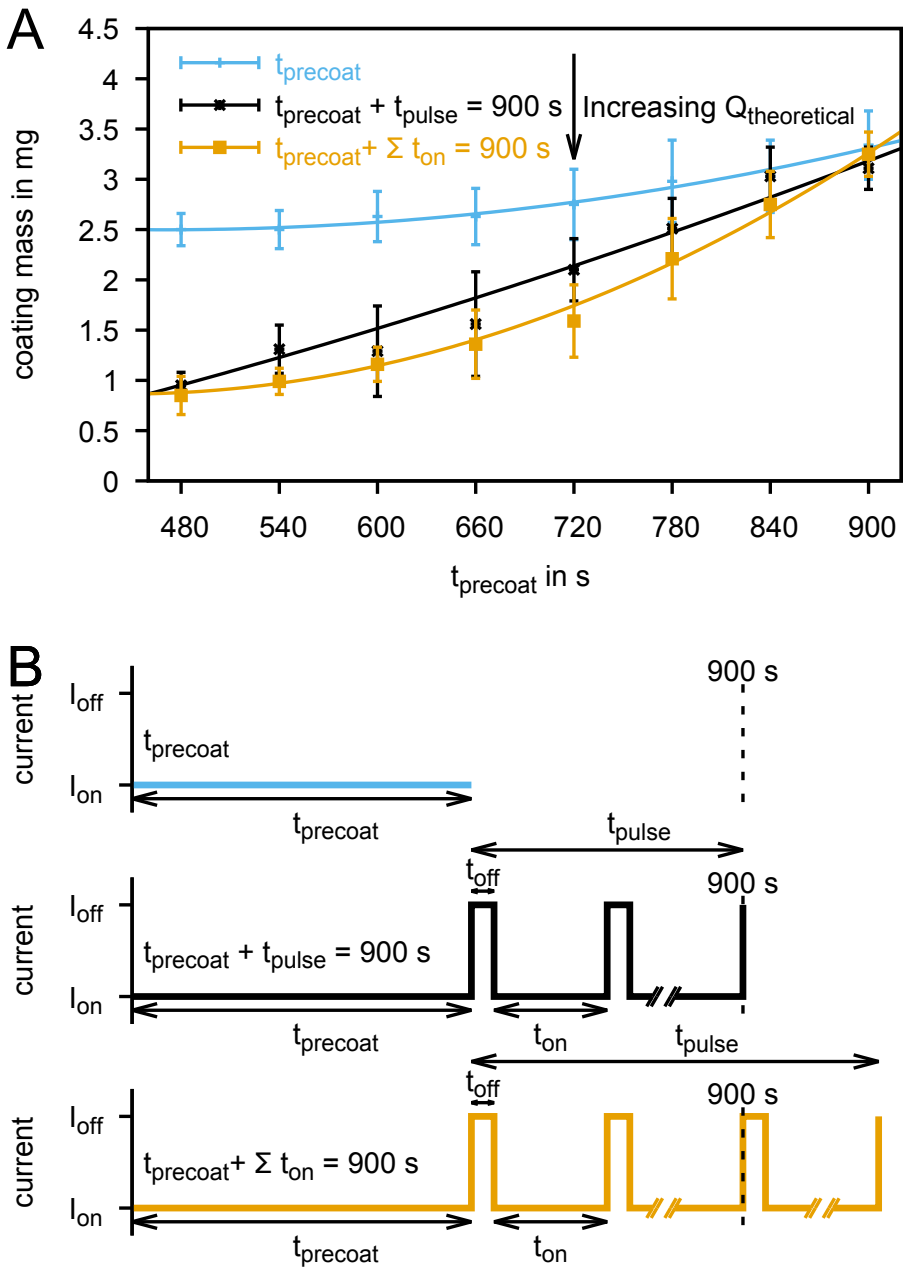

Figure 4.9: A) Coating masses after deposition with three different current patterns. B) Schematic illustration of applied pulse patterns. Coating masses are highest for $t_{precoat}$ followed by $t_{precoat} + t_{pulse} = 900\,s$ and then $t_{precoat} + \Sigma\ t_{on} = 900\,s$. Interestingly, the deposited mass decreased with longer t_{pulse}, thus during t_{off} already deposited mass seemed to be dissolved again.

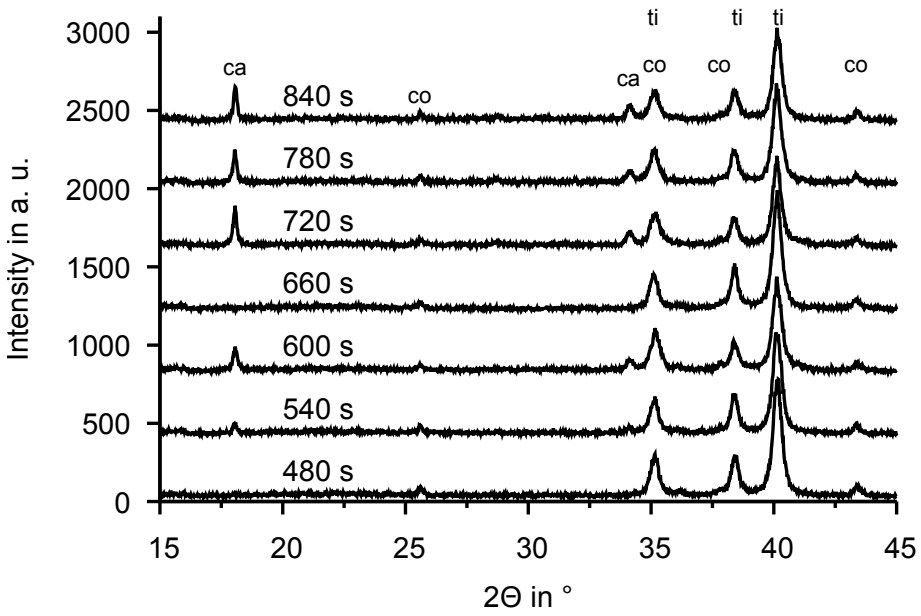

Figure 4.10: X-ray diffraction patterns of coatings produced with $t_{precoat} + t_{pulse} = 900\,s$. The diffraction patterns are labeled with the respective $t_{precoat}$. Longer $t_{precoat}$ led to increased calcium hydroxide diffraction peaks (ca). Remaining diffraction peaks are attributed to titanium (ti) and corundum (co).

for $t_{precoat} + t_{pulse} = 900\,s$ (compare figure 4.10). Titanium and corundum diffraction peaks originated from the Al_2O_3-sandblasted titanium substrate and remained nearly unchanged. The intensity of the calcium hydroxide peak at 18° increased with increasing $t_{precoat}$ and was a result of the higher coating mass.

Scanning electron microscopy images were taken to investigate the effect of the three different time patterns used for coating on the surface morphology (see figure 4.11). For illustration samples with $t_{precoat} = 480\,s$ were chosen, because here the greatest differences between the three current patterns existed. The biggest difference in coating mass was measured for the samples produced with $t_{precoat}$ compared with those produced with $t_{precoat} + t_{pulse} = 900\,s$ or $t_{precoat} + \Sigma\, t_{on} = 900\,s$. Overview images with 200x magnification showed homogeneous coatings for all coating parameters investigated. At higher magnification, the structures of coatings differed from each other. Coating with $t_{precoat}$ led to crater-like structures distributed over the whole surface, which most likely grew around hydrogen bubbles from the water electrolysis. When pulsing was applied crater-like structures were hardly visible (see figure 4.11) or were at least flatter, but the visible cracks seemed to get wider. This does not necessarily mean that cracks got wider, but the contrast between shadows and cracks was pronounced by a smoother surface. Moreover, the samples produced with $t_{precoat} + \Sigma\, t_{on} = 900\,s$ seemed to be smoother than those produced with the same $t_{precoat} + t_{pulse} = 900\,s$. This could be caused by increased precipitation in the inner part of the crater, because the coating is thinner there. Therefore,

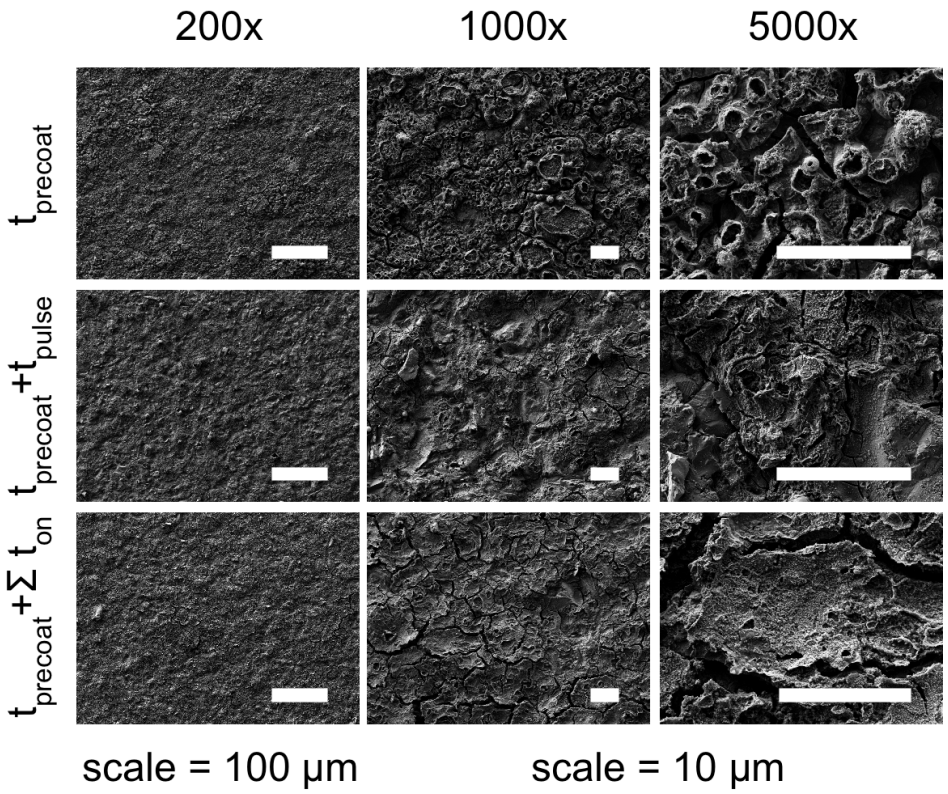

Figure 4.11: Scanning electron microscopy images from coatings produced with $t_{precoat}$, $t_{precoat}$ + t_{pulse} = 900 s or $t_{precoat}$ + Σ t_{on} = 900 s. For all $t_{precoat}$ was set to 480 s. At 200x magnification all samples show a homogeneous and dense coating. At higher magnification (1000x and 5000x) crater-like structures can be seen for $t_{precoat}$. For $t_{precoat}$ + t_{pulse} = 900 s and $t_{precoat}$ + Σ t_{on} = 900 s the crater-like structures appear more and more smoothened, but the cracks seem to broaden.

the electric resistance is lower, which allows more current to flow and more coating to deposit. Consequently, the crater-like structures could fill up from within. Another explanation was that thin crater-like structures could be dissolved during t_{off} by the surrounding acidic electrolyte, which would also explain the decreasing coating mass.

4.3.3. Stirring instead of pulsing after precoating

Stirring was applied after precoating instead of pulsing to investigate the difference between both. Stirring with 200 rpm after precoating had nearly no effect on the coating mass. On the contrary, increased stirring speed (500 rpm) changed the coating mass: the longer $t_{precoat}$ and thus the shorter $t_{500\,rpm}$ was, the higher the coating mass got (compare figure 4.12). When compared to precoating not followed by pulsing or stirring ($t_{precoat}$) and pulsing (compare figure 4.12), precoating followed by stirring with 500 rpm ($t_{precoat}$ + $t_{500\,rpm}$) yielded in similar coating mass as $t_{precoat}$. Consequently, during $t_{500\,rpm}$ no further deposition of coating took place. This led to the conclusion that the deposition rate during stirring with 500 rpm was as high as the dissolution rate.

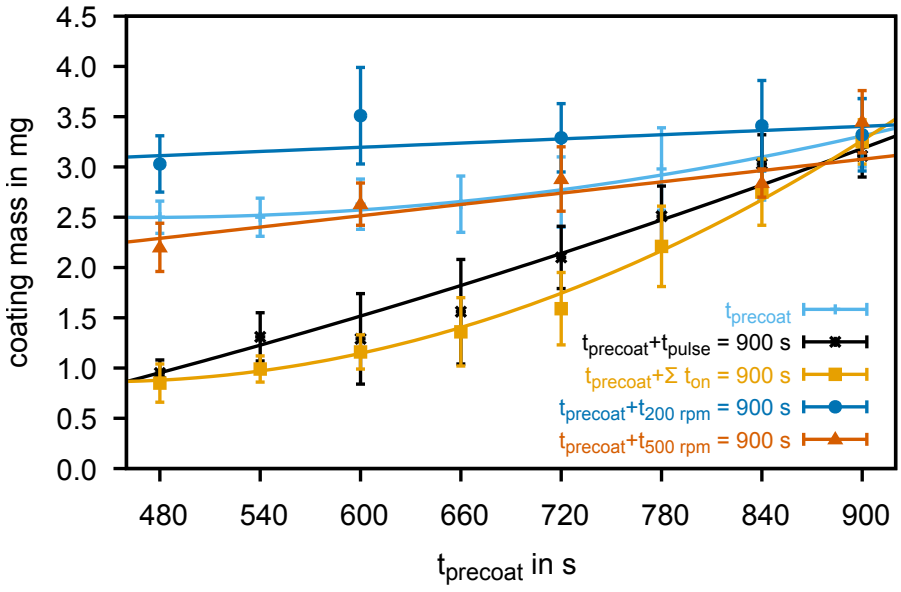

Figure 4.12: Variation of the stirring speed that was used instead of pulsing. Comparison of coatings produced with direct current ($t_{precoat}$), pulsing ($t_{precoat}$+t_{pulse} = 900 s, $t_{precoat+\Sigma\ t_{on}}$ = 900 s) and stirring ($t_{precoat}$+$t_{200\ rpm}$, $t_{precoat}$+$t_{500\ rpm}$).

Scanning electron microscopy images of the coatings revealed no significant difference that could be linked to the production parameter (compare figure 4.13). Thus, stirring instead of pulsing could change the coating masses, but had no noticeable influence on the surface morphology.

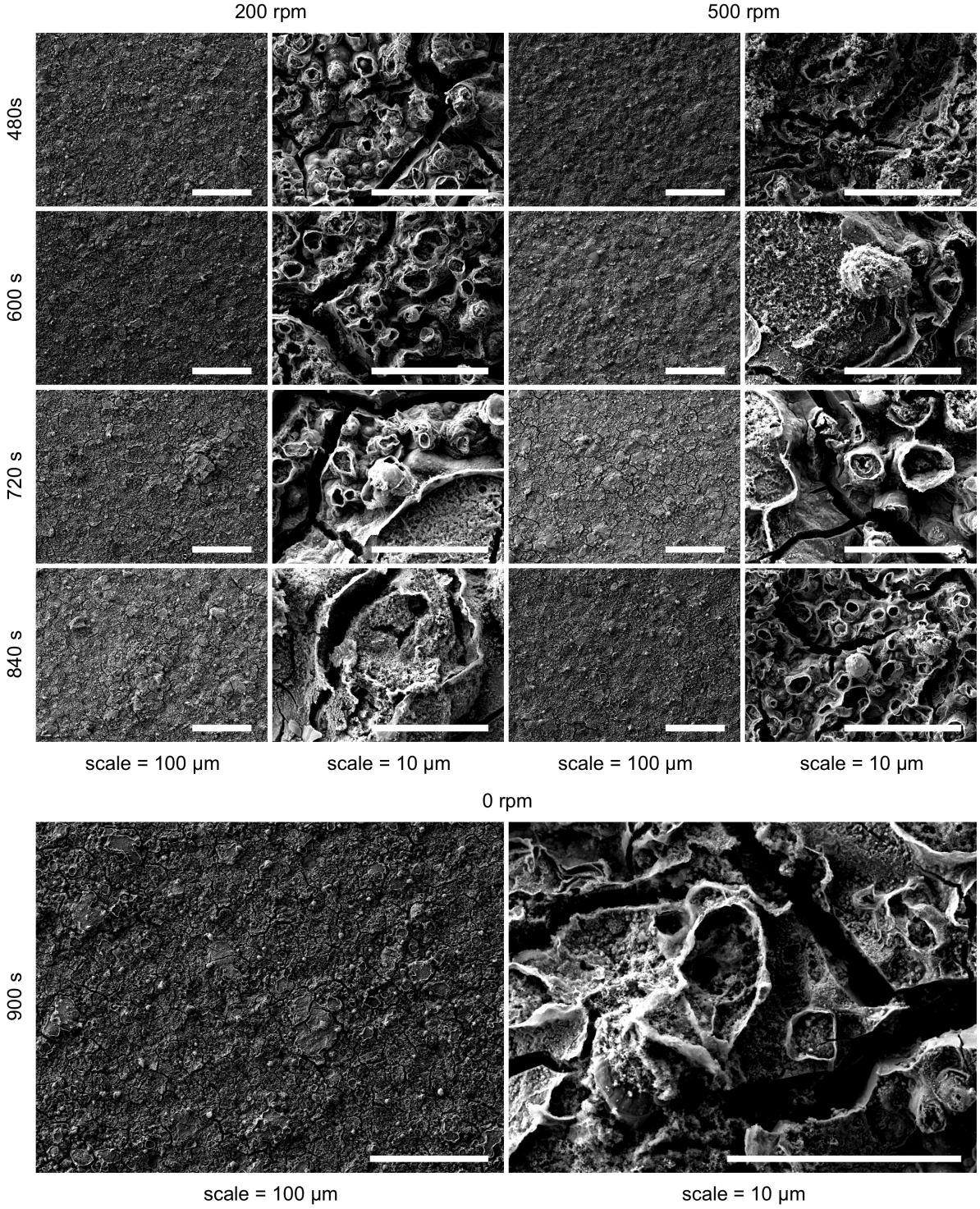

Figure 4.13: Scanning electron microscopy images of samples produced with stirring instead of pulsing. Given times are $t_{precoat}$. Stirring was applied until t_{total}= 900 s.

4.3.4. Influences of combined pulsing and stirring

Stirring and pulsing applied alone during coating deposition reduced the coating mass, as shown in section 4.3.1 and 4.3.2. Therefore, it was interesting to investigate, how the two effects may interact with each other. Stirring lead to higher flow that could dissolve more coating during t_{off}, but also transports calcium ions faster to the surface that are needed for coating and could therefore lead to higher mass deposition during t_{on}. The experiments revealed that combining stirring and pulsing led to lower coating masses than only pulsing without stirring (compare figure 4.14), thus dissolution of the coating was the dominating process. Scanning electron microscopy images in figure 4.15 showed typical crater-like structures that were smoothed by longer pulsing times (G, H, I compared to A, B, C and M, N, O to J, K, L), but not noticeable affected by stirring speed.

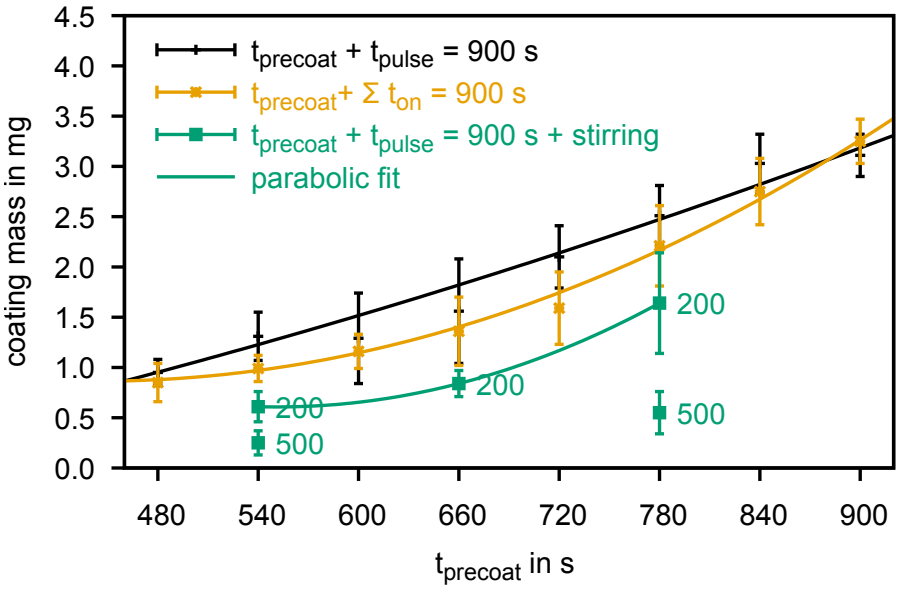

Figure 4.14: Additional stirring of the electrolyte during coating deposition further reduced the coating mass and higher stirring speeds led to lower coating masses. This is in accordance with figure 4.6. Thus, the effects of stirring and pulsing add up.

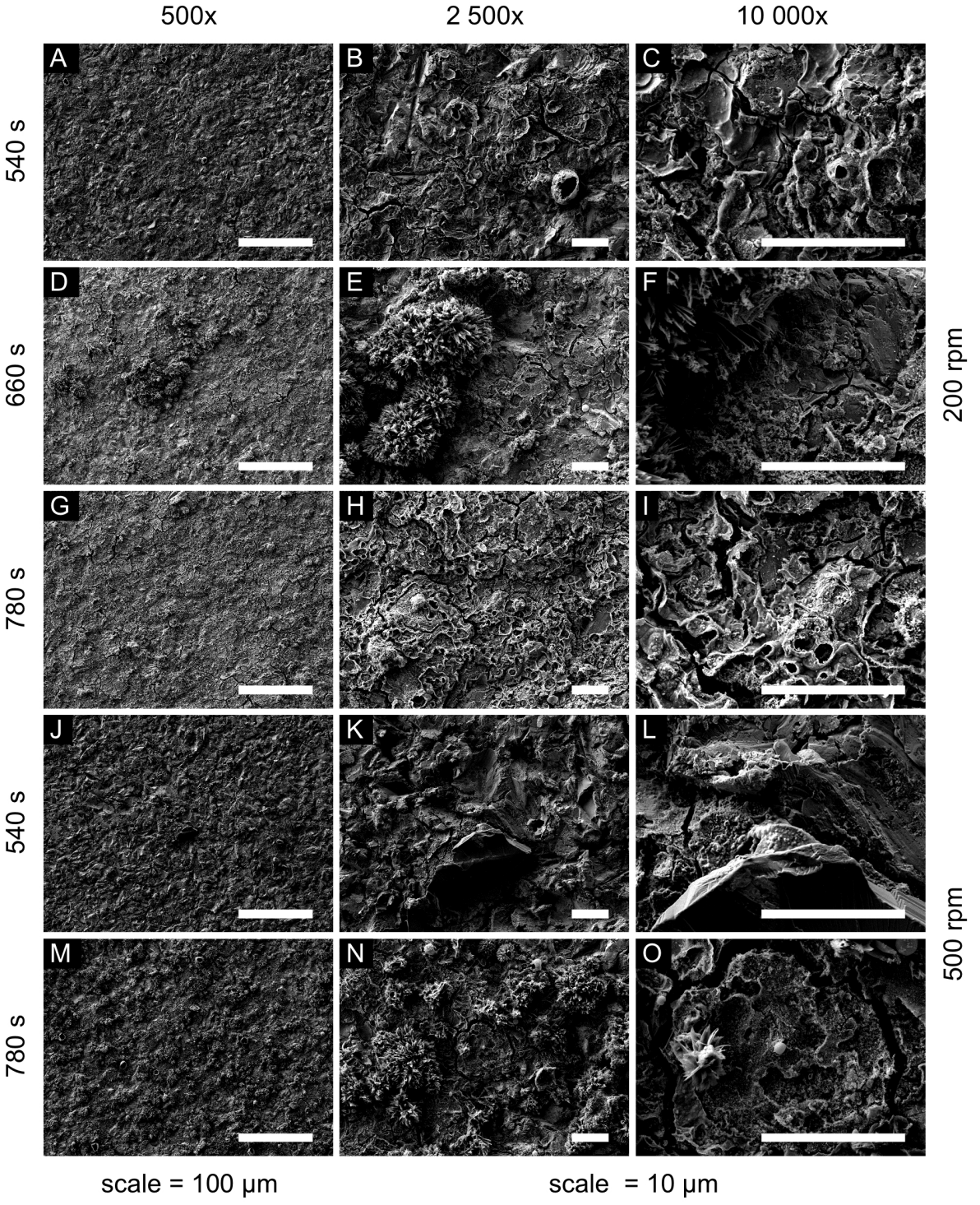

Figure 4.15: Scanning electron microscopy images of calcium hydroxide coatings produced with combined pulsing ($t_{precoat}$+t_{pulse}=900 s) and stirring. The time shown represents $t_{precoat}$. Typical crater-like structures are visible that were smoothed by longer pulsing times (G, H, I compared to A, B, C and M, N, O to J, K, L), but not noticeable affected by stirring speed.

4.3.5. Dissolution of calcium hydroxide coating

Dissolution of the calcium hydroxide coating was investigated without and with stirring at 500 rpm for 1 s, 5 s, 10 s, 20 s and 40 s dissolution time, to further investigate the dissolution rate and the influence on surface morphology.

Longer dissolution times led to higher dissolved masses and even more coating dissolved when stirring was applied (compare figure 4.16). During the first second (0.59±0.12) mg dissolved without stirring, which was (16±1) % of the coating and about 36 % of the mass dissolved after 40 s ((1.60±0.11) mg) (compare figure 4.16 A). Consequently, dissolution was fastest during the first second. The remaining mass after 40 s was (16±5) % when stirring was applied and (43±4) % without stirring (compare figure 4.16 B).

When stirring with 500 rpm was applied, the coating mass dissolved faster than without stirring. With stirring (0.75±0.06) mg dissolved during the first second and after 40 s (2.90±0.44) mg dissolved, which is nearly the whole coating, only (16±5) % remained. Interestingly, stirring during dissolution also resulted in flower-like structures as did stirring during deposition (compare figures 4.8 and 4.17 B). These flower-like structures seemed to be the most robust morphology produced during deposition.

From the results of the pulsing experiments (see section 4.3.2), the assumption arose that at the beginning of dissolution, finest structures on the surface are present which provide a large surface area for the electrolyte to attack and dissolve these structures. However, this assumption is not supported by these experiments. SEM-images (compare figure 4.17) showed no differences between as-produced coatings (0 s) and coatings after dissolution without stirring for all time points. Therefore, dissolution most likely took place within the structure and may have led to a higher porosity, which is not visible in the images in figure 4.17 A. Stirring with 500 rpm changed the surface morphology, however, crater-like structures seemed not to be smoothened, but flower-like structures were revealed. It is unlikely, that flower-like structures grew during dissolution with stirring but originated from the coating process and presented the most robust structure against dissolution. Accordingly, the circumstances during t_{off} of the pulsing cycle were different than during pure dissolution. One difference is that during t_{off} hydrogen bubbles were present at the surface and predominantly in the crater-like structures. The electrolyte could only attack the rim of the crater and not the bottom to dissolve the calcium hydroxide coating. A dissolved rim resulted in a smoother structure as seen in figure 4.11. In contrast, pure dissolution experiments showed unchanged crater-like structures, even after 40 s dissolution. During these experiments, no protecting hydrogen bubbles were present. Therefore, the dissolution took place evenly at the rim and the bottom of the crater-like structures, not changing the morphology.

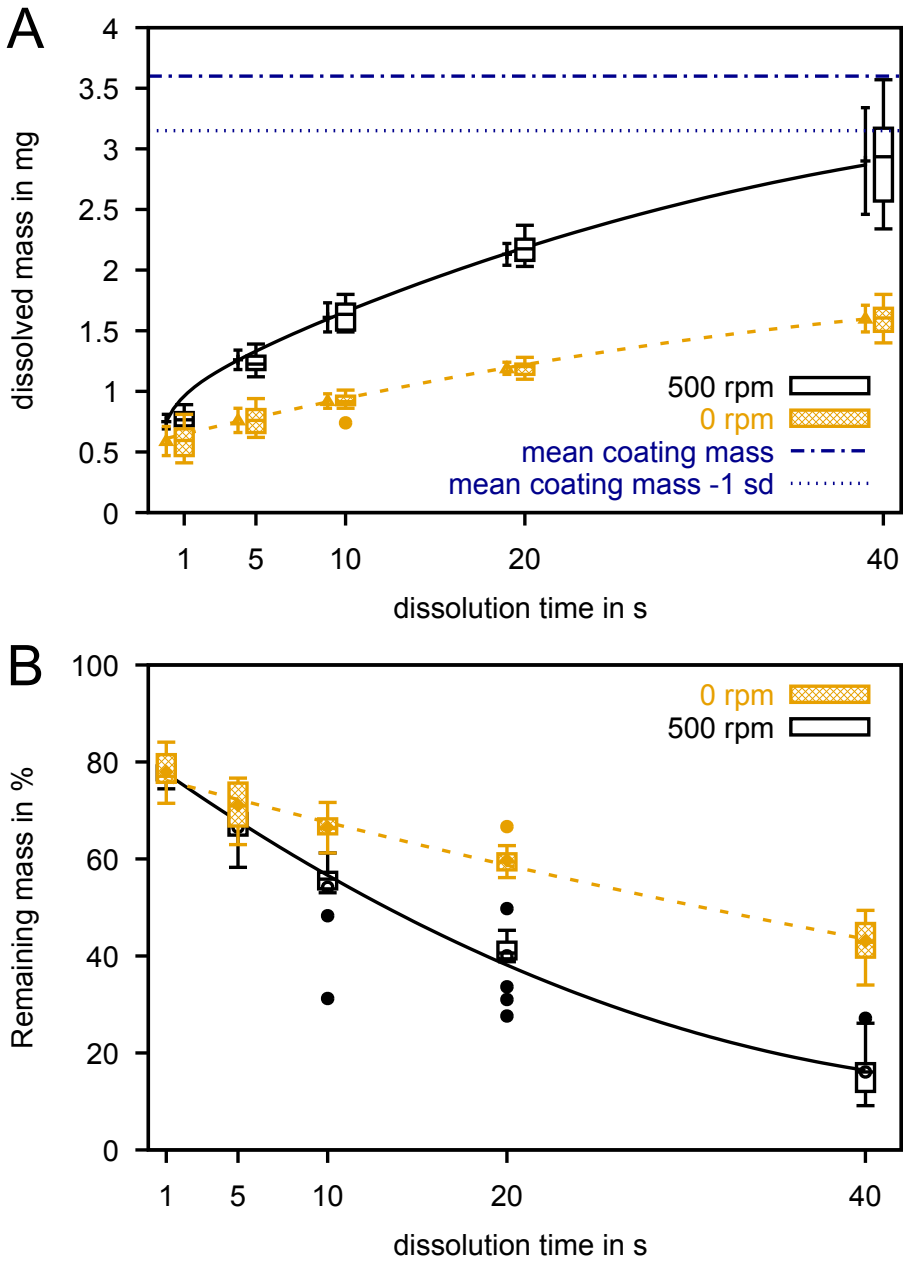

Figure 4.16: Dissolution of calcium hydroxide coatings on titanium samples fixed to the 4-fold sample holder with and without stirring. A) Boxplot, mean and −1 standard deviation (sd) of dissolved coating masses are displayed. Stirring with 500 rpm resulted in significantly higher dissolution of coating mass. B) Percent of remaining masses. After 40 s without stirring the coating mass is reduced to (42±4) % but goes down to only (16±5) % with stirring. Fits are displayed to visualize the trend but are not meant to explain the physical background.

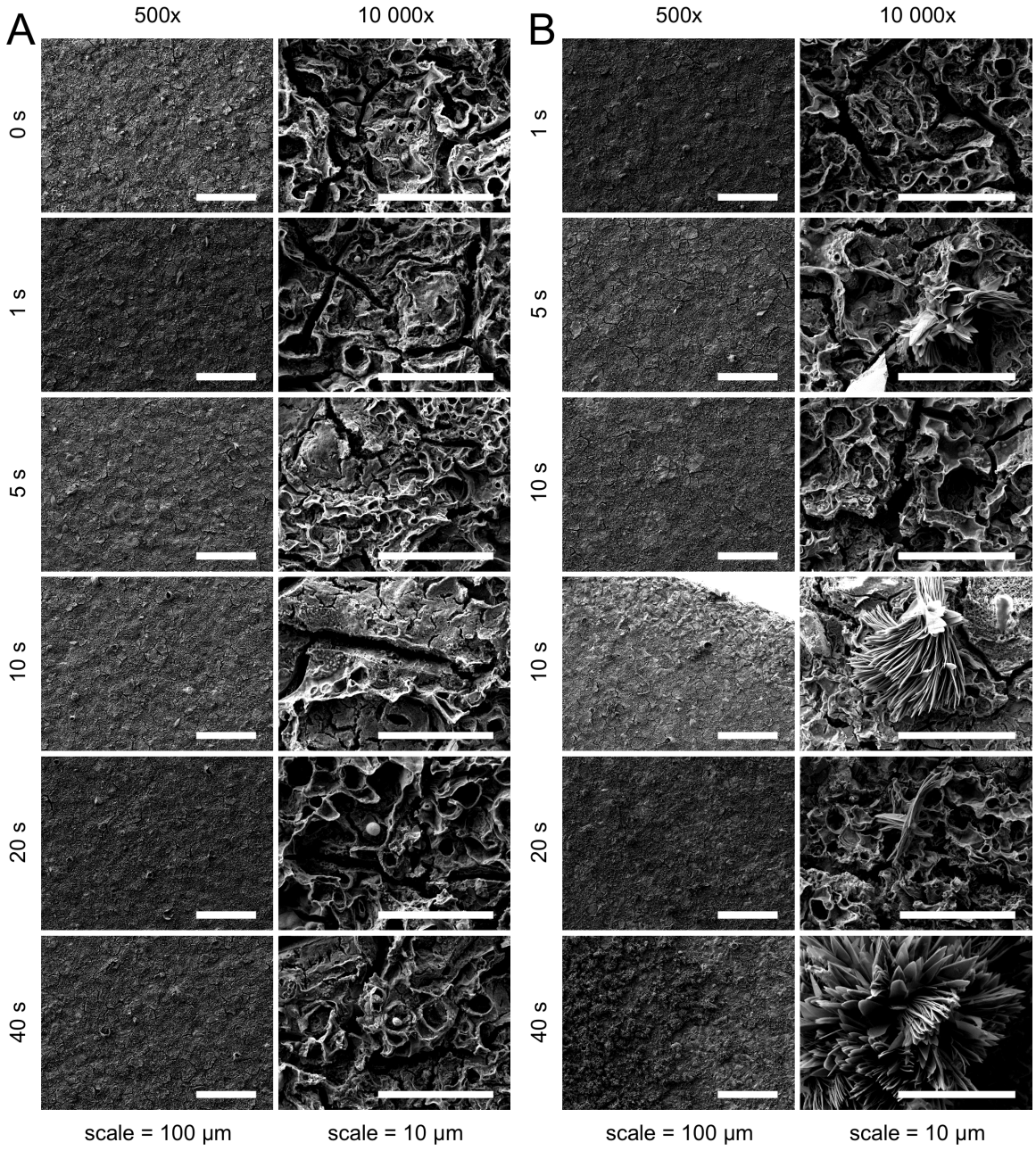

Figure 4.17: Scanning electron microscopy images of the coatings after dissolution A) without stirring and B) stirring at 500 rpm. A) For all dissolution times there are no noticeable changes in the surface morphology. B) Dissolution for up to 10 s does not influence the surface morphology, but longer dissolution times reveal more and more flower-like structures. Most likely the crater-like structures were dissolved leaving behind the flower-like ones.

4.3.6. Relationship of pulsing, stirring and dissolution

All experiments described above have in common, that they altered the coating mass and the surface morphology of the coating. Applying stirring during the whole deposition of calcium hydroxide led to lower coating masses and changed the surface morphology to flower-like structures. Pulsing with different time-patterns revealed that coating mass was dissolved during pulsing and led to smoother surfaces. When stirring was applied instead of pulsing, the coating mass was lowered, but the surface morphology stayed unchanged. A combination of pulsing and stirring confirmed the results from the isolated experiments, because both had an influence on coating mass and surface morphology. Flower-like structures where less present than with stirring alone.

The coating mass is relevant because it determines how much antibacterial agent is present. More calcium hydroxide will be able to reduce the pH to a lower value or keep the pH longer at a low value, but the surface morphology of the thinner coatings might be favorable. Surface morphology has a big influence on bacterial and cell response. Pegg et al. [18] separated the chemistry from the morphology of ECAD-HA with a thin gold layer and investigated the response of human osteoblast-like cells (human osteosarcoma TE-85). The surface roughness and morphology of uncoated and gold coated ECAD-HA was measured with optical profilometry and SEM and showed both needle-like structures with no difference in roughness. Moreover, X-ray photoelectron spectroscopy of the two surfaces ensured full coating with gold, thus the separation of chemistry and morphology could be assumed. Cell proliferation and markers of osteoblastic phenotype were significantly higher on gold coated and uncoated ECAD-HA than on the uncoated and gold coated Thermanox control that is optimized for cell adhesion and growth. Since gold coated and uncoated ECAD-HA have the same morphology, this effect can be attributed to the morphology and not the chemistry of ECAD-HA. However, the chemistry had an effect because the average results for uncoated ECAD-HA were higher compared to the gold coated ECAD-HA, but not statistically significant.

How size and shape of material entering the body influence the foreign body immune response was investigated by Veiseh et al. [317]. A large variety of tests and an *in vivo* non-human primate animal models revealed less fibrotic tissue around sphere sized implants larger than 1.5 mm than on cylinders or smaller spheres. Interestingly, this was independent from the used materials alginate, stainless steel, glass, polycaprolactone and polystyrene. Hence, size and shape and not other material properties like stiffness seemed more important for biocompatibility. Of course, implants cannot be sphere shaped, but the study clearly showed the importance of shape and size. Shape and size of the deposited calcium hydroxide coatings could be altered by pulsing, stirring or a combination and may enable further tuning of their biocompatibility.

4.4. Further modifications with metal ions

This section was already published in [297]. Reprinted with permission from Springer Nature, Copyright © 2018

Silver and copper ions were added to enhance the antibacterial effect of the calcium hydroxide coatings. The addition of silver and copper ions to the electrolyte did not inhibit the precipitation of $Ca(OH)_2$. $Ca(OH)_2$ was still the main phase of X-ray diffraction patterns of Ag-$Ca(OH)_2$ and Cu-$Ca(OH)_2$ on the titanium background (see figure 4.18). While the positions of the peaks stayed the same, the height was affected by the addition of metal ions. However, no other calcium phosphate phases occurred. Diffraction peaks corresponding to corundum were found in most samples and resulted from the incorporation of Al_2O_3 into the titanium surface during sandblasting pre-treatment. The addition of Ag^+ lead to a significantly decreased $Ca(OH)_2$-peak at $2\theta = 18°$, while at the same time the coating mass increased by a factor of about 4 ($(5.22\pm0.43)\,mg\,cm^{-2}$, compared to $(1.34\pm0.03)\,mg\,cm^{-2}$ for pure $Ca(OH)_2$). Additional peaks could be found at 38.2° and 44.5° and indicated the deposition of metallic silver. However, no peaks for metallic copper occurred in Cu-$Ca(OH)_2$ and intensities of portlandite peaks and coating masses were nearly the same as for undoped coatings. Copper may still have precipitated as metallic copper but was not detected by XRD due to the detection limit of $\approx$1 %. Another possibility is an amorphous copper phosphate that is also not detectable by XRD.

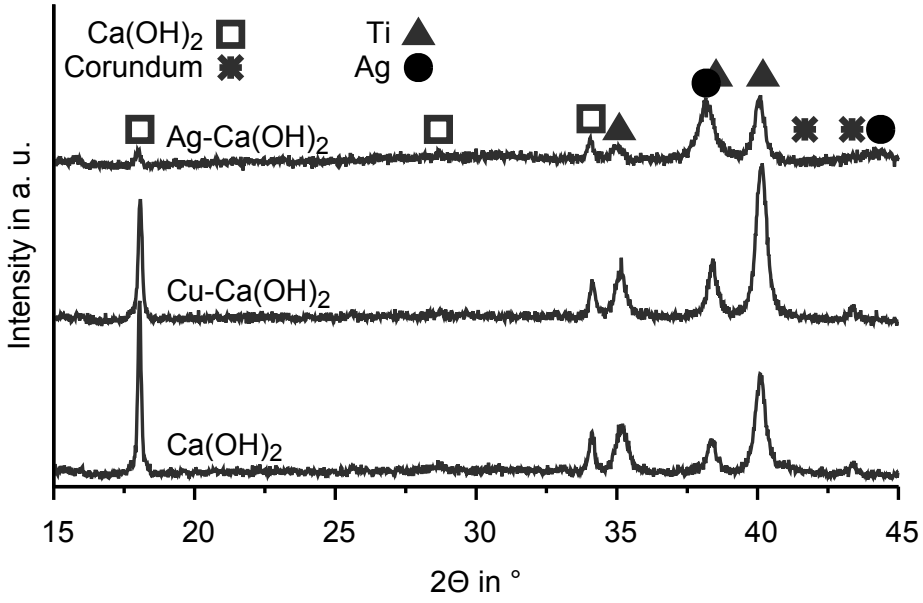

Figure 4.18: "X-ray diffraction pattern of Ag-$Ca(OH)_2$ and Cu-$Ca(OH)_2$ coatings on titanium. The main product can be identified as $Ca(OH)_2$. Metal incorporation only changed the crystallinity." Reprinted from [297] with permission from Springer Nature, Copyright © 2018.

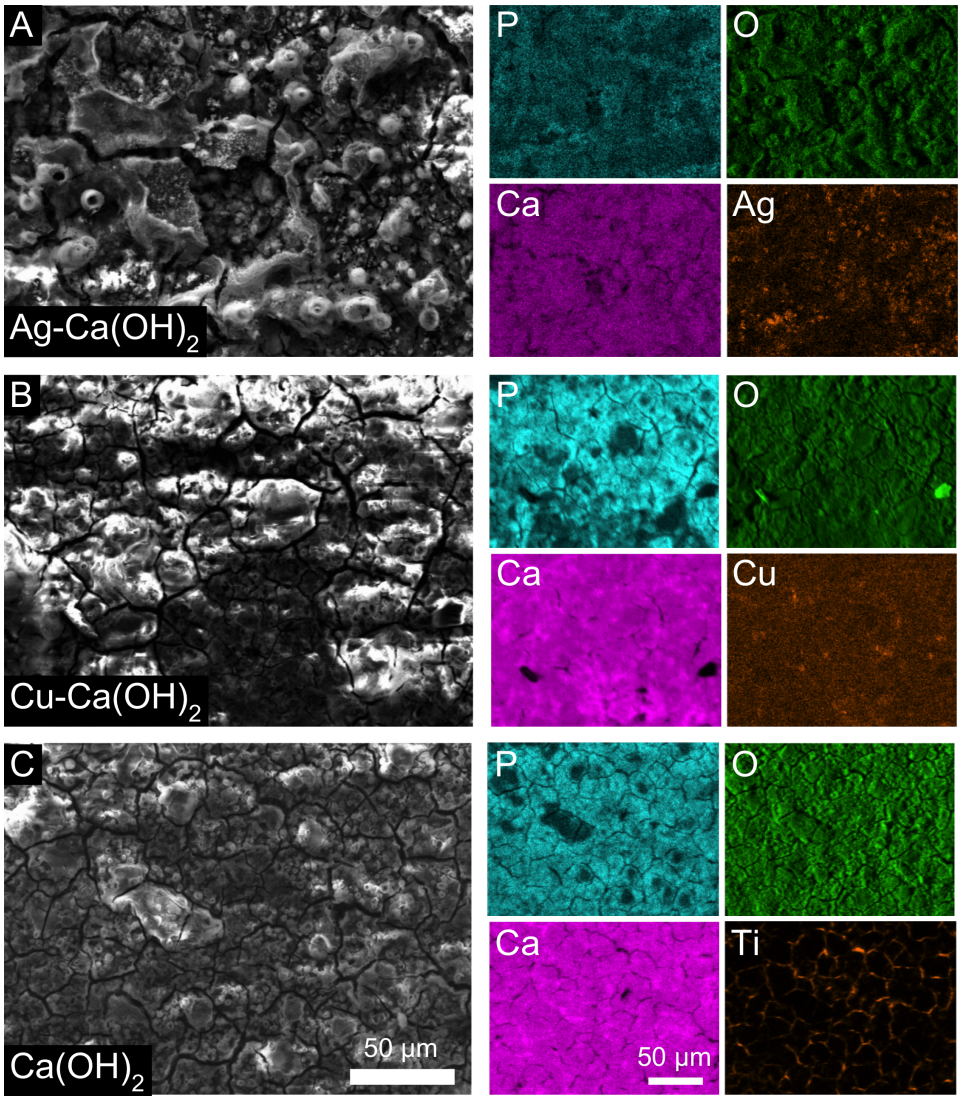

Figure 4.19: "Scanning electron microscope picture and EDS mapping of Ag-$Ca(OH)_2$ (A), Cu-$Ca(OH)_2$ (B) and $Ca(OH)_2$ (C). Silver and copper are homogeneously distributed within the coating surface." Reprinted from [297] with permission from Springer Nature, Copyright © 2018.

Table 4.2: Ion content of the coatings measured by ICP-MS. Reprinted from [297] with permission from Springer Nature, Copyright © 2018.

Sample	metal content in µg	metal content in wt. %	coating mass in mg	Ca content in µg	metal/Ca in mol. %
Cu-$Ca(OH)_2$	17.7±2.6	0.28±0.06	6.3±0.3	2060±55	0.6
Ag-$Ca(OH)_2$	722 ±159	4.4 ±0.1	16.5±2.9	4500±1300	6

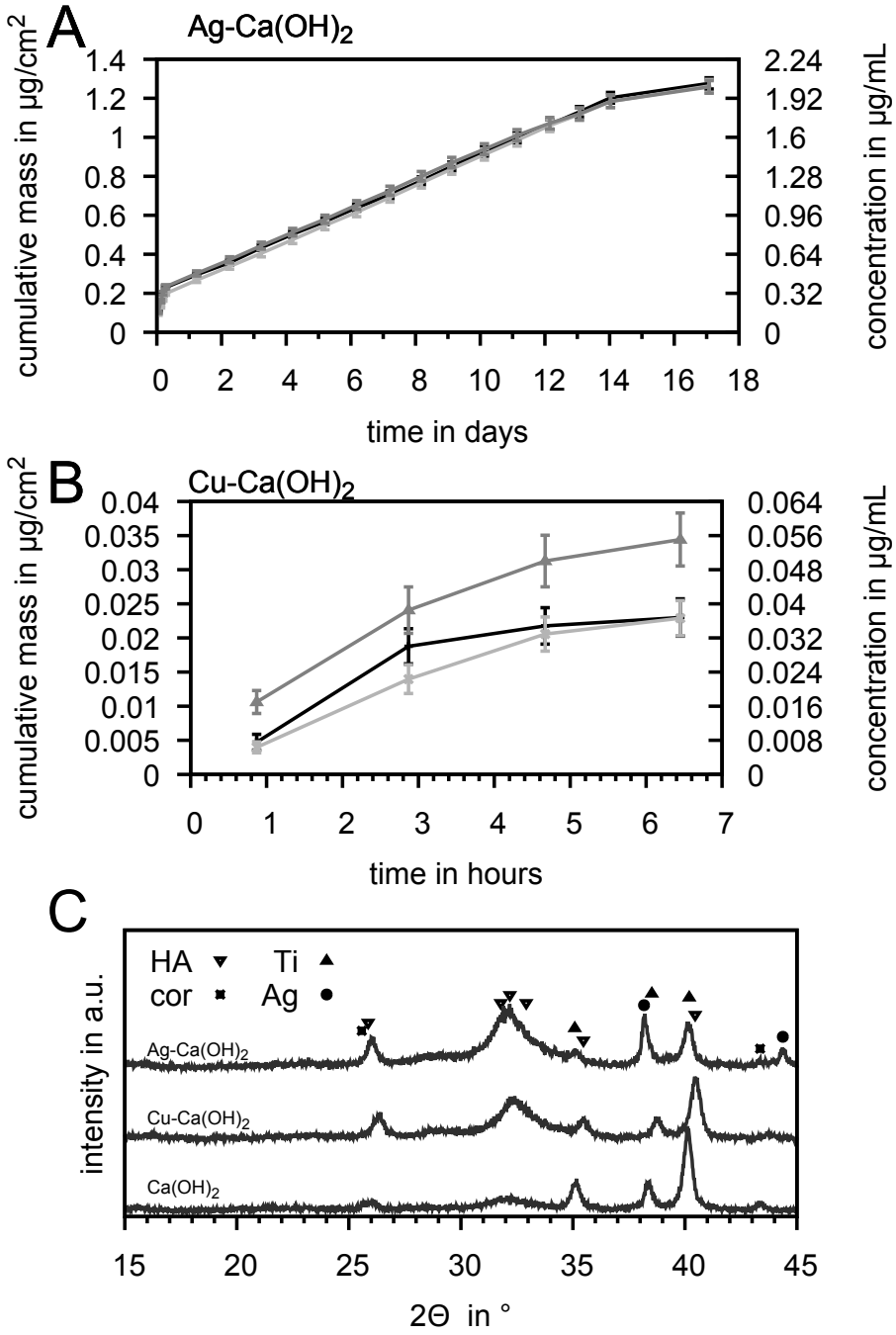

Figure 4.20: "Release study of Ag-$Ca(OH)_2$ and Cu-$Ca(OH)_2$ in simulated body fluid. Silver was released constantly over 17 days (A), copper only during the first hours (B). Both coatings were converted to hydroxyapatite after 17 days in the same way as pure $Ca(OH)_2$ (C)." cor stands for corundum that was incorporated during sandblasting. Reprinted and adapted from [297] with permission from Springer Nature, Copyright © 2018.

Metal ion addition obviously changed the surface morphology of the coatings. Investigation with SEM revealed rounder and more volcano-like structures for Ag-$Ca(OH)_2$ coatings and smoother structures for pure $Ca(OH)_2$ and Cu-$Ca(OH)_2$ coatings. The titanium substrate was detected for all modifications where cracks occurred in the coatings (see figure 4.19 C). Additionally, aluminum and oxygen were found originating from Al_2O_3 that was incorporated during sandblasting. On that spots no other elements were present, because the non-conductive Al_2O_3 hindered the deposition of coatings with ECAD. Silver contributed (7.7±2.6) wt % to the coating mass and copper (0.2±0.1) wt % and both were equally distributed all over the coating (see figure 4.19). These findings were well in accordance with the ICP-MS measurements where (4.4±1.0) wt % silver and (0.28±0.06) wt % copper were recorded (see table 4.2).

This is an about 40-fold metal content in Ag-$Ca(OH)_2$ compared to Cu-$Ca(OH)_2$, moreover the coating mass of Ag-$Ca(OH)_2$ was more than double. This is surprising because the applied current density was lower. The metal-ion/Ca molar ratio of the coatings was 6 % in Ag-$Ca(OH)_2$ and only 0.6 % in Cu-$Ca(OH)_2$, which is half of the 1 % of the electrolyte. Thus, silver deposited in higher amounts and also caused a higher deposition of $Ca(OH)_2$ than copper. Obviously, the silver deposition was favored to copper.

In terms of antibacterial activity, the release of metal ions is more important than the mere metal content, because only ions are active against bacteria [318, 319]. Silver was practically constantly released into SBF solution over 14 days with an average release of (1.11±0.09) µg per day and a maximum of (1.60±0.13) µg after the first hour (see figure 4.20A). In total (20±1) µg (0.07 µg cm^{-2}) of silver were released after 17 days which is about 2.8 % of the silver in the coating. This led to a silver concentration in the release medium of 110 ppb that was well above the minimal effective dose of 0.1 ppb [320] and lead to the antibacterial effect visible in figure 4.27. Since only 2.8 % of silver was released, a longer release seems possible. Copper behaved differently because the release of $Cu_2{}^+$ could only be measured for the first 7 h. During the first hour (0.01±0.05) µg was released, but after that only (0.18±0.15) µg. The total amount of released copper was (0.43±0.11) µg (0.027 µg cm^{-2}). This is a ratio of 2.4 % of the incorporated copper, which is, however, similar to the ratio of released silver. Thus, the lower total copper amount most likely led to the lower release. Another possibility is the formation of Cu(II) phosphates with solubility products of $Cu_3(PO_4)_2$ of 1.40×10^{-37} $mol^5\,L^{-5}$ compared to Ag_3PO_4 with 8.89×10^{-17} $mol^4\,L^{-4}$ [321].

After 17 days in SBF X-ray diffraction patterns of Ag-$Ca(OH)_2$ and Cu-$Ca(OH)_2$ indicated the transformation of $Ca(OH)_2$ into HA (see figure 4.20C). Thus, the transformation (see 4.5) was not affected by the metal ions.

$$5\,Ca(OH)_2 + 3\,HPO_4{}^{2-} \longrightarrow Ca_5(PO_4)_3OH + 3\,H_2O + 6\,OH^- \tag{4.5}$$

This is well in accordance with the transformation of $Ca(OH)_2$ coatings without metal into HA from a previous study [30].

4.5. Coating thickness

The thickness of the calcium hydroxide coatings was evaluated after cutting a rectangle hole with a focused ion beam (see figure 4.21). To distinguish titanium substrate and coating an EDS was recorded. Two samples were measured each 9 times at equal lateral distribution and the thickness was determined to be (3.54±0.81) µm and (3.16±0.50) µm. The thickest and thinnest parts were 4.82 µm and 1.49 µm as well as 3.77 µm and 1.61 µm, respectively.

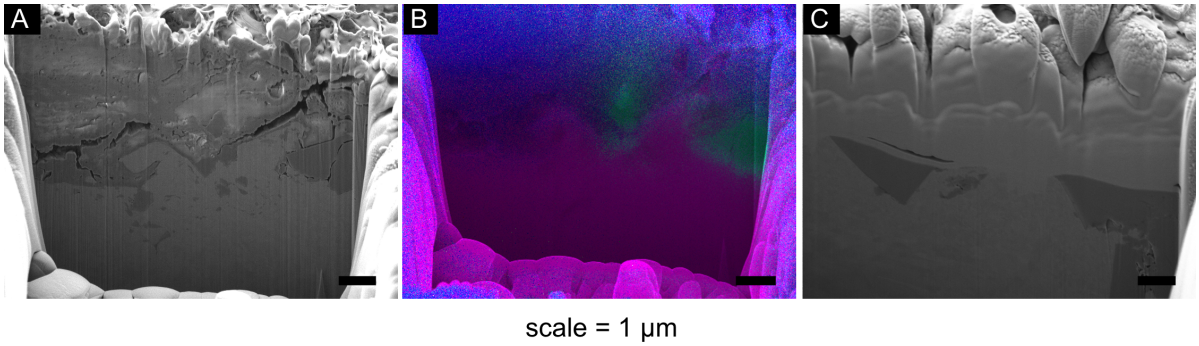

Figure 4.21: A) and C) Scanning electron microscopy images of focused ion beam cuts. The coating thickness was determined to be A)(3.54±0.81) µm and C) (3.16±0.50) µm. Image B shows energy dispersive X-ray spectroscopy where the coating (blue), the titanium substrate (pink) and the Al_2O_3 grains (green) can be distinguished, which is important for correct thickness determination.

The thickness is well in accordance with thicknesses of 5 µm found for ECAD-HA [31]. The lower values compared to plasma-spraying are thought to prevent delamination.

4.6. Adhesion

An important feature of coatings is their adhesion on the substrate, as it determines the resistance of the coating to mechanical stresses. Since adhesion tests were not yet performed on calcium hydroxide coatings, standard tests for coating adhesion were transferred to these coatings. Therefore, standard parameters were chosen to coat calcium hydroxide coatings. As standard tests tape and scratch test were evaluated and also a method using an ultrasonic bath was investigated.

For evaluation of the tape test (compare ASTM D3359), a piece of Tesa©-Tape was pressed onto the coating (compare figure 4.22 A) and carefully removed by hand. On the titanium a dense coating was preserved (figure 4.22 B) and only the top layer of the coating could be found on the tape (figure 4.22 C). This indicated that the cohesion within the coating was lower than its adhesion to the titanium surface. A second Tesa-tape was applied and again the coating was not removed from the substrate, but only got a little thinner (figure 4.22 D), as the top layer stuck to the tape (figure 4.22 E). Thus, tape-test was unsuitable for testing the

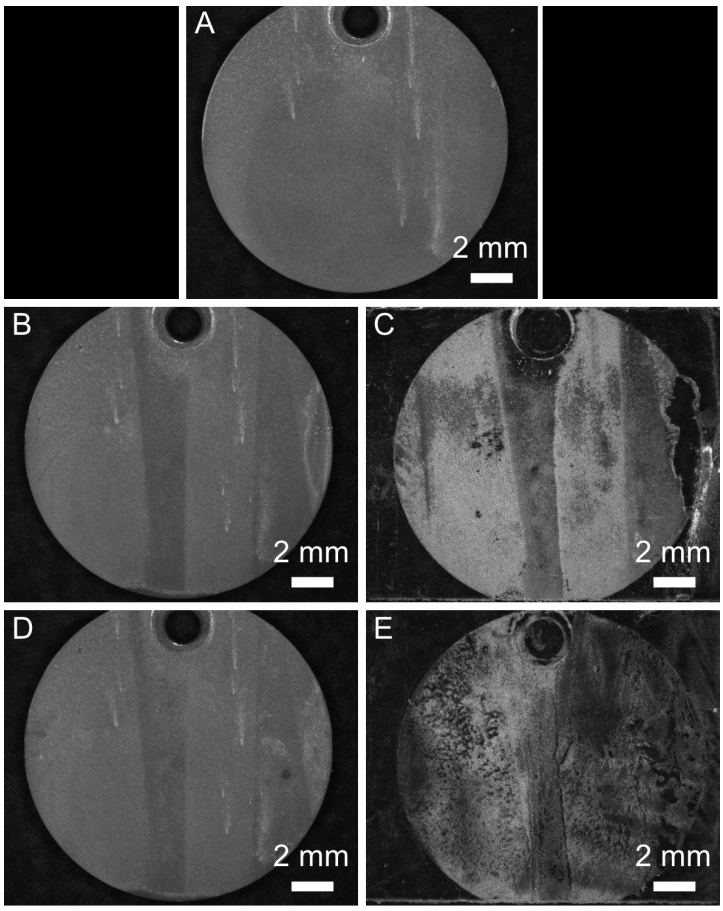

Figure 4.22: A) Coating as deposited before tape test, B) coating after first tape test, C) tape of the first test, D) coating after second tape test, E) tape of the second test.

adhesion of the investigated calcium hydroxide coatings but revealed that the adhesion of the coating to the titanium surface is higher than the cohesion within the coating.

Another test for adhesion of the coating was to use an ultrasonic bath and to measure how long the coating withstands removal. Ultrasonic baths can apply an about isotropic mechanical stress to the coating that is not dependent on glues. The acoustic waves penetrate the whole sample and can agitate the coating and the interface directly. This method is only semi-quantitative, as no adhesion force can be measured or calculated. Moreover, the force attacking the interface is dependent on the geometry and the power of the ultrasonic bath as well as the placement of the samples and the amount of water filled into the bath. For samples where the coating is clearly visible and can be distinguished from the titanium substrate photographs can be taken. One big advantage of this method is that it can be applied to different shapes and rough surfaces, because the acoustic waves are not limited to a connection as glues and tapes are. Ultrasound can be applied in different ways. Either with a frequency sweep and differences in amplitude [322] or different amplitudes at fixed frequency [323]. Another possibility are unchanged frequency and amplitude, where the time the coating

withstands removal is a comparable value for adhesion [324], as done here.

First measurements were done comparing calcium hydroxide coatings on titanium disks that were either blasted with Korox 110 (Al_2O_3) or used as manufactured and then coated. Homogeneous coatings could be achieved on both surfaces (compare figure 4.23 A and G). The

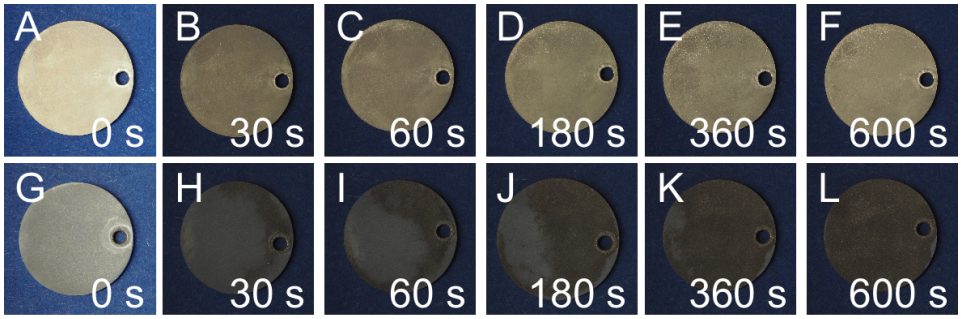

Figure 4.23: Differently pretreated titanium disks coated with calcium hydroxide after ultrasonication in ultrapure water for the given times. A-F: machined, G-L: Ti sandblasted with Korox 110.

coating was homogeneous and could be seen as grayer regions that turn shinier with time going by (figure 4.23 B-F). But the visible differences before (figure 4.23 A) and after ultrasonication (figure 4.23 B-F) were not big enough for a meaningful evaluation of the as-manufactured samples. Even though the ultrasonic bath seems the only possibility concerning mechanical stress, the evaluation is difficult and depends strongly on the reflection of the surface during photography. For future investigations EDS suggests itself to clearly determine residual coating. For Korox-pretreated samples a removal of the coating can clearly be seen in pictures G-L in figure 4.23. The coating is more and more removed during the ultrasonic treatment, is hardly visible after 360 s and completely removed after 600 s. Hence, a calcium hydroxide coating on Korox 110 pretreated surfaces can withstand at least 360 s ultrasonication.

Scratch testing is a standardized method and is often used to test the adhesion of bioceramic coatings [325]. As a standardized method scratch testing was performed and the scratches evaluated with SEM and EDS. Scanning electron microscopy of all samples up to a load of 1.0 kg showed a surface crazed with cracks, indicating a layer of calcium hydroxide. In addition, EDS detected calcium within the scratch supporting the assumption of remaining calcium hydroxide (compare figure 4.24). With increasing mass load more calcium hydroxide coating was scratched from the titanium substrate. Until 1.0 kg the scratches were clearly visible in the coating but have fewer protruding parts with increasing load. For 1.5 kg and 2 kg hardly any cracks could be found. The crack on the calcium hydroxide coated sample after 2 kg scratch test were smaller and all nearly orthogonal to the moving direction of the Rockwell indenter.

To investigate the behavior of the titanium substrate, uncoated titanium was tested as well. After 2 kg scratch test it showed orthogonal cracks and other tribological phenomena. Deep scratches parallel to the testing direction occurred from abrasion and the orthogonal cracks

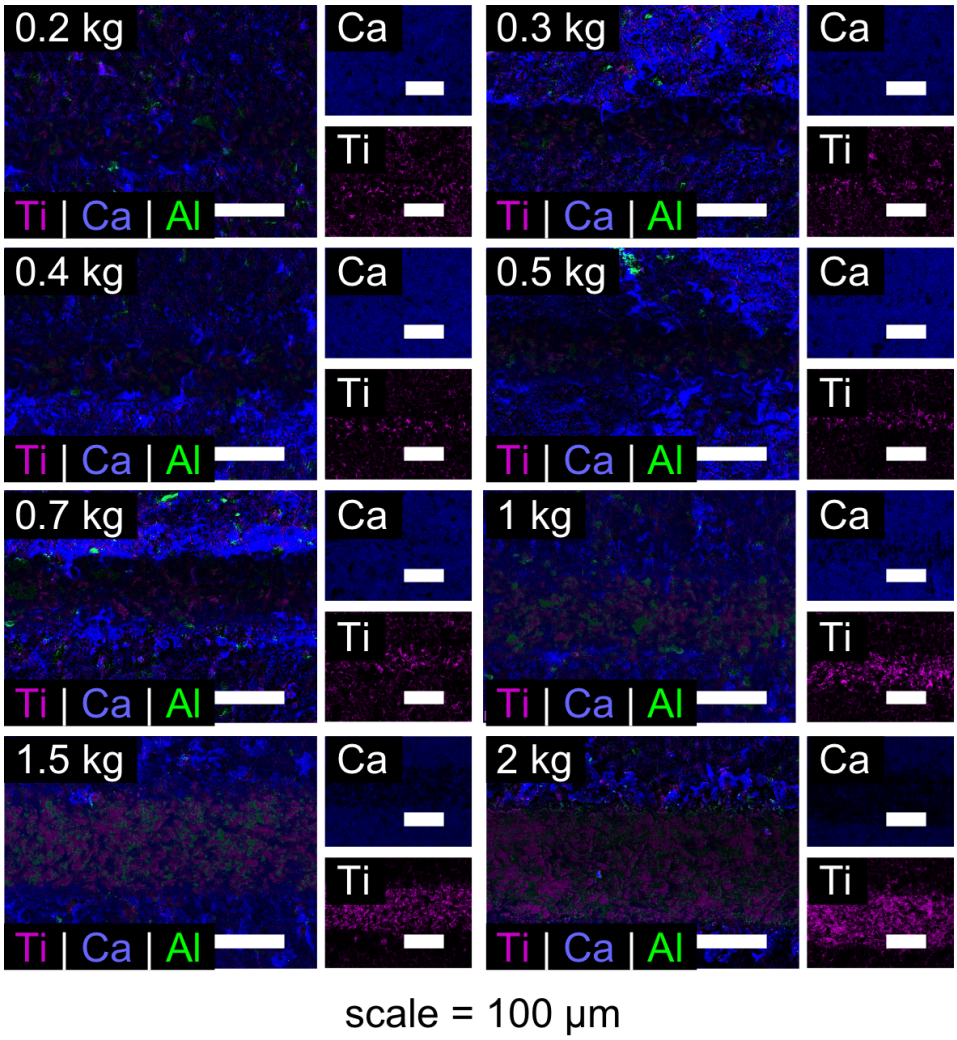

Figure 4.24: Energy dispersive X-ray spectroscopy measurements of scratch tests with loads between 0.2 kg and 2 kg. Overlaid images and separate images of calcium (Ca) and titanium (Ti) are given. A scratch in the calcium hydroxide coating is visible for all loadings (overlaid images), but noticeable higher titanium backgrounds were only visible from 0.4 kg. Starting from a load of 1 kg black spots with no remaining calcium appear in the scratch in the calcium image, thus calcium is noticeable removed. A load of 2 kg completely stripped the coating from the titanium disk.

most likely from surface fatigue or a smearing of titanium [326]. These observations were supported by EDS measurements and are shown in figure 4.25.

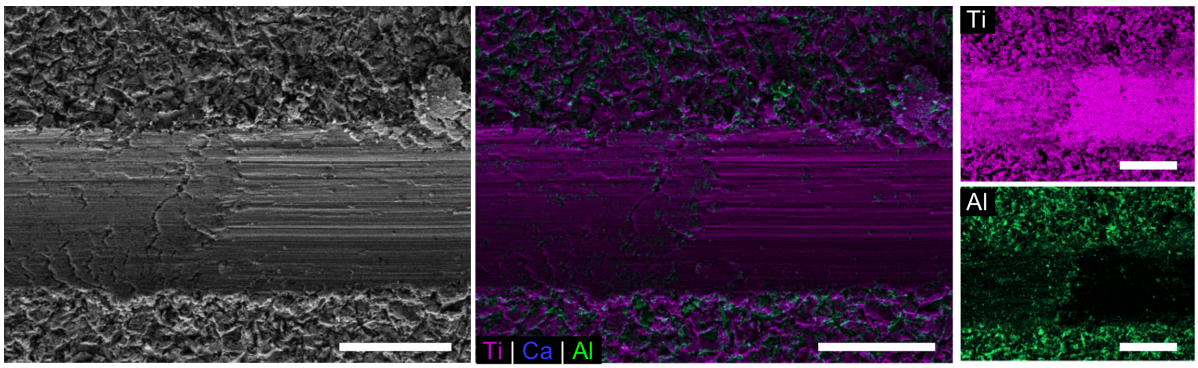

Figure 4.25: Scanning electron microscopy images and energy dispersive X-ray spectroscopy measurements on uncoated titanium after scratch test with a load of 2 kg. Deep scratches parallel to the testing direction occur from abrasion and the orthogonal cracks most likely from surface fatigue or a smearing of titanium.

With increasing load, the signal of calcium on the surface decreased and, on the contrary, the signals for titanium and aluminum increased. Aluminum signals result from implanted aluminum oxide from the Korox sandblasting and stand for the substrate. Considering the about 1 µm depth EDS signals are occurring from, it is obvious that titanium signals can be detected if the coating thickness is about or less than 1 µm. Therefore, the missing of a calcium signal is more reliable to detect the complete stripping of the calcium hydroxide coating. Thus, the almost missing calcium signal in the scratch at 1.5 kg and 2.0 kg (figure 4.24) is a sign for the complete stripping of the calcium hydroxide coating. In conclusion calcium hydroxide coatings on Korox 50 sandblasted titanium could withstand complete stripping until a load of 1.0 kg during scratch test.

Determining the complete removal of the coating is not easy for bioceramic coatings and done differently [325, 327], but mostly with light microscopy. Here the use of EDS is considered as a big advantage because a clear distinction between coating and substrate is possible. Comparison with measurements done on hard coatings is also difficult because the endpoint is defined by a visible and/or audible crack, which is more precise [153, 328]. Nijhuis et al. [179] stated, that comparison of adhesion of different coatings is quite difficult, because the values strongly depend on experimental conditions, especially for scratch test. Therefore, values found in literature ranged over two orders of magnitude and make further comparisons meaningless.

4.7. Biological properties

Calcium hydroxide is known as antibacterial agent and used widely in dentistry for root channel infections. When used as coating material, it is important to determine the antibacterial potential of this type of application. Tests were performed with the most common bacteria in implant infections: *S. aureus* and *S. epidermidis*.

4.7.1. Agar diffusion test

Agar diffusion test is a standard test for antibacterial properties of different materials. Neither the calcium hydroxide coatings nor the uncoated titanium controls showed an inhibition zone around the sample (compare figure 4.26). Therefore, the coated calcium hydroxide was not able to lower the pH-value in the vicinity and consequently did not exhibit a long-distance effect against *S. aureus*.

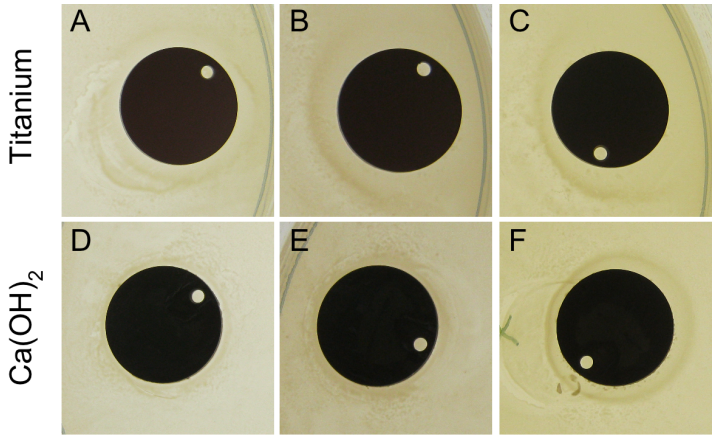

Figure 4.26: Agar diffusion test of calcium hydroxide coatings and titanium controls. No inhibition zones are visible and there are no differences between titanium and calcium hydroxide coatings.

Studies about agar diffusion test on calcium hydroxide with different bacteria were summarized in [276]. They also showed no inhibition zone and the hypothesis arouse, that the buffer substances of the medium in the agar plates were the reason. In contrast, NaOH and KOH were able to kill bacteria and create an inhibition zone. Since OH^- from NaOH, KOH or $Ca(OH)_2$ should show no difference in diffusion, the main reason could be the different solubility. NaOH and KOH have a higher solubility ($1090\,g\,L^{-1}$ [329] and $1130\,g\,L^{-1}$ [330], respectively) than $Ca(OH_2)$ ($1.7\,g\,L^{-1}$ [331]) and can release more OH^-. However, this advantage concerning antibacterial activity comes with the drawback of cytotoxicity of NaOH and KOH. In addition, the crystallinity of calcium hydroxide seemed to influence the antibacterial activity in the agar diffusion test [332]. A commercial calcium hydroxide/salicylate cement showed clear reflection peaks for $Ca(OH)_2$ in XRD while mechanically activated tetracalcium phosphate revealed no reflection peaks, despite up to 13 % calcium hydroxide that precipitated during setting. From

that the authors concluded an amorphous character and thus better solubility of the calcium hydroxide from mechanically activated tetracalcium phosphate, which in turn explains the better antibacterial results from the agar diffusion test [332]. Therefore, changing the surface morphology and crystallinity of calcium hydroxide with stirring or pulsing might be a chance to further tune the antibacterial properties if required. In addition, an altered surface pretreatment could lead to changed crystallinity as shown in section 4.2. Still, the effects on cytocompatibility and conversion to HA must be considered.

4.7.2. Bactericidity test

This section was already published in [297]. Reprinted with permission, Copyright © 2018, Springer Nature

A test that is more independent from the dissolution of $Ca(OH)_2$ is the WST-test, because it measures the activity of bacteria seeded on the coated samples. Here Ag-$Ca(OH)_2$ and Cu-$Ca(OH)_2$ were tested against *S. epidermidis* and $Ca(OH)_2$, sandblasted titanium and PS served as control (PS set to 100 % in figure 4.27). All coatings showed highly significantly lower bacterial activity than PS and titanium. The bacterial activity of $Ca(OH)_2$ was only about 40 % of PS, Ag-$Ca(OH)_2$ only 25 % and Cu-$Ca(OH)_2$ only 13 % (see figure 4.27). Hence, silver significantly increased the antibacterial potential of the coating and copper even showed a highly significant effect.

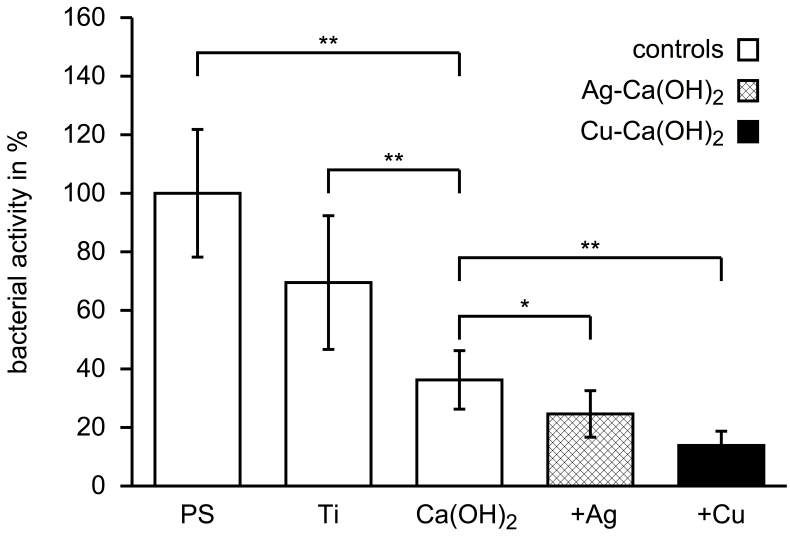

Figure 4.27: "Bacterial test with *Staphylococcus epidermidis* with polystyrene (PS) set as 100 %. All coatings containing $Ca(OH)_2$ showed a high-significantly (**, $p < 0.01$) lower bacterial activity than PS and titanium (Ti). The addition of silver significantly (*, $p < 0.05$) or copper high-significantly decreased the bacterial activity even further." Reprinted from [297] with permission from Springer Nature, Copyright © 2018.

$Ca(OH)_2$ coatings without metal ions could show antibacterial properties against *Staphylococ-*

cus epidermidis and *Klebsiella pneumonia* in a WST-1 test of a previous study [30]. Braissant et al. confirmed this for *Staphylococcus epidermidis* by means of a novel microcalorimetric assay and Kirby-Bauer assay [295]. The study at hand showed significant inhibitory effects against bacteria for pure $Ca(OH)_2$ coatings and increased effect for coatings with metal ion additions. Surprisingly, copper was most effective despite its low release rate. The copper mass released in the first hours ((0.10 ± 0.06) µg, $(0.16\pm0.09)\,\mu mol\,L^{-1}$) was lower than the lowest value found in literature for antibacterial activity ($55\,\mu mol\,L^{-1}$ against *Enterococcus hirae* [214]). Here a synergistic effect of the low pH caused by $Ca(OH)_2$ and the $Cu_2{}^+$ comes into mind.

4.7.3. Bacterial growth over time

S. aureus and *S. epidermidis* are common bacteria that cause most of the implant infections [80, 98, 101]. Therefore, the short time antibacterial efficacy of the calcium hydroxide coatings against these strains where evaluated. Different time points within 7 h catch bacteria in their different states. This is important, because in some states bacteria might be more susceptible to $Ca(OH)_2$. Thus, a bigger picture of the efficacy of $Ca(OH)_2$ is shown. Moreover, the number of cells is more meaningful than the activity that can depend among others on the single states, on the sample surface and on the environmental conditions. During animal studies at the Department for Functional Materials in Medicine and Dentistry University of Würzburg the bacterial count was determined with a sonification protocol. For comparability, the same protocol was used for these experiments. Sonication was used for removing the bacteria and plating on agar plates for the bacterial count.

After 1 h, 3 h, 5 h and 7 h for all dilutions and both germs no colonies were found on the agar plates belonging to the calcium hydroxide coated samples. After 3 h one agar plate of a titanium sample showed one colony at the 10^{-2}-dilution. Since at 10^{-1}-dilution no colonies grew, the colony was considered a contamination and not considered for further calculations. All in all, only the 0-dilutions showed some colonies on the agar-plates belonging to the titanium samples. It is commonly accepted that only plates with 20-30 up to 200-300 colonies should be considered for evaluation, because plates with less than 20-30 colonies are not statistically acceptable and the chance that a colony is formed from more than one bacterium is too high for more than 200-300 colonies on one plate [333, p. 98] and [334]. The titanium control samples after the different times of inoculation with bacteria should show at least the same number of bacteria that was seeded. On the plates seeded with 100 µL bacteria suspension these numbers should be counted: (*S. aureus*/ *S. epidermidis*) 40/3 for 0-dilution, 4/0 for 10^{-1}-dilution and 0/0 for 10^{-2}-dilution. Consequently, the numbers of colonies on the plates were too low to be statistically acceptable. This experiment showed that seeding with 445 CFU/mL did not yield high enough bacteria counts after 1 h, 3 h, 5 h and 7 h to have a statistically acceptable result. Few *S. aureus* colonies counted on the agar plates of the titanium controls after 7 h could be a weak sign for starting bacterial growth. Since no colonies were found on the agar plates of the

calcium hydroxide coatings, this may indicate an inhibiting effect of calcium hydroxide.

The experiment for 7 h, 9 h, 11 h and 13 h showed higher bacterial counts for 7 h and the following time points and made interpretation of the data possible (compare figure 4.28). For both germs, a clear difference between calcium hydroxide and the titanium control was detectable. On titanium surfaces *S. epidermidis* grew well and about doubled its number from $(2.0\pm0.6)\times10^4$ at 7 h to $(4\pm1)\times10^4$ at 13 h, but on the calcium hydroxide coating the number stayed approximately the same $(7\pm4)\times10^3$ at 7 h and $(8\pm3)\times10^3$ at 13 h. This difference showed that calcium hydroxide was promisingly antibacterial against *S. epidermidis*. The *S. aureus* count could also be reduced by calcium hydroxide from $(6\pm6)\times10^3$ to $(1.5\pm0.9)\times10^3$ from 7 h to 13 h, while the number stayed at about $(2.0\pm0.4)\times10^4$ on titanium. Consequently, calcium hydroxide exhibited antibacterial action against *S. epidermidis* and *S. aureus* for 13 h. Bacterial counts were also determined for 1, 2 and 3 days. All in all, the experiment was repeated 4 times with the same protocol and under the same conditions, but meaningful results were only found for one run. The results are shown in figure 4.29. On day 1 the bacterial count was more than that seeded on titanium and calcium hydroxide. On day two the count on titanium was higher than on day one, but the count on calcium hydroxide was significantly lower. On day three the count on both surfaces was lower than on day one and day two. No medium change was performed, thus the low bacterial count on day 3 was most likely caused by starvation of the bacteria. Otherwise, the count on titanium should be at least as high as on day 2. This indicated that biological experiments are not predictable and are affected by many parameters, even if conducted following the same protocol. Thus, more repetitions should be done, to get verifiable results.

S. aureus has a high affinity to bone tissue and is very active in contaminating implants. Studies showed that *S. aureus* adheres to calcium phosphate coatings more readily than on pure metallic implants [208]. On calcium hydroxide, however, the adhesion seemed to be reduced for 13 h. The formation of biofilm in dependency of the pH-value was investigated for *S. aureus* ATCC 25923 and 46 strains isolated from auricular infections at the pH levels 3, 5, 7, 9 and 12 by Zmantar et al. [128]. High acidic (pH 3) or alkaline (pH 12) levels reduced the formation of biofilm compared to pH 7. While no biofilm formation was found at pH 3 two stains showed biofilm formation at pH 12. At pH 9 16 out of 28 strains showed lower grade of biofilm formation than at pH 7, but for two strains biofilm formation increased. For the strains tested in my experiments a reduction could be achieved, but the efficacy against other strains can be different and has to be investigated in more detail. Attributing antibacterial activity to a single surface property is hardly possible because surface morphology, surface energy, surface chemistry, porosity and leaching of bactericides influences the response and adherence of bacteria. Nonetheless, calcium hydroxide coatings could reduce the load of *S. aureus* and *S. epidermidis* for 13 h and are a promising antibacterial implant coating.

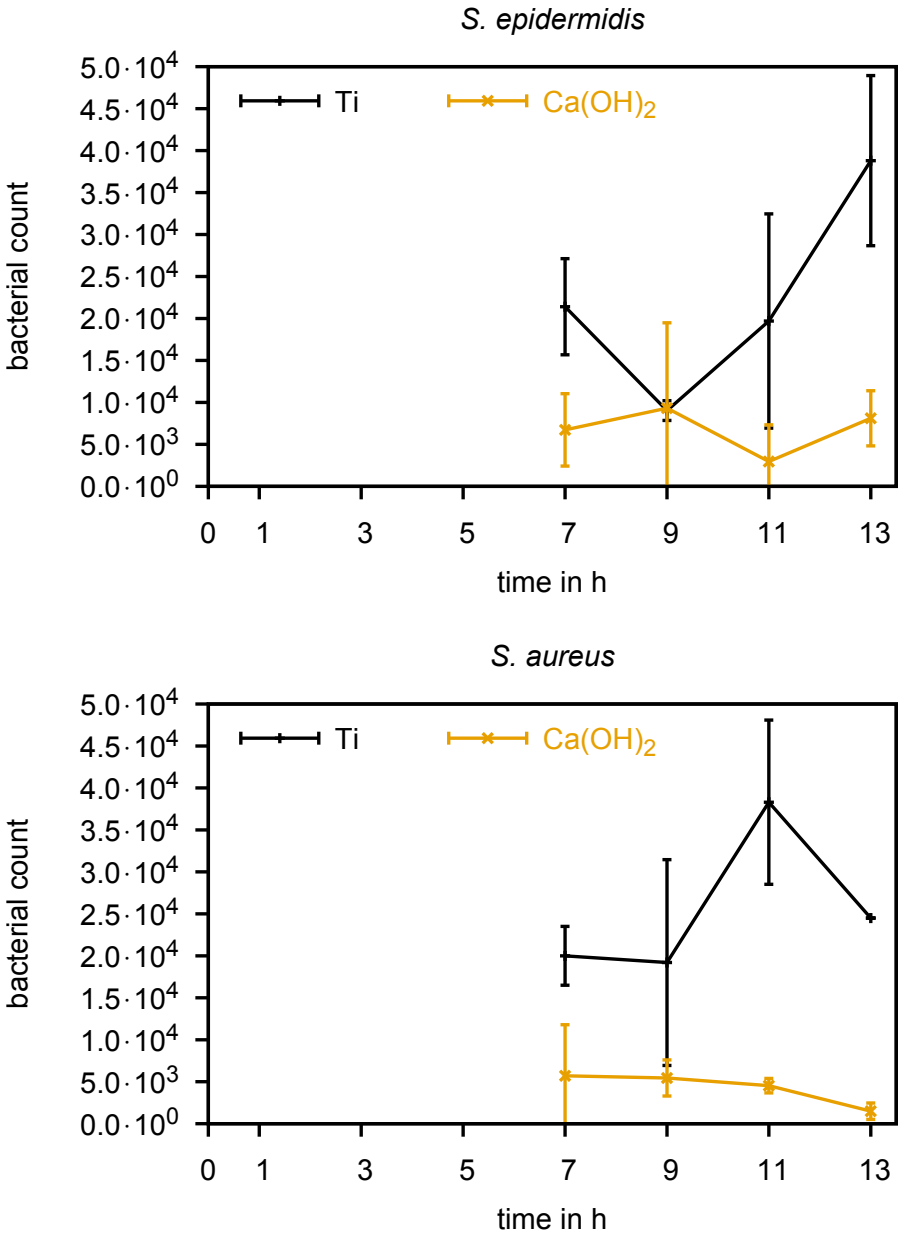

Figure 4.28: Calcium hydroxide could reduce the bacterial count of *S. aureus* and *S. epidermidis* for the time points 7 h, 9 h, 11 h and 13 h below the titanium control, thus calcium hydroxide shows antibacterial properties.

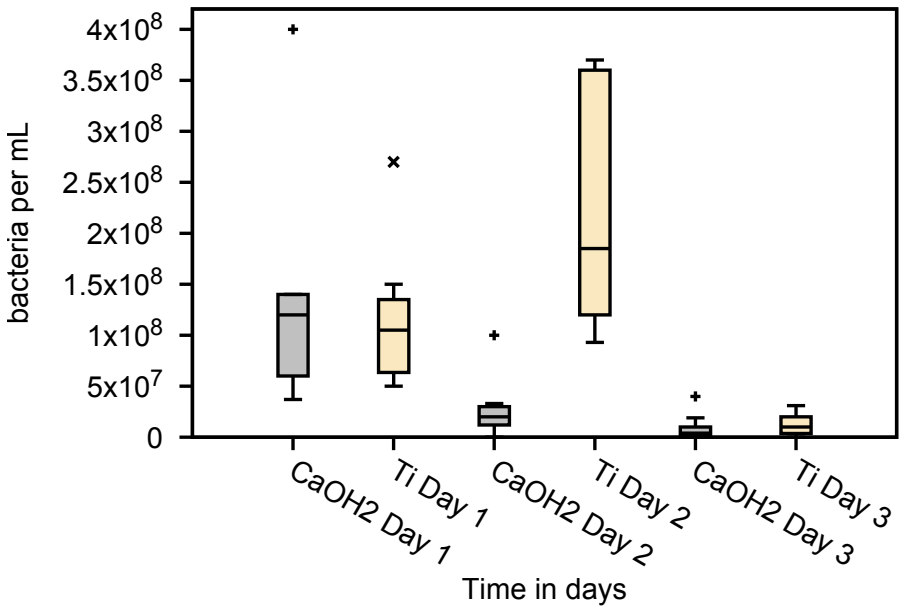

Figure 4.29: *S. aureus* count on titanium and calcium hydroxide after 1, 2 and 3 days.

4.8. Biofilm growth

Implant infections are feared by patients and doctors, especially when biofilms are involved. Biofilms are produced by bacteria to protect themselves against the host immune system and as storage for water and nutrients. Bacteria within a biofilm also withstand treatment with antibiotics and can hardly be removed. Therefore, it is vital to understand the formation of a biofilm and the time it needs for formation. Thus, after investigating for bacterial growth in the sections above, this section also looks for the biofilm-marker concanavalin A. Bacteria and a biofilm that may have formed were stained with FITC-labeled concanavalin A (ConA) and Hoechst or SYBR-green. Concanavalin A binds to alpha-linked mannose rests that are present in many glycoproteins that are involved in biofilm formation [335] and was therefore used to detect a biofilm. The DNA of bacteria was stained with Hoechst 33342 to see if the bacteria were located within the biofilm or not covered by biofilm.

Fluorescence microscopy could detect the stained bacteria already at the first day of incubation (see figure 4.31). On the next days, the bacteria formed larger three-dimensional aggregates,

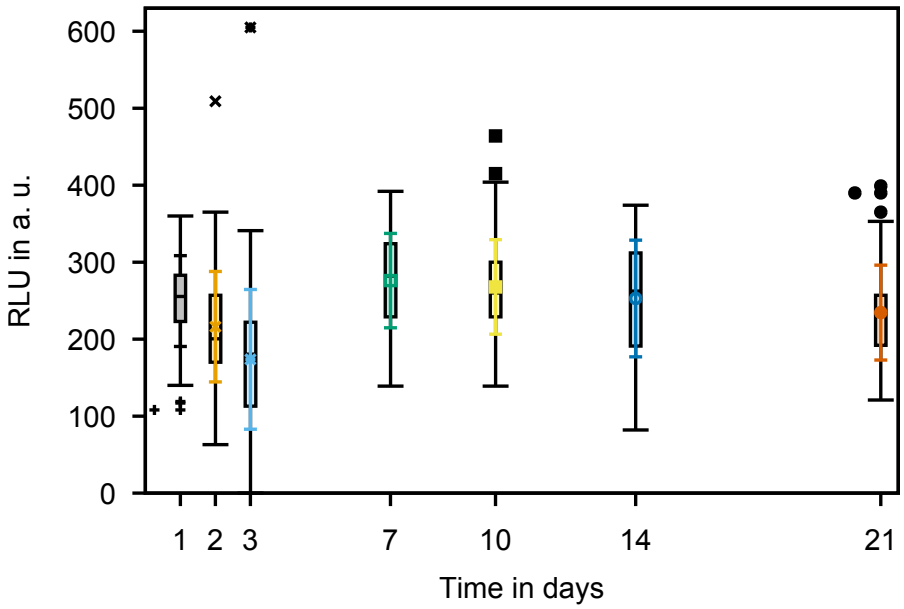

Figure 4.30: Relative bacterial count measured by SYBR-green fluorescence. SYBR-green binds to DNA and is therefore connected to the bacterial count. The number of bacteria decreased during the first three days, which can be a hint for a forming biofilm. On day 7 the count was higher than on day 1, stayed at about that level until day 14 and dropped significantly on day 21. The drop in bacterial count could be a hint for biofilm formation.

but only slowly increased in number, if at all. Biofilm formation seemed to correspond to the formation of aggregates, as these aggregates were clearly visible on the ConA-staining. Even at day one ConA bound to a single aggregate. In addition, SYBR-green was used to stain the

bacterial DNA [336] and the measured fluorescence was used to compare the relative bacterial count for all days of investigation (see figure 4.30). The number of bacteria decreased for day 1, 2 and 3 significantly, but increased until the 7th day significantly to again decrease slowly until the 21st day. On day 7 the count was higher than on day 1, stayed at about that level until day 14 and dropped significantly on day 21. The drop in bacterial count could be a hint for biofilm formation. Medium changes seemed not to influence the bacteria count, because after the first change on day 2 the numbers still decreased, but after the changes on day 4 and day 6, the number measured on day 7 was higher. After that, the medium was changed two days before measurement and a significant decrease could only be detected between 7th and 21st as well as 10th and 21st day. Comparing the first with the 21st day the bacterial count did not change significantly.

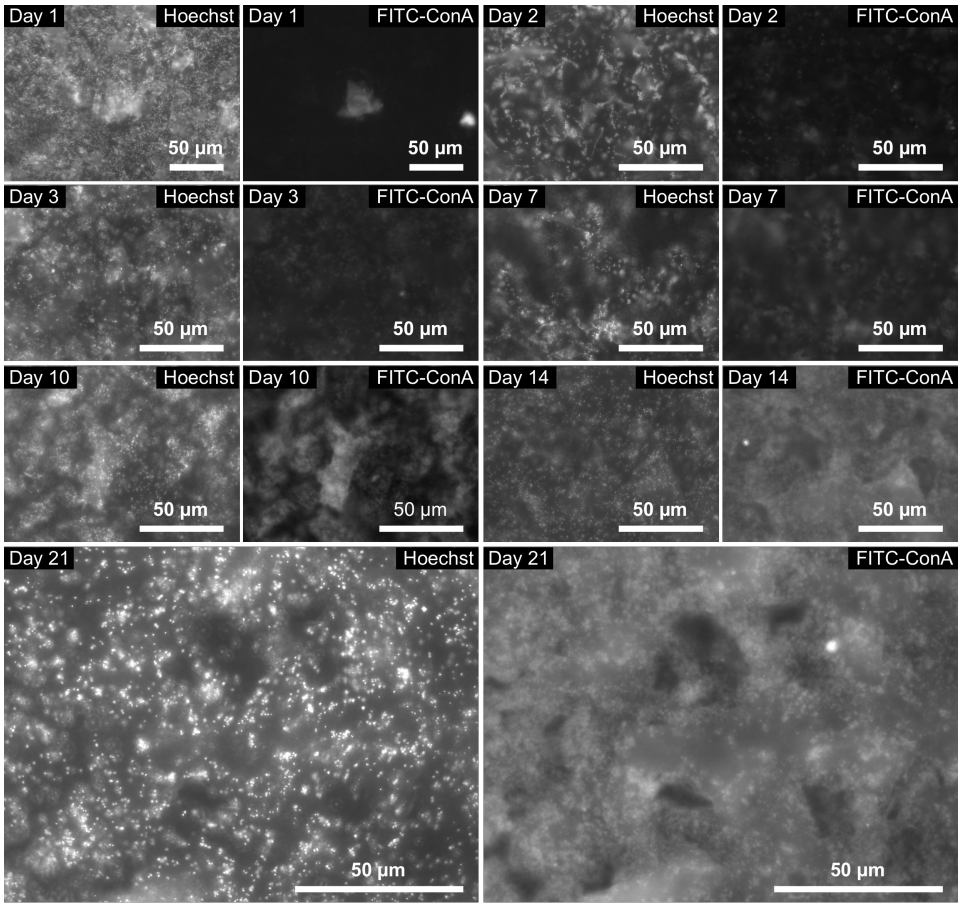

Figure 4.31: Fluorescence microscopic images of titanium disks seeded with *S. aureus*. Bacterial DNA was stained with Hoechst to visualize their distribution and labeling with FITC-ConA monitored biofilm formation. Bacteria are visible on the images of each day and are quite dense from the beginning on. On day 1 ConA bound only to a point with high bacteria aggregation. On further days increasing ConA-staining could be found, so exposure times for taking the images could be reduced. The ConA-stained structures clearly coincide with areas of high bacterial density and cloudy areas. Brightness and contrast of images were adjusted.

The biofilm was also examined on calcium hydroxide coated titanium disks. Pure calcium hydroxide coatings were tested and did not fluoresce (see 4.32 A-A"). Calcium hydroxide coatings not seeded with bacteria were stained with the same protocol as the seeded ones, and the images excluded fluorescence of the dye together with coating components (see 4.32 B-B"). Unfortunately, as soon as medium or medium with bacteria were in contact with the coatings, they showed high auto-fluorescence (see figure 4.32 C-E"). Thus, it was not possible to distinguish between auto-fluorescence of the calcium hydroxide coating together with medium and a stained biofilm (see figure 4.32 F). Bright spots on the background of auto-fluorescence marked bacteria stained with Hoechst and made it possible to detect bacteria after one day of culture (see figure 4.32 F'). This indicates that bacteria also grew on calcium hydroxide coatings and were not killed successfully. Since staining of biofilm on calcium hydroxide coatings was not possible due to auto-fluorescence, the samples were fixated, dried and examined in the SEM (see figure 4.39). The images show a biofilm formation on day 21, but no indication for that on day 10 or 14. The change in the surface morphology between day 3 and 10 was obvious. On days 1,2 and 3 the surface morphology did not change much and was as expected for a calcium hydroxide coating: rough with cracks and crater-like structures. From day 10 on, the coating seemed to be gone, because the surface looked like the uncoated titanium at that days (compare figure 4.38). The number of visible bacteria also differed not much from that on titanium. Therefore, from SEM images no clear antibacterial activity could be concluded. That a biofilm formed after 21 days could be explained by the dissolution of the calcium hydroxide coating, as no signs of a coating could be seen anymore. Hence, the antibacterial agent was depleted and not able to fight the bacteria.

The measurement of fluorescence indicated that there was about the same number of bacteria on the titanium samples over the time (SYBR-green) and that the biofilm slightly increased from day 1 to day 5 and then stayed at approximately the same level or decreased slightly (ConA) (compare figure 4.33). Epifluorescence microscopy was used to control the results from fluorescence measurement and the first biofilm agglomerates could be found on day 5 and then an about equal bacterial count could be seen for the following days (see figure 4.34). This was in accordance with the results from fluorescence measurement.

In a next step the experimental protocol was optimized to increase day to day reproducibility of the results. Washing and staining were not done on hooks and in a wet chamber but in the well. This should minimize handling deviations and difference in washing intensity. In addition, the fluorescence of Hoechst was measured on the same samples as ConA, giving a better correlation of the biofilm and bacterial count data. Instead of SYBR-green staining Live/Dead-staining was performed. Figure 4.35 shows the results for ConA and Hoechst staining. The fluorescence of the Hoechst-stained DNA stayed at about the same level for all days and showed no increase as would be expected for an increased bacterial count. However, the fluorescence of ConA increased for day 10 and day 14, consequently a formed biofilm

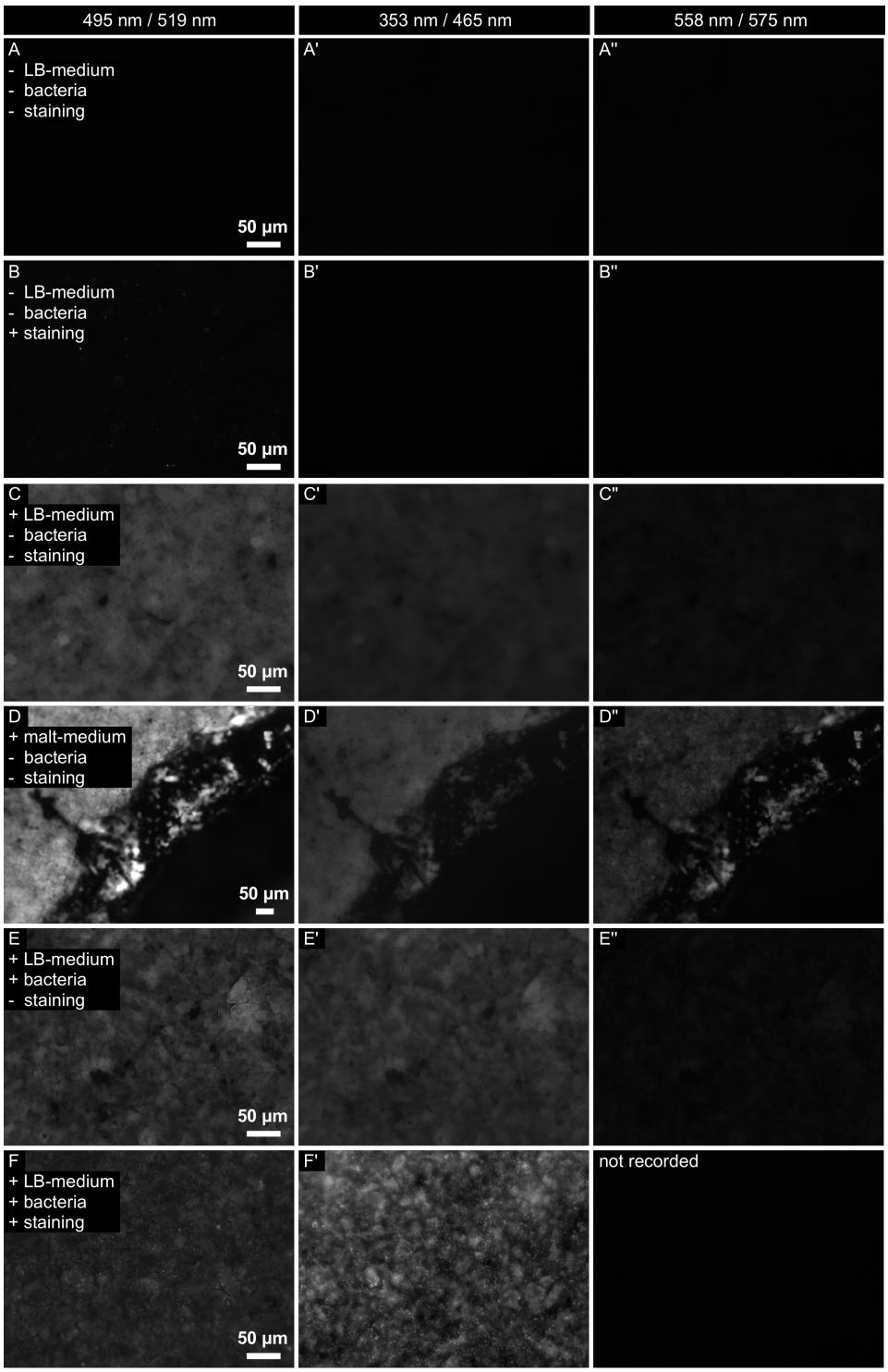

Figure 4.32: Calcium hydroxide coatings show no auto-fluorescence (A-A') and no fluorescence when stained with FITC-ConA (B-B'), but as soon as LB- or malt-medium with or without bacteria is present the structure of the coating is clearly visible (C-E"). Therefore, it is not possible to distinguish between the contributions of auto-fluorescence and stained biofilm (F). Bacteria stained with Hoechst can be distinguished because they appear as bright dots (F') on the auto-fluorescing background.

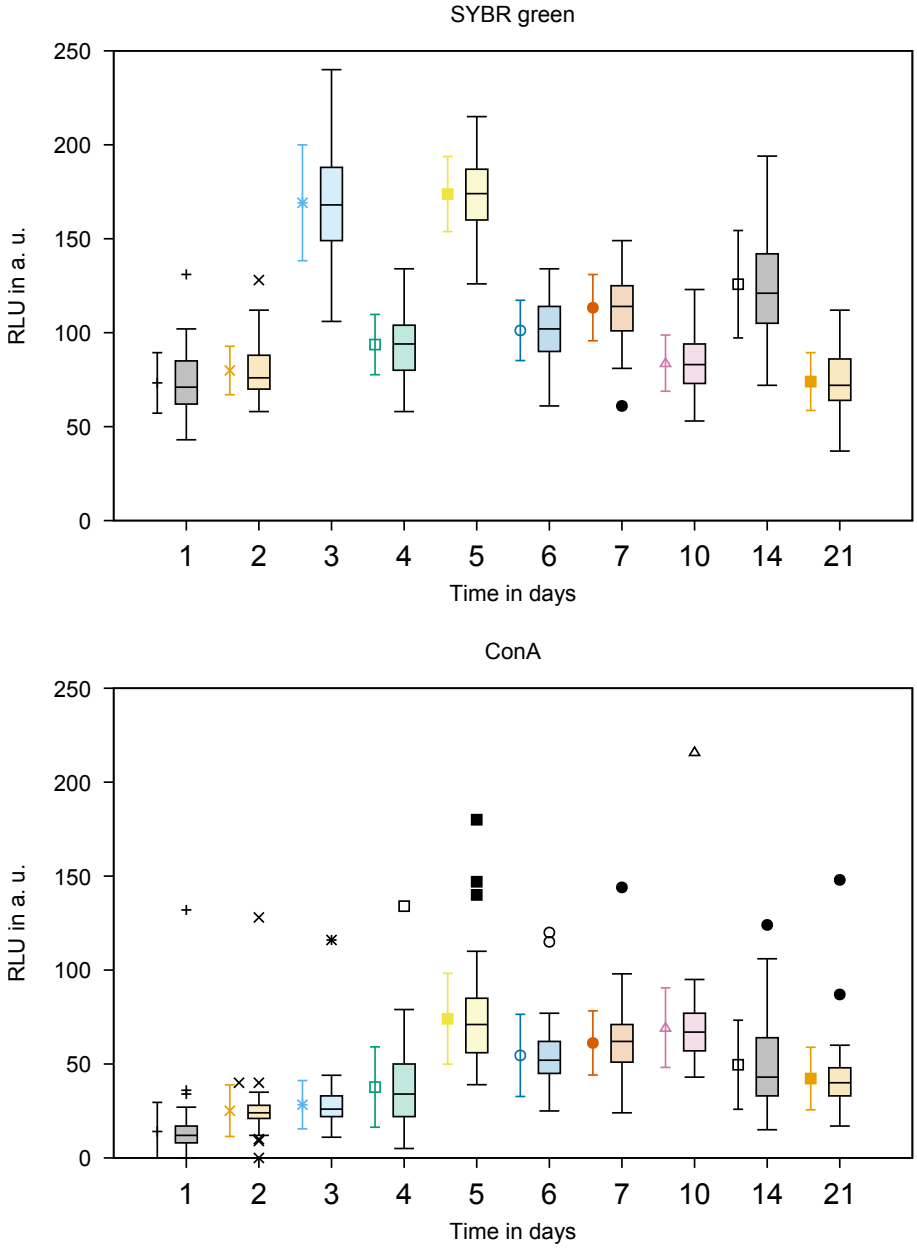

Figure 4.33: Fluorescence measurement for the DNA-staining SYBR-green and the biofilm staining with FITC-labeled concanavalin A (ConA) of *S. aureus* on titanium surfaces.

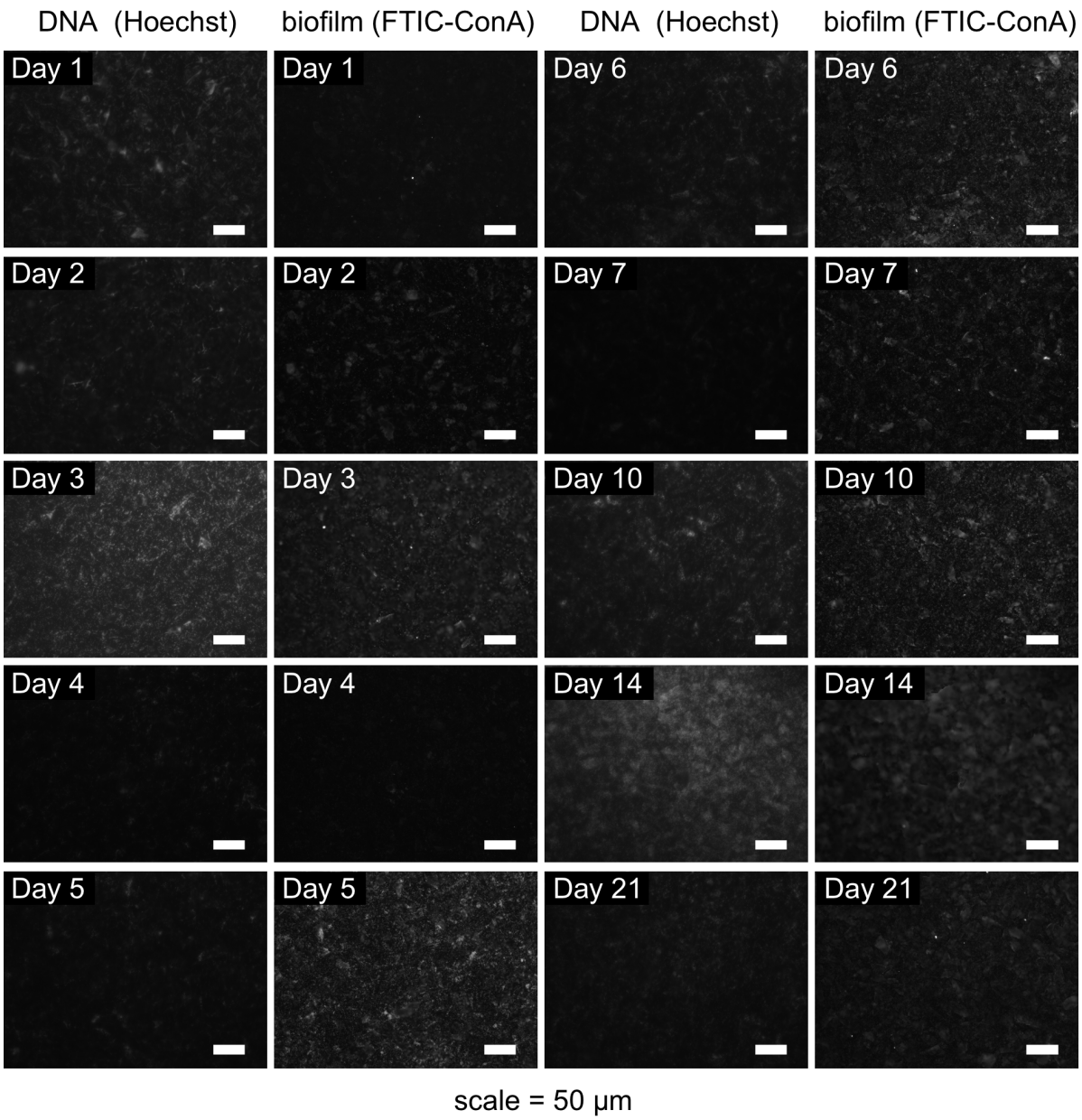

Figure 4.34: Microscopic images of FITC-labeled concanavalin A-stained biofilm. The first biofilm agglomerates can be seen on day 5. Thereafter, the bacterial count stayed about the same and equally distributed bacteria can be seen for day 7, 10, 14 and 21.

was most likely. The results of the fluorescence measurements for the quantification of the Live/Dead-staining are shown in figure 4.36. The calibration curve and the limit of detection of 20.52 % and the limit of determination of 67.12 % were calculated from all calibration values measured at all 7 time points. At day 2 around 80 % bacteria were alive and at all time points after that below 67 %, which is below the calculated limit of determination, excluding the determination of their precise values. However, even when neglecting the limit of determination, the calculated values showed no trend, despite that more than 20 % living bacteria were present.

X-ray diffraction patterns were recorded for all days investigated (compare figure 4.37) and showed no peaks for calcium hydroxide from the first day on, thus there was no crystalline calcium hydroxide on the coating anymore. However, the rising and broadening peak between 30° and 35° indicated the formation of calcium phosphates and among others different forms of HA. The peak was visible at day 7 and 21, that means that conversion to HA took longer than in SBF, as investigated by [30]. However, this indicates, that auto-biocompatibilization is not inhibited by bacterial growth and could support bone ingrowth even in this critical situation.

Additional to the staining, samples were fixated with glutaraldehyde and examined in the SEM (see figure 4.38). The images are in good accordance with the results from staining, regarding the bacterial count. However, signs for a biofilm were doubtful for day 10 and day 14 where a clear biofilm could be detected with ConA. Only the images of day 21 showed bacteria adhering to one another and small filaments between them. Titanium is a standard material for implants and is used with good success. Unfortunately, studies show that good biocompatibility does not only allow cells to grow, but also bacteria and that implants are especially prone to microbial colonization [130]. The aim is to overcome this drawback of the highly biocompatible titanium with antibacterial coatings. Fixation of the bacteria was also possible on calcium hydroxide coatings and the resulting SEM images are shown in figure 4.39. Until day 3 the coating with its crater-like structures and cracks were clearly visible in all magnifications. The bacteria were singly spread over the surface or only loosely agglomerated (on day 3) and the visual impression was the same on all days as for titanium (compare figure 4.38). On day 21 formation of fibrillar structures were visible and were a strong hint for a biofilm.

SEM images were similar to biofilms in literature [100, 337, 338]. The number of bacteria at the surface seen on the SEM images were about the same for titanium samples and calcium hydroxide coated titanium samples. Of course, this is unwanted, as calcium hydroxide should kill bacteria and prevent the formation of a biofilm. However, calcium hydroxide converts to HA in cultural media within about 3 days, which is the auto-biocompatibilization that enhances bone growth but terminates the antibacterial activity. Thus, surviving bacteria can multiply and form a biofilm. It must be considered that the number of bacteria was large as compared to contaminations during surgery.

Laminar airflow systems can reduce the bacteria down to 1 CFU/m^3 to 10 CFU/m^3 in the operation theater and further down to 1 CFU/m^3 when space suits are used [339, 340]. Despite

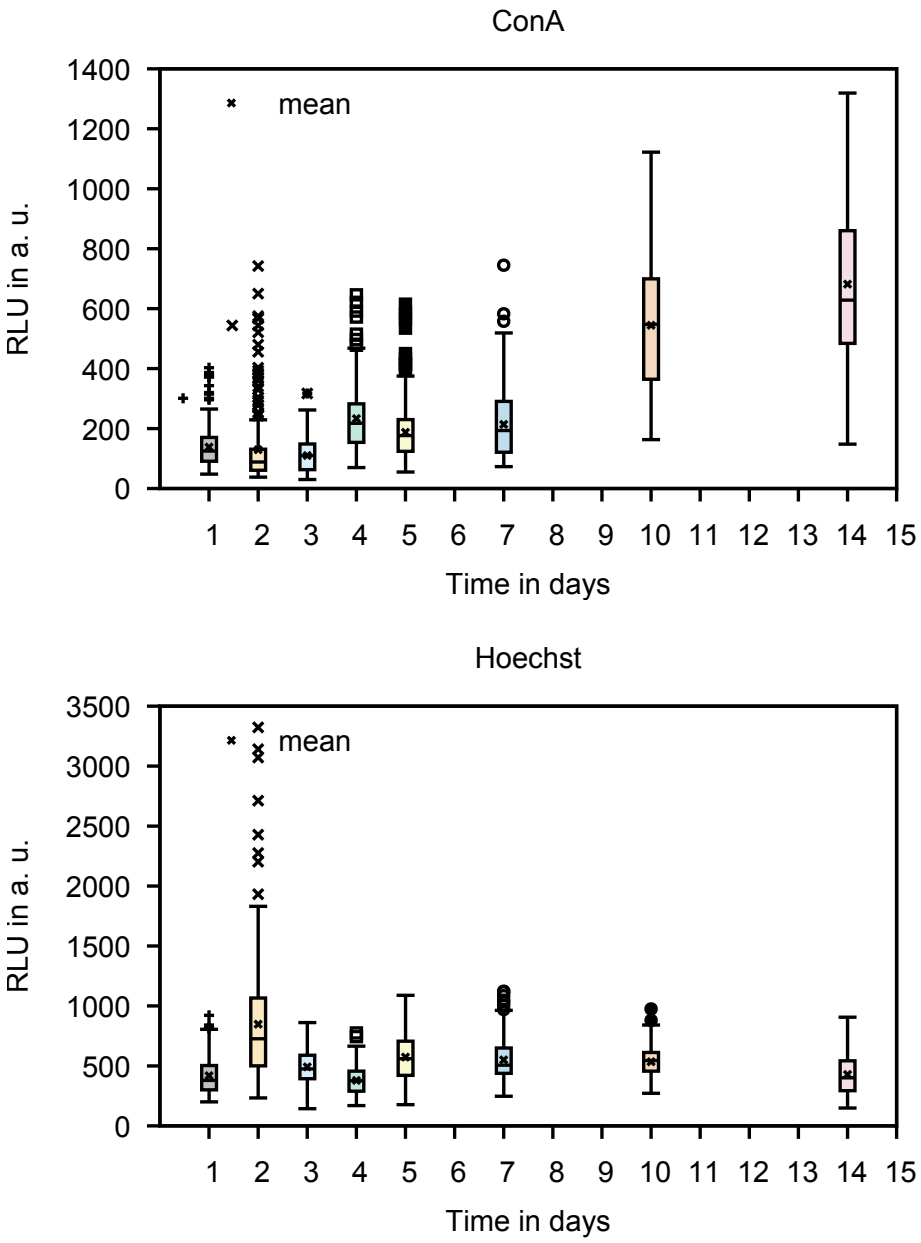

Figure 4.35: Biofilm (ConA) and bacterial DNA (Hoechst) staining measured on the same samples to have a measure for biofilm development and bacterial count. The bacterial count stayed at about the same level on all days. Many outliers can be seen on day 2 that also occurred in ConA-fluorescence but are not undoubtedly assignable. Fluorescence of ConA stayed at the same level until day 7 but significantly rose on day 10 and 14. Hence, biofilm started noticeable growing after day 7.

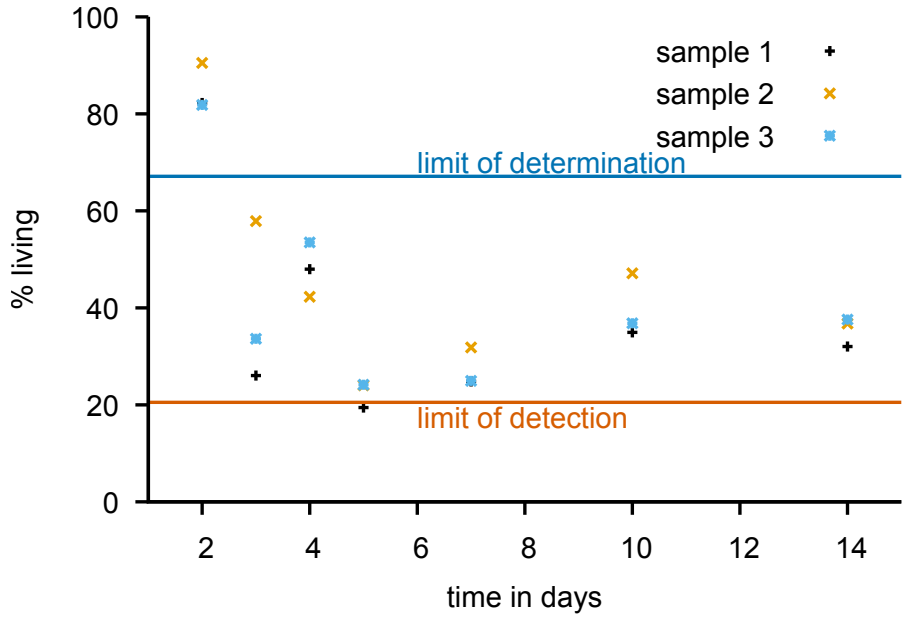

Figure 4.36: Evaluated Live/Dead-Staining. All values, except one at day 5 lie above the limit of detection, but only the values of day 2 above the limit of determination. Therefore, quantitative values can only be given for day 2. For all other days, the only possible conclusion is that living bacteria are present. Nevertheless, their values were plotted, but show no trend.

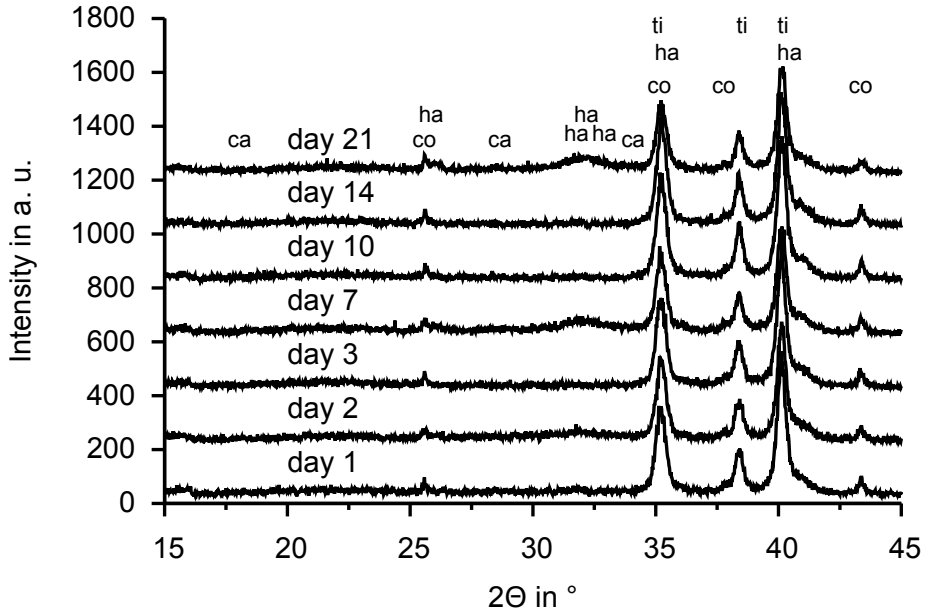

Figure 4.37: X-ray diffraction patterns of calcium hydroxide coated titanium disks after colonization with *S. aureus*. Crystalline calcium hydroxide was not detectable, but between 30° and 35° a broad peak appeared that is related to calcium phosphate i. e. HA formation. Peaks are labeled with ti for titanium, ca for calcium hydroxide, co for corundum and ha for calcium phosphate/HA.

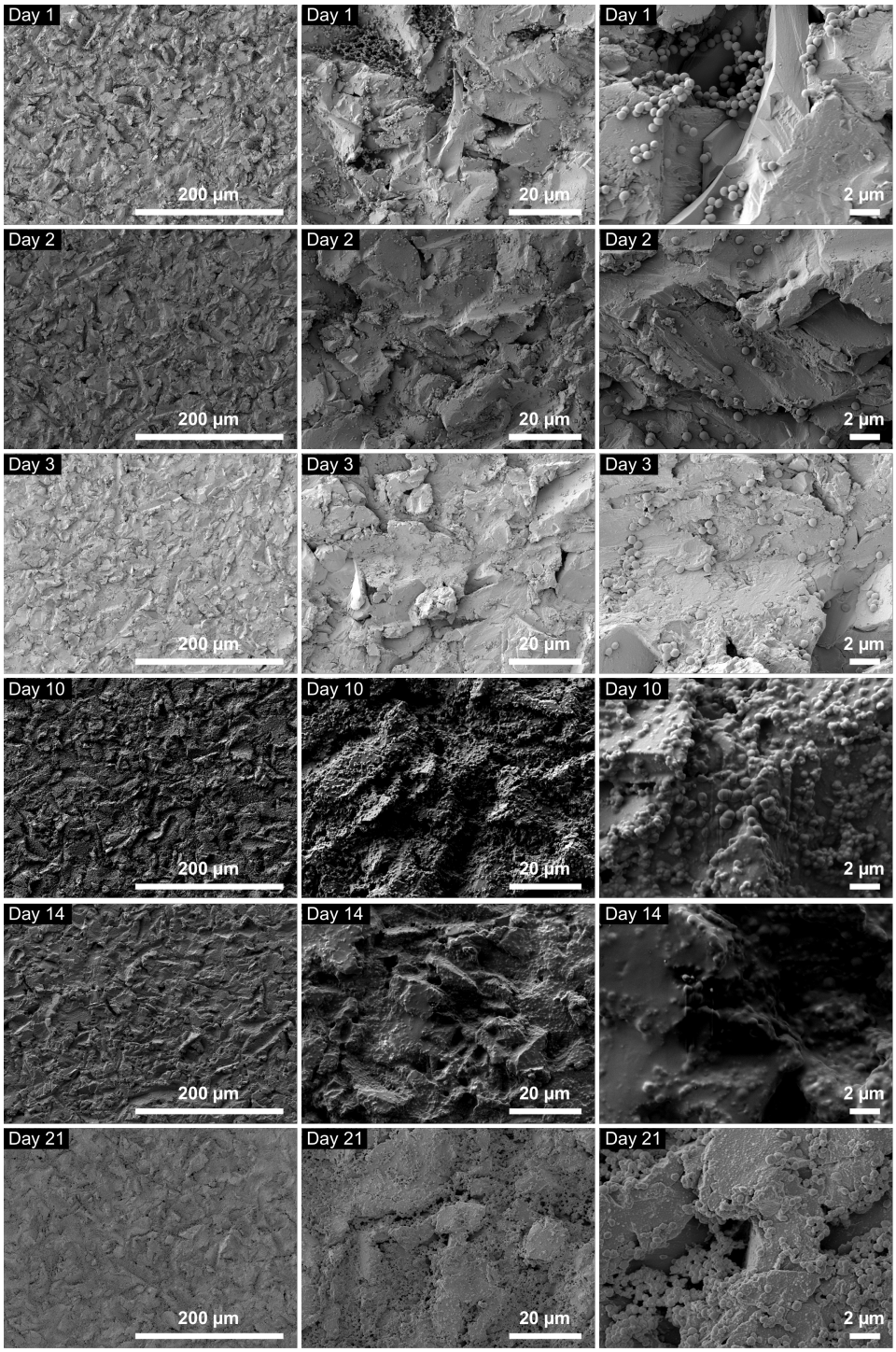

Figure 4.38: Scanning electron microscopy images of *S. aureus* on titanium. On day 1, 2 and 3 about the same number of bacteria can be seen on the titanium, but no hints for a biofilm formation. More bacteria are visible on day 10 and 14 and the amount increases again for day 21. At day 21 bacteria adhere to each other and thin filaments can be seen between them.

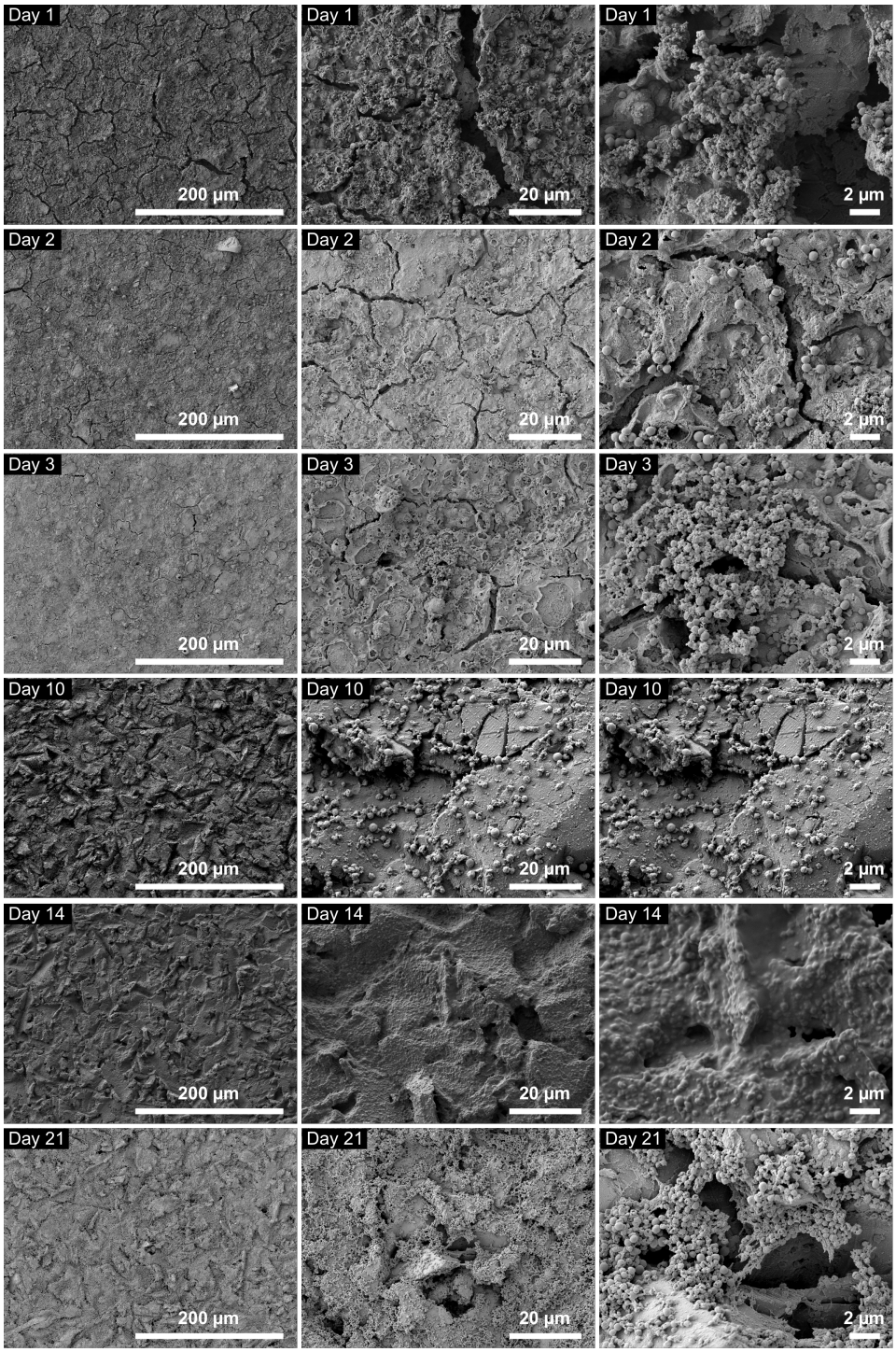

Figure 4.39: Scanning electron microscopy images of *S. aureus* on calcium hydroxide coated titanium. The coating with its cracks and crater-like structures is clearly visible on day 1, 2 and 3, but seem to disappear from day 10 on. The number of bacteria on the surface is comparable with that on titanium (see figure 4.38). On day 10 and 14 no signs of a biofilm formation are visible, but on day 21 aggregated bacteria and fibers reveal a formed biofilm.

the use of these techniques the infection rate seemed not to be reduced, but to increase [16].

Determination of biofilm formation is difficult, and currently under intense investigation [119, 130, 131, 341]. My experiments are only a tiny step to shed further light into the formation of *S. aureus* and *S. epidermidis* biofilms and could detect biofilm formation starting between day 5 and 10 of bacterial incubation and a pronounced biofilm with SEM after 21 days.

4.8.1. Cytocompatibility

Cytocompatibility is very important for an implant. Tests for $Ca(OH)_2$, Ag-$Ca(OH)_2$ and Cu-$Ca(OH)_2$ were made with hFOB over 10 days. The cell number as well as cell activity of hFOB on sandblasted titanium increased over all days and showed a normal cell behavior (see figure 4.27 A and B). Cu-$Ca(OH)_2$ showed about the same activity per cell as $Ca(OH)_2$ (see figure 4.27 C). The cell number of Cu-$Ca(OH)_2$ stayed practically constant, but the cell activity slightly increased. Cell number and cell activity on Ag-$Ca(OH)_2$ were immensely reduced.

In a previous study MG63 cells were used and revealed high cytocompatibility for $Ca(OH)_2$ coatings. MG63 is a human osteosarcoma cell line and thus perhaps less sensitive against material modifications. Therefore, the human cell line (hFOB 1.19) was used for this experiment, as it is not degenerated. Compared to the uncoated sandblasted titanium substrates all coated samples showed a significantly lower cell number and cell activity on all days. However, the cell activity and number rose on $Ca(OH)_2$ and Cu-$Ca(OH)_2$ during the 10 days of the test period. On Ag-$Ca(OH)_2$ only few cells after 10 days and no proliferation could be detected. The cells should not have been harmed by the silver concentrations, because, regarding to the release profiles, the silver concentration should have been below the minimal toxic dose of 300 ppb [262]. A difference in the studies was the release medium SBF for the release study and Dulbecco's Modified Eagle Medium (DMEM) in the cell study, which can affect release rates of silver. Especially proteins in the cell culture Medium DMEM can lead to higher silver release [342] and thus explain higher toxicity. Together with the lower antibacterial activity of silver compared to copper, silver is less promising as additive for the $Ca(OH)_2$ coatings than copper. Also, Heidenau et al. [39] could show the tendency of a lower cytotoxicity and a higher antibacterial activity of copper.

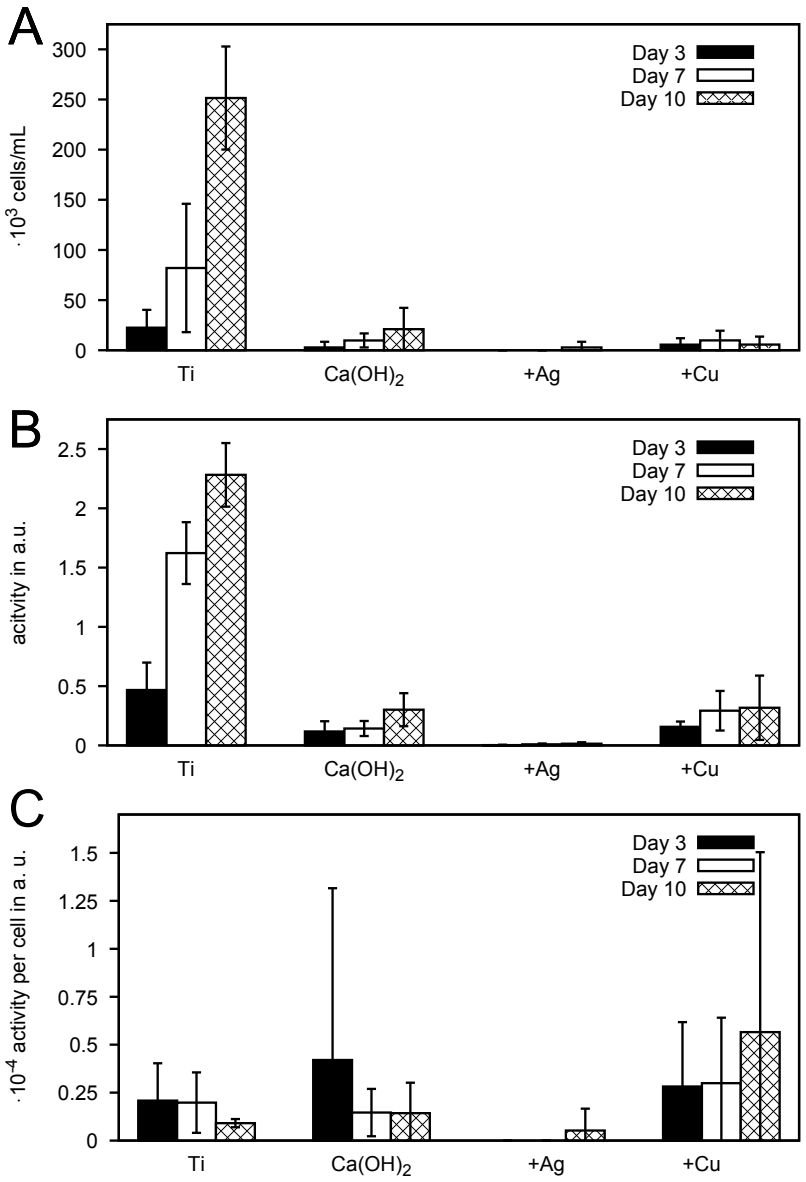

Figure 4.40: "Cell tests with hFOB. The cells showed an increased cell number (A) and activity (B) on the titanium (Ti) control, pure $Ca(OH)_2$ and Cu-$Ca(OH)_2$ and comparable activity per cell (C). Only on Ag-$Ca(OH)_2$ no cells grew over 10 days." Reprinted from [297] with permission, Copyright © 2018, Springer Nature.

4.9. Coating of clinically relevant geometries

The big advantage of ECAD is, that it is a non-line-of-sight technique and complex geometries can easily be coated. Besides medical application [343, 344] it is therefore under investigation to produce protecting HA coatings on marble artwork [345] and calcium phosphate coatings on carbon fiber cloth [346]. In order to get the same current density, the actual current must be adapted to the larger surface area of larger and more complex shaped items. Further changes to the process are not necessary. Adjusting the stirring speed to the size of the implant and the size of the electrolytic cell can improve the coating. Another aspect that must be considered are parts that must not be coated like screw threads, the part where the head is put on the stem of a hip implant or the distal part of the stem. The easiest way is not to put these parts into the electrolyte, but, if this is unavoidable, they need to be covered. To prove the feasibility of calcium hydroxide coatings on clinically relevant geometries, a structured surface, a hip stem, a tooth implant and a hip cup were coated.

A structured titanium sample of about 40 cm^2 was coated with -2 A ($\approx 50\,mA\,cm^{-2}$) with stirring of the electrolyte at 200 rpm for 30 min (see figure 4.41 A). The stem of the hip implant shown in figure 4.41 B was coated at the same parameters for 15 min. For the tooth implant -110 mA were applied for 15 min without stirring (see figure 4.41 C). All geometries were coated homogeneously and showed good coating quality, independent of their different sizes and morphologies. As proof of concept a commercially available hip cup was coated with calcium hydroxide to show that even complex structures could be coated homogeneously (compare figure 4.41 D). The screw threads that should be left un-coated were sealed with wax for the first trial. In order to get a good, homogeneous coating around the screw threads but not in the threads themselves, fitting plastic screws are a promising choice. They could additionally fixate a sealing part for the inside of the cup. The coating parameter were estimated based on experience from earlier experiments and only changed once during the experiment because the bubble formation seemed to be too high. Coating was performed at -5 A at 500 rpm for 30 min and then at -3 A at 0 rpm for 2 h. Even at the first try with not optimized parameters the hip cup could be coated homogeneously. Further analyses like SEM and XRD could not be performed due to the geometry of the implant. The clinical partner wanted the implant returned intact, therefore it was not possible to cut pieces that fit the analytical needs.

The experiments clearly showed the advantages of electrochemically assisted deposited calcium hydroxide coatings and its high potential as antibacterial implant coating. Moreover, this technique is easy to adapt to new implant geometries with only minor changes in the setup of the coating device.

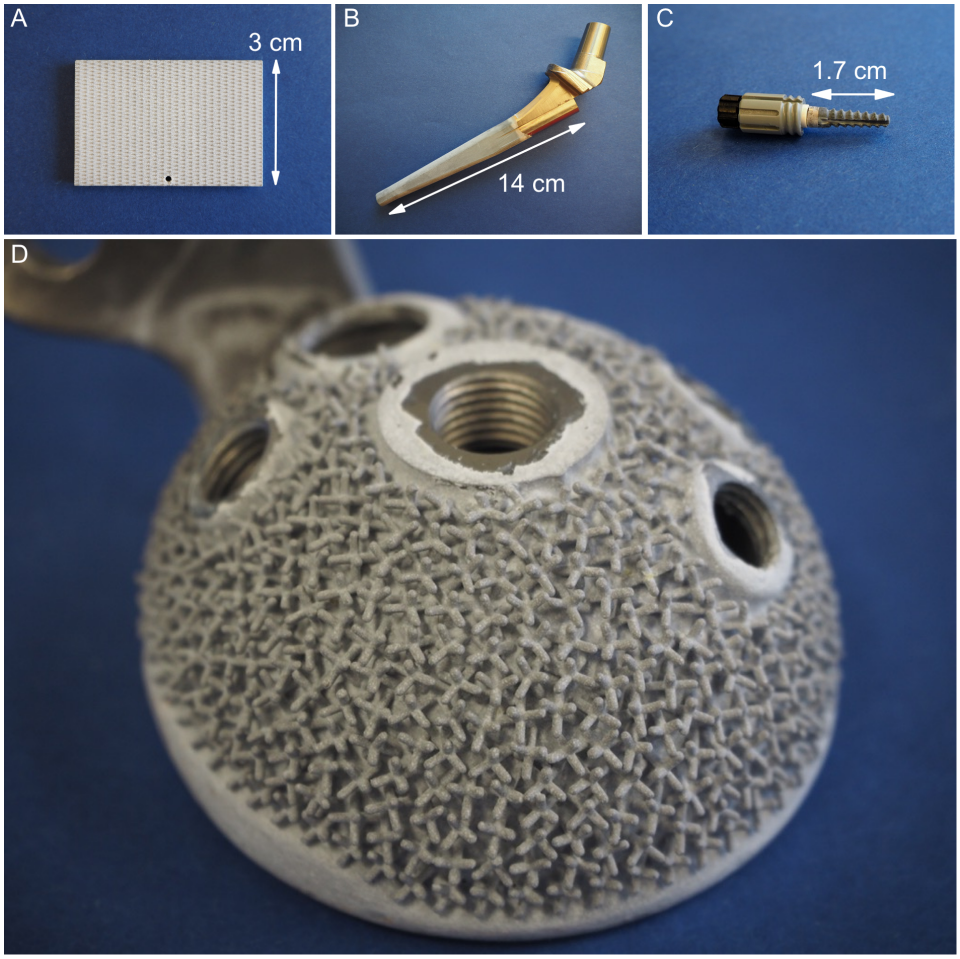

Figure 4.41: Complex geometries coated with calcium hydroxide. A) Structured surface, B) hip stem, C) dental implant and D) hip cup. The complex geometry of the hip cup was homogeneously coated, and sealed screw threads were not coated. This indicates the huge potential of electrochemically assisted deposition for implant coatings.

5. Conclusion

Calcium hydroxide coatings produced with electrochemically assisted deposition (ECAD) showed the potential to combine antibacterial properties and enhanced bone ingrowth. Thus, they are a step in fighting aseptic loosening and implant infections, the two major problems for implants, as implant registers and publications revealed and that occur in about 2 % of surgeries. Due to the promising results calcium hydroxide coatings where filed as patent DE102016007126.5.

ECAD utilizes the pH-gradient for coating deposition, which was visualized with phenolphthalein and found to be surface confined. This is advantageous for thin coatings with good adhesion. Surface pretreatment influenced the coating mass and the morphology of the calcium hydroxide coating. The best compromise between coating mass and surface homogeneity was the surface pretreatment with Korox 50. A mechanical surface pretreatment in combination with a bioactive coating like calcium hydroxide is also favorable in terms of osseointegration [347]. In addition, the morphology of the surface coating could be altered by applying pulsed current, stirring or a combination of both during deposition. Thus, these parameters can be used to further tune biocompatibility as well as antibacterial properties, because both are affected by the surface morphology [310, 311, 314]. Experiments showed that morphology can be different at the edge of the samples. Here voltage spikes occur that are dependent on the radius of the tip and thus influence the deposition. To address this phenomenon a systematic approach with different tip radii is suggested for further investigations. Studies showed that laminar air-flow systems and space suits, were able to reduce the bacterial load in the operation theater [339, 340], but infection rates were not reduced, in contrast, they rose [16]. Microbiological evaluation of calcium hydroxide coatings revealed an antibacterial effect for at least the first 13 h and could prevent colonization of the implant with bacteria during surgery. To eradicate an infection 100 % of bacteria must be killed. As seen in this thesis and nearly all publications dealing with bacteria, a 100 % reduction of bacteria is hardly ever measured. Here a measurement problem occurs. The minimal number of bacteria needed for meaningful measurements is dramatically higher than the concentration of bacteria that might enter a wound during surgery. Therefore, the coatings could be way more effective than the tests reveal. From the tests, however, only a certain antibacterial activity, but not a 100 % reduction of bacteria can be found. Nevertheless, a lower bacterial burden helps the immune system to fight the remaining bacteria. Whenever the antibacterial effect should be enhanced and prolonged, the addition of silver and copper ions can help significantly. Copper proved most promising, as the increase in antibacterial activity was higher than for silver while the impact

on cytocompatibility was less pronounced. Additionally, copper is known to be angiogenic and to stimulate bone growth, which is favorable for the use in implant coatings [348]. Former studies showed, that after about 3 days the auto-biocompatibilization, that is the conversion of calcium hydroxide to hydroxyapatite (HA), is finished in simulated body fluid (SBF) for pure and coatings with copper or silver addition. This study showed that auto-biocompatibilization is not inhibited by bacterial growth and could support bone ingrowth even in this critical situation. The situation gets even more critical when bacteria form a biofilm. Treatments against biofilm are commonly started after 3 weeks, where scanning electron microscope (SEM) revealed pronounced biofilm formation. With the results of biofilm formation starting after 5 to 10 days in mind, a rethinking should start. It may be advantageous to treat infections as if a biofilm is present from day 5 on and not after 3 weeks as common practice.

Since calcium hydroxide coatings were applied with ECAD, such coatings can be produced on complex geometries. This was proven by successfully coating a commercially available hip cup with a very complex macroscopic surface geometry. Calcium hydroxide coating together with ECAD is a promising tool for the easy improvement of commercial and patient-specific implants in terms of biocompatibility as well as antibacterial properties.

Bibliography

[1] S. Kurtz, K. Ong, E. Lau, F. Mowat, M. Halpern, „Projections of primary and revision hip and knee arthroplasty in the United States from 2005 to 2030“, *J. Bone Jt. Surg.* **2007**, *89*, 780–785.

[2] The NJR Editorial Board, NJR 13th Annual Report 2016, **2016**.

[3] American Joint Replacement Registry, American Joint Replacement Registry Annual Report 2016, **2016**.

[4] J. Kärrholm, H. Lindahl, H. Malchau, M. Mohaddes, C. Rogmark, O. Rolfson, Eds., Swedish Hip Arthroplasty Register Annual Report 2015, **2016**.

[5] M. Sundberg, L. Lidgren, A. W-Dahl, O. Robertsson, Eds., Swedish Knee Arthroplasty Register Annual Report 2016, **2016**.

[6] A. Grimberg, V. Jansson, T. Liebs, O. Melsheimer, A. Steinbrück, EPRD-Jahresbericht 2015, **2015**.

[7] J. Kärrholm, C. Rogmark, E. Nauclér, J. Vinblad, M. Mohaddes, O. Rolfson, Eds., Swedish Hip Arthroplasty Register Annual Report 2018, **2018**.

[8] P. H. Gundtoft, A. B. Pedersen, C. Varnum, S. Overgaard, „Increased Mortality After Prosthetic Joint Infection in Primary THA“, *Clin. Orthop. Relat. Res.* **2017**, 1–9.

[9] J. A. Browne, J. M. Cancienne, W. M. Novicoff, B. C. Werner, „Removal of an Infected Hip Arthroplasty Is a High-Risk Surgery: Putting Morbidity Into Context With Other Major Nonorthopedic Operations“, *J. Arthroplasty* **2017**, *32*, 2834–2841.

[10] C. Otto-Lambertz, A. Yagdiran, F. Wallscheid, P. Eysel, N. Jung, „Periprosthetic infection in joint replacement“, *Deutsches Aerzteblatt Online* **2017**, *114*, 347–353.

[11] R. Pivec, A. J. Johnson, S. C. Mears, M. A. Mont, „Hip arthroplasty“, *The Lancet* **2012**, *380*, 1768–1777.

[12] C. L. Romanò, H. Tsuchiya, I. Morelli, A. G. Battaglia, L. Drago, „Antibacterial coating of implants: are we missing something?“, *Bone Joint Res* **2019**, *8*, 199–206.

[13] J. Beldame, B. Lagrave, L. Lievain, B. Lefebvre, N. Frebourg, F. Dujardin, „Surgical glove bacterial contamination and perforation during total hip arthroplasty implantation: When gloves should be changed“, *Orthop. Traumatol. Surg. Res.* **2012**, *98*, 432–440.

[14] P. G. M. Maathuis, D. Neut, H. J. Busscher, H. C. van der Mei, J. R. van Horn, „Perioperative Contamination in Primary Total Hip Arthroplasty.“, *Clin. Orthop.* **2005**, *433*, 136–139.

[15] B. A. S. Knobben, J. R. van Horn, H. C. van der Mei, H. J. Busscher, „Evaluation of measures to decrease intra-operative bacterial contamination in orthopaedic implant surgery“, *J. Hosp. Infect.* **2006**, *62*, 174–180.

[16] G. J. Hooper, A. G. Rothwell, C. Frampton, M. C. Wyatt, „Does the use of laminar flow and space suits reduce early deep infection after total hip and knee replacement?“, *Bone Jt. J.* **2011**, *93-B*, 85–90.

[17] J. Raphel, M. Holodniy, S. B. Goodman, S. C. Heilshorn, „Multifunctional coatings to simultaneously promote osseointegration and prevent infection of orthopaedic implants“, *Biomaterials* **2016**, *84*, 301–314.

[18] E. C. Pegg, F. Matboli, T. Marriott, I. Khan, C. A. Scotchford, „Topographical and chemical effects of electrochemically assisted deposited hydroxyapatite coatings on osteoblast-like cells“, *J. Biomater. Appl.* **2014**, *28*, 946–953.

[19] J. Redepenning (J. G. Redepenning), 5310464, U.S. Classification: 205/318; 204/490; 623/901; 623/923 International Classification: C25D 1136, **1994**.

[20] R. Pérez-Tanoira, X. Han, A. Soininen, A. A. Aarnisalo, V.-M. Tiainen, K. K. Eklund, J. Esteban, T. J. Kinnari, „Competitive Colonization of Prosthetic Surfaces by Staphylococcus Aureus and Human Cells“, *J. Biomed. Mater. Res. A* **2017**, *105*, 62–72.

[21] C. A. S. de Souza, R. P. Teles, R. Souto, M. A. E. Chaves, A. P. V. Colombo, „Endodontic Therapy Associated with Calcium Hydroxide as an Intracanal Dressing: Microbiologic Evaluation by the Checkerboard DNA-DNA Hybridization Technique“, *J. Endod.* **2005**, *31*, 79–83.

[22] T. Albrektsson, C. Johansson, „Osteoinduction, osteoconduction and osseointegration“, *Eur. Spine J.* **2001**, *10*, 96–101.

[23] S. V. Dorozhkin, M. Epple, „Biological and Medical Significance of Calcium Phosphates“, *Angew. Chem. Int. Ed.* **2002**, *41*, 3130–3146.

[24] A. L. Boskey, „Bone composition: relationship to bone fragility and antiosteoporotic drug effects“, *BoneKEy Reports* **2013**, *2*, 447.

[25] L. Sun, C. C. Berndt, K. A. Gross, A. Kucuk, „Material Fundamentals and Clinical Performance of Plasma-Sprayed Hydroxyapatite Coatings: A Review“, *J. Biomed. Mater. Res.* **2001**, *58*, 570–592.

[26] W. Tong, J. Chen, Z. Xingdong, „Amorphorization and recrystallization during plasma spraying of hydroxyapatite“, *Biomaterials* **1995**, *16*, 829–832.

[27] R. Z. LeGero, D. Mijares, J. Park, X.-F. Chang, I. Khairoun, R. Kijkowska, R. Dias, J. P. LeGeros, „Amorphous Calcium Phosphates (ACP): Formation and Stability“, *Key Eng. Mater.* **2005**, *284-286*, 7–10.

[28] D. Gopi, J. Indira, L. Kavitha, „A comparative study on the direct and pulsed current electrodeposition of hydroxyapatite coatings on surgical grade stainless steel“, *Surf. Coat. Technol.* **2012**, *206*, 2859–2869.

[29] X. Lu, Z. Zhao, Y. Leng, „Calcium phosphate crystal growth under controlled atmosphere in electrochemical deposition“, *J. Cryst. Growth* **2005**, *284*, 506–516.

[30] C. Moseke, W. Braun, A. Ewald, „Electrochemically Deposited $CaOH_2$ Coatings as a Bactericidal and Osteointegrative Modification of Ti Implants“, *Adv. Eng. Mater.* **2009**, *11*, B1–B6.

[31] S. Rössler, A. Sewing, M. Stölzel, R. Born, D. Scharnweber, M. Dard, H. Worch, „Electrochemically assisted deposition of thin calcium phosphate coatings at near-physiological pH and temperature“, *J. Biomed. Mater. Res. A* **2003**, *64*, 655–663.

[32] E. Fernandez, F. J. Gil, M. P. Ginebra, F. C. M. Driessens, J. A. Planell, S. M. Best, „Calcium Phosphate Bone Cements for Clinical Applications. Part I: Solution Chemistry“, *J. Mater. Sci.: Mater. Med.* **1999**, *10*, 169–176.

[33] I. Greenwald, „The solubility of calcium phosphate I. The effect of pH and of amount of solid phase“, *J. Biol. Chem.* **1942**, *143*, 703–710.

[34] H. C. Vogely, C. J. M. Oosterbos, E. W. A. Puts, M. W. Nijhof, P. G. J. Nikkels, A. Fleer, A. J. Tonino, W. J. A. Dhert, A. J. Verbout, „Effects of hydroxyapatite coating on Ti-6 Al-4V implant-site infection in a rabbit tibial model“, *J. Orthop. Res.* **2000**, *18*, 485–493.

[35] P. Drechsler, W. Braun, R. Thull, „Elektrochemische Abscheidung von $Ca(OH)_2$ auf Titan zur Unterstützung der Osteointegration“, *Fortbildung Osteologie 2* **2008**, 112–115.

[36] Q. Chen, G. A. Thouas, „Metallic Implant Biomaterials“, *Mater. Sci. Eng. R-Rep.* **2015**, *87*, 1–57.

[37] S. Bauer, P. Schmuki, K. von der Mark, J. Park, „Engineering Biocompatible Implant Surfaces: Part I: Materials and Surfaces“, *Prog. Mater Sci.* **2013**, *58*, 261–326.

[38] S. Grosse, H. K. Haugland, P. Lilleng, P. Ellison, G. Hallan, P. J. Høl, „Wear particles and ions from cemented and uncemented titanium-based hip prostheses—A histological and chemical analysis of retrieval material“, *J. Biomed. Mater. Res. B.* **2015**, *103*, 709–717.

[39] F. Heidenau, W. Mittelmeier, R. Detsch, M. Haenle, F. Stenzel, G. Ziegler, H. Gollwitzer, „A novel antibacterial titania coating: metal ion toxicity and in vitro surface colonization“, *J. Mater. Sci.: Mater. Med.* **2005**, *16*, 883–888.

[40] C. A. Grillo, M. L. Morales, M. V. Mirífico, M. A. Fernández Lorenzo de Mele, „Synergistic cytotoxic effects of ions released by zinc–aluminum bronze and the metallic salts on osteoblastic cells“, *J. Biomed. Mater. Res. A* **2013**, *101A*, 2129–2140.

[41] Y. Okazaki, E. Gotoh, „Metal ion effects on different types of cell line, metal ion incorporation into L929 and MC3T3-E1 cells, and activation of macrophage-like J774.1 cells“, *Mater. Sci. Eng. C.* **2013**, *33*, 1993–2001.

[42] U. G. K. Wegst, H. Bai, E. Saiz, A. P. Tomsia, R. O. Ritchie, „Bioinspired structural materials“, *Nat. Mater.* **2015**, *14*, 23–36.

[43] M. Sundfeldt, L. V. Carlsson, C. B. Johansson, P. Thomsen, C. Gretzer, „Aseptic loosening, not only a question of wear: A review of different theories“, *Acta Orthop.* **2006**, *77*, 177–197.

[44] E. Wintermantel, S.-W. Ha, *Medizintechnik Life Science Engineering*, 4th ed., Springer Berlin Heidelberg, Berlin, Heidelberg, **2008**.

[45] B. M. Holzapfel, J. C. Reichert, J.-T. Schantz, U. Gbureck, L. Rackwitz, U. Nöth, F. Jakob, M. Rudert, J. Groll, D. W. Hutmacher, „How smart do biomaterials need to be? A translational science and clinical point of view“, *Adv. Drug Delivery Rev.*, Bionics - Biologically inspired smart materials **2013**, *65*, 581–603.

[46] M. Pilia, T. Guda, M. Appleford, „Development of Composite Scaffolds for Load-Bearing Segmental Bone Defects“, *BioMed Res. Int.* **2013**, *2013*, e458253.

[47] C. K. Seal, K. Vince, M. A. Hodgson, „Biodegradable surgical implants based on magnesium alloys ? A review of current research“, *IOP Conf. Ser.: Mater. Sci. Eng.* **2009**, *4*, 012011.

[48] S. Bose, G. Fielding, S. Tarafder, A. Bandyopadhyay, „Understanding of Dopant-Induced Osteogenesis and Angiogenesis in Calcium Phosphate Ceramics“, *Trends Biotechnol.* **2013**, *31*, 594–605.

[49] V. Goriainov, R. Cook, J. M. Latham, D. G. Dunlop, R. O. C. Oreffo, „Bone and Metal: An Orthopaedic Perspective on Osseointegration of Metals“, *Acta Biomater.* **2014**, *10*, 4043–4057.

[50] R. D. Guyer, J.-j. Abitbol, D. D. Ohnmeiss, C. Yao, „Evaluating Osseointegration Into a Deeply Porous Titanium Scaffold: A Biomechanical Comparison With Peek and Allograft“, *Spine* **2016**, *41*, E1146–E1150.

[51] Q. Li, Y. Zhang, D. Wang, H. Wang, G. He, „Porous Polyether Ether Ketone: A Candidate for Hard Tissue Implant Materials“, *Mater. Des.* **2017**, *116*, 171–175.

[52] S. Najeeb, M. S. Zafar, Z. Khurshid, F. Siddiqui, „Applications of Polyetheretherketone (PEEK) in Oral Implantology and Prosthodontics“, *J. Prosthodont. Res.* **2016**, *60*, 12–19.

[53] C. Rey, C. Combes, C. Drouet, M. J. Glimcher, „Bone mineral: update on chemical composition and structure“, *Osteoporos. Int.* **2009**, *20*, 1013–1021.

[54] K. A. Hing, „Bone repair in the twenty–first century: biology, chemistry or engineering?“, *Phil. Trans. R. Soc. A* **2004**, *362*, 2821–2850.

[55] M. E. Launey, M. J. Buehler, R. O. Ritchie, „On the Mechanistic Origins of Toughness in Bone“, *Annu. Rev. Mater. Res.* **2010**, *40*, 25–53.

[56] I. Jäger, P. Fratzl, „Mineralized Collagen Fibrils: A Mechanical Model with a Staggered Arrangement of Mineral Particles“, *Biophys. J.* **2000**, *79*, 1737–1746.

[57] K. J. Koester, J. W. Ager, R. O. Ritchie, „The true toughness of human cortical bone measured with realistically short cracks“, *Nat. Mater.* **2008**, *7*, 672–677.

[58] R. K. Nalla, J. J. Kruzic, J. H. Kinney, R. O. Ritchie, „Mechanistic aspects of fracture and R-curve behavior in human cortical bone“, *Biomaterials* **2005**, *26*, 217–231.

[59] I. Gotman, „Characteristics of Metals Used in Implants“, *J. Endourol.* **1997**, *11*, 383–389.

[60] Y. Okazaki, E. Gotoh, „Comparison of metal release from various metallic biomaterials in vitro“, *Biomaterials* **2005**, *26*, 11–21.

[61] M. Geetha, A. K. Singh, R. Asokamani, A. K. Gogia, „Ti based biomaterials, the ultimate choice for orthopaedic implants – A review“, *Prog. Mater Sci.* **2009**, *54*, 397–425.

[62] P. J. Yates, N. A. Quraishi, A. Kop, D. W. Howie, C. Marx, E. Swarts, „Fractures of Modern High Nitrogen Stainless Steel Cemented Stems“, *J. Arthroplasty* **2008**, *23*, 188–196.

[63] P. Thomas, B. Summer, „Metallimplantatallergie“ in *Ossäre Integration*, (Eds.: R. Gradinger, H. Gollwitzer), Springer Berlin Heidelberg, Berlin, Heidelberg, **2006**, pp. 75–80.

[64] M. Thomsen, „Update Implantatallergie“, *Der Orthopäde* **2013**, *42*, 596–596.

[65] G. Lütjering, J. C. Williams, *Titanium*, *Vol. 2*, Springer, **2003**.

[66] H. Rotaru, R. Schumacher, S.-G. Kim, C. Dinu, „Selective laser melted titanium implants: a new technique for the reconstruction of extensive zygomatic complex defects“, *Maxillofac. Plast. Reconstr. Surg.* **2015**, *37*, 1.

[67] A. Mellal, H. W. A. Wiskott, J. Botsis, S. S. Scherrer, U. C. Belser, „Stimulating effect of implant loading on surrounding bone“, *Clin. Oral Implants Res.* **2004**, *15*, 239–248.

[68] E. Eisenbarth, J. Breme, H. Hildebrand, „Einfluss des Vanadiumgehalts von Ti-Al-V-Legierungen“, *BIOmaterialien* **2001**, *2*, 203–210.

[69] L. S. Morais, G. G. Serra, C. A. Muller, L. R. Andrade, E. F. A. Palermo, C. N. Elias, M. Meyers, „Titanium alloy mini-implants for orthodontic anchorage: Immediate loading and metal ion release“, *Acta Biomater.*, 2nd TMS Symposium on biological materials science **2007**, *3*, 331–339.

[70] V. S. A. Challa, S. Mali, R. D. K. Misra, „Reduced toxicity and superior cellular response of preosteoblasts to Ti-6Al-7Nb alloy and comparison with Ti-6Al-4V“, *J. Biomed. Mater. Res. A* **2013**, *101A*, 2083–2089.

[71] Z. Wang, X. Wei, J. Yang, J. Suo, J. Chen, X. Liu, X. Zhao, „Chronic exposure to aluminum and risk of Alzheimer's disease: A meta-analysis“, *Neurosci. Lett.* **2016**, *610*, 200–206.

[72] C. Exley, T. Vickers, „Elevated brain aluminium and early onset Alzheimer's disease in an individual occupationally exposed to aluminium: a case report“, *J. Med. Chase Rep.* **2014**, *8*, 41.

[73] S. A. Virk, G. D. Eslick, „Occupational Exposure to Aluminum and Alzheimer Disease: A Meta-Analysis“, *J. Occup. Environ. Med.* **2015**, *57*, 893–896.

[74] C. C. Willhite, N. A. Karyakina, R. A. Yokel, N. Yenugadhati, T. M. Wisniewski, I. M. F. Arnold, F. Momoli, D. Krewski, „Systematic review of potential health risks posed by pharmaceutical, occupational and consumer exposures to metallic and nanoscale aluminum, aluminum oxides, aluminum hydroxide and its soluble salts“, *Crit. Rev. Toxicol.* **2014**, *44*, 1–80.

[75] S. Galli, R. Jimbo, Y. Naito, S. Berner, M. Dard, A. Wennerberg, „Chemically modified titanium–zirconium implants in comparison with commercially pure titanium controls stimulate the early molecular pathways of bone healing“, *Clin. Oral Implants Res.* **2017**, *28*, 1234–1240.

[76] D. R. N. Correa, F. B. Vicente, T. A. G. Donato, V. E. Arana-Chavez, M. A. R. Buzalaf, C. R. Grandini, „The effect of the solute on the structure, selected mechanical properties, and biocompatibility of Ti–Zr system alloys for dental applications“, *Mater. Sci. Eng. C.* **2014**, *34*, 354–359.

[77] The NJR Editorial Board, NJR 12th Annual Report 2015, **2015**.

[78] T. Gehrke, P. Alijanipour, J. Parvizi, „The Management of an Infected Total Knee Arthroplasty“, *Bone Jt. J.* **2015**, *97-B*, 20–29.

[79] A. Tzeng, T. H. Tzeng, S. Vasdev, K. Korth, T. Healey, J. Parvizi, K. J. Saleh, „Treating periprosthetic joint infections as biofilms: key diagnosis and management strategies“, *Diagn. Microbiol. Infect. Dis.* **2015**, *81*, 192–200.

[80] K. Anagnostakos, D. Kohn, „Hüftgelenkinfektionen – Ergebnisse einer Umfrage unter 28 orthopädischen Universitätskliniken“, *Der Orthopäde* **2011**, *40*, 781–792.

[81] American Joint Replacement Registry, American Joint Replacement Registry Annual Report 2014, 9400 West Higgins Road, Suite 210 Rosemont, IL 60018-4975, **2014**.

[82] G. Garellick, J. Kärrholm, H. Lindahl, H. Malchau, C. Rogmark, O. Rolfson, Eds., Swedish Hip Arthroplasty Register Annual Report 2014, **2015**.

[83] C. L. Nelson, A. C. McLaren, S. G. McLaren, J. W. Johnson, M. S. Smeltzer, „Is aseptic loosening truly aseptic?“, *Clin. Orthop.* **2005**, 25–30.

[84] J. Parvizi, D. Suh, S. M. Jafari, A. Mullan, J. J. Purtill, „Aseptic Loosening of Total Hip Arthroplasty: Are They All Truly Aseptic?“, *J. Arthroplasty* **2010**, *25*, e24.

[85] A. C. Rothenberg, A. E. Wilson, J. P. Hayes, M. J. O'Malley, B. A. Klatt, „Sonication of Arthroplasty Implants Improves Accuracy of Periprosthetic Joint Infection Cultures“, *Clin. Orthop. Relat. Res.* **2017**, 1–10.

[86] E. Witso, „The rate of prosthetic joint infection is underestimated in the arthroplasty registers“, *Acta Orthop.* **2015**, *86*, 277–278.

[87] N. Renz, C. Perka, A. Trampuz, „Management periprothetischer Infektionen des Kniegelenks“, *Der Orthopäde* **2016**, *45*, 65–71.

[88] A. F. Kamath, P. B. Voleti, T. W. B. Kim, J. P. Garino, G.-C. Lee, „Impaction Bone Grafting With Proximal and Distal Femoral Arthroplasty“, *J. Arthroplasty* **2011**, *26*, 1520–1526.

[89] D. R. Osmon, E. F. Berbari, A. R. Berendt, D. Lew, W. Zimmerli, J. M. Steckelberg, N. Rao, A. Hanssen, W. R. Wilson, „Diagnosis and Management of Prosthetic Joint Infection: Clinical Practice Guidelines by the Infectious Diseases Society of America“, *Clin. Infect. Dis.* **2013**, *56*, e1–e25.

[90] M. R. Streit, D. Haeussler, T. Bruckner, T. Proctor, M. M. Innmann, C. Merle, T. Gotterbarm, S. Weiss, „Early Migration Predicts Aseptic Loosening of Cementless Femoral Stems: A Long-Term Study“, *Clin. Orthop. Relat. Res.* **2016**, *474*, 1697–1706.

[91] E. S. Hartmann, M. I. Köhler, F. Huber, J. I. Redeker, B. Schmitt, M. Schmitt-Sody, B. Summer, A. Fottner, V. Jansson, S. Mayer-Wagner, „Factors Regulating Bone Remodeling Processes in Aseptic Implant Loosening“, *J. Orthop. Res.* **2017**, *35*, 248–257.

[92] Y. Abu-Amer, I. Darwech, J. C. Clohisy, „Aseptic Loosening of Total Joint Replacements: Mechanisms Underlying Osteolysis and Potential Therapies“, *Arthritis Res. There.* **2007**, *9*, S6.

[93] Z. Deng, Z. Wang, J. Jin, Y. Wang, N. Bao, Q. Gao, J. Zhao, „SIRT1 Protects Osteoblasts against Particle-Induced Inflammatory Responses and Apoptosis in Aseptic Prosthesis Loosening“, *Acta Biomater.* **2017**, *49*, 541–554.

[94] J. Chandrananth, A. Rabinovich, A. Karahalios, S. Guy, P. Tran, „Impact of Adherence to Local Antibiotic Prophylaxis Guidelines on Infection Outcome after Total Hip or Knee Arthroplasty“, *J. Hosp. Infect.* **2016**, *93*, 423–427.

[95] J. Parvizi, B. Adeli, B. Zmistowski, C. Restrepo, A. S. Greenwald, „Management of Periprosthetic Joint Infection: The Current Knowledge, AAOS Exhibit Selection“, *J. Bone Jt. Surg.* **2012**, *94*, e104 1–9.

[96] C. Friesecke, J. Wodtke, „Management Des Protheseninfektes“, *Der Chirurg* **2008**, *79*, 777–794.

[97] S. V. Duijf, F. J. Vos, J. F. Meis, J. H. Goosen, „Debridement, Antibiotics and Implant Retention in Early Postoperative Infection with Enterococcus Sp.“, *Clin. Microbiol. Infect.* **2015**, *21*, e41–e42.

[98] H. Sakai, G. W. Procop, N. Kobayashi, D. Togawa, D. A. Wilson, L. Borden, V. Krebs, T. W. Bauer, „Simultaneous Detection of Staphylococcus aureus and Coagulase-Negative Staphylococci in Positive Blood Cultures by Real-Time PCR with Two Fluorescence Resonance Energy Transfer Probe Sets“, *J. Clin. Microbiol.* **2004**, *42*, 5739–5744.

[99] C. Liu, A. Bayer, S. E. Cosgrove, R. S. Daum, S. K. Fridkin, R. J. Gorwitz, S. L. Kaplan, A. W. Karchmer, D. P. Levine, B. E. Murray, M. J. Rybak, D. A. Talan, H. F. Chambers, „Clinical Practice Guidelines by the Infectious Diseases Society of America for the Treatment of Methicillin-Resistant Staphylococcus Aureus Infections in Adults and Children“, *Clin. Infect. Dis.* **2011**, *52*, e18–e55.

[100] L. G. Harris, R. G. Richards, „Staphylococci and implant surfaces: a review“, *Injury*, Infection in Fracture Fixation. From basic research, to diagnosis, to evidence-based treatment **2006**, *37*, S3–S14.

[101] S. Hogan, N. Stevens, H. Humphreys, J. O'Gara, E. O'Neill, „Current and Future Approaches to the Prevention and Treatment of Staphylococcal Medical Device-Related Infections“, *Curr. Pharm. Des.* **2015**, *21*, 100–113.

[102] C. Weidenmaier, A. Peschel, „Teichoic Acids and Related Cell-Wall Glycopolymers in Gram-Positive Physiology and Host Interactions“, *Nat. Rev. Microbiol.* **2008**, *6*, 276–287.

[103] W. W. Navarre, O. Schneewind, „Surface Proteins of Gram-Positive Bacteria and Mechanisms of Their Targeting to the Cell Wall Envelope“, *Microbiol. Mol. Biol. Rev.* **1999**, *63*, 174–229.

[104] M. Masalha, I. Borovok, R. Schreiber, Y. Aharonowitz, G. Cohen, „Analysis of Transcription of the Staphylococcus Aureus Aerobic Class Ib and Anaerobic Class III Ribonucleotide Reductase Genes in Response to Oxygen“, *J. Bacteriol.* **2001**, *183*, 7260–7272.

[105] G. H. Dayan, N. Mohamed, I. L. Scully, D. Cooper, E. Begier, J. Eiden, K. U. Jansen, A. Gurtman, A. S. Anderson, „Staphylococcus Aureus: The Current State of Disease, Pathophysiology and Strategies for Prevention“, *Expert Rev. Vaccines* **2016**, *15*, 1373–1392.

[106] R. P. Novick, „Mobile Genetic Elements and Bacterial Toxinoses: The Superantigen-Encoding Pathogenicity Islands of Staphylococcus Aureus“, *Plasmid* **2003**, *49*, 93–105.

[107] T. J. Foster, „The Staphylococcus Aureus "Superbug"“, *J. Clin. Invest.* **2004**, *114*, 1693–1696.

[108] A.-C. N. Winkler, PhD thesis, Julius-Maximilians-Universität Würzburg, **2015**, 111 pp.

[109] Y. Gillet, B. Issartel, P. Vanhems, J.-C. Fournet, G. Lina, M. Bes, F. Vandenesch, Y. Piémont, N. Brousse, D. Floret, J. Etienne, „Association between Staphylococcus Aureus Strains Carrying Gene for Panton-Valentine Leukocidin and Highly Lethal Necrotising Pneumonia in Young Immunocompetent Patients“, *The Lancet* **2002**, *359*, 753–759.

[110] G. Lina, Y. Piémont, F. Godail-Gamot, M. Bes, M.-O. Peter, V. Gauduchon, F. Vandenesch, J. Etienne, „Involvement of Panton-Valentine Leukocidin—Producing Staphylococcus Aureus in Primary Skin Infections and Pneumonia“, *Clin. Infect. Dis.* **1999**, *29*, 1128–1132.

[111] K. R. Matthews, J. Roberson, B. E. Gillespie, D. A. Luther, S. P. Oliver, „Identification and Differentiation of Coagulase-Negative Staphylococcus Aureus by Polymerase Chain Reaction“, *J. Food Prot.* **1997**, *60*, 686–688.

[112] M. Otto, „Staphylococcus Epidermidis — the 'Accidental' Pathogen“, *Nat. Rev. Microbiol.* **2009**, *7*, 555–567.

[113] J. E. Coia, „MRSA – Seeing the Bigger Picture“, *J. Hosp. Infect.* **2016**, *93*, 364–365.

[114] M. Y. Pavlov, M. Ehrenberg, „Optimal control of gene expression for fast proteome adaptation to environmental change., Optimal control of gene expression for fast proteome adaptation to environmental change“, *PNAS* **2013**, *110, 110*, 20527–20532.

[115] A. Borg, M. Ehrenberg, „Determinants of the Rate of mRNA Translocation in Bacterial Protein Synthesis“, *J. Mol. Biol.*, Translation: Regulation and Dynamics **2015**, *427*, 1835–1847.

[116] E. J. O'Brien, B. O. Palsson, „Computing the functional proteome: recent progress and future prospects for genome-scale models“, *Curr. Opin. Biotechnol.*, Systems biology • Nanobiotechnology **2015**, *34*, 125–134.

[117] J. A. Lindsay, M. T. G. Holden, „Staphylococcus Aureus: Superbug, Super Genome?“, *Trends Microbiol.* **2004**, *12*, 378–385.

[118] C. van Pelt, J. Nouwen, E. Lugtenburg, C. van der Schee, S. De Marie, P. Schuijff, H. Verbrugh, B. Löwenberg, A. van Belkum, M. Vos, „Strict infection control measures do not prevent clonal spread of coagulase negative staphylococci colonizing central venous catheters in neutropenic hemato-oncologic patients“, *FEMS Immunol. Med. Microbiol.* **2003**, *38*, 153–158.

[119] P. D. Fey, M. E. Olson, „Current Concepts in Biofilm Formation of Staphylococcus Epidermidis“, *Future Microbiol.* **2010**, *5*, 917–933.

[120] Y. Achermann, E. J. C. Goldstein, T. Coenye, M. E. Shirtliff, „*Propionibacterium acnes*: from Commensal to Opportunistic Biofilm-Associated Implant Pathogen“, *Clin. Microbiol. Rev.* **2014**, *27*, 419–440.

[121] M. Vert, Y. Doi, K.-H. Hellwich, M. Hess, P. Hodge, P. Kubisa, M. Rinaudo, F. Schué, „Terminology for biorelated polymers and applications (IUPAC Recommendations 2012)“, *Pure Appl. Chem.* **2012**, *84*, 377–410.

[122] K. K. Jefferson, „What drives bacteria to produce a biofilm?“, *FEMS Microbiol. Lett.* **2004**, *236*, 163–173.

[123] M. E. Olson, H. Ceri, D. W. Morck, A. G. Buret, R. R. Read, „Biofilm Bacteria: Formation and Comparative Susceptibility to Antibiotics“, *Can. J. Vet. Res.* **2002**, *66*, 86.

[124] D. Monroe, „Looking for Chinks in the Armor of Bacterial Biofilms“, *PLoS Biol.* **2007**, *5*, e307.

[125] M. R. Kiedrowski, A. R. Horswill, „New Approaches for Treating Staphylococcal Biofilm Infections“, *Ann. N.Y. Acad. Sci.* **2011**, *1241*, 104–121.

[126] J. W. Costerton, P. S. Stewart, E. P. Greenberg, „Bacterial Biofilms: A Common Cause of Persistent Infections“, *Science* **1999**, *284*, 1318–1322.

[127] C. R. Arciola, L. Baldassarri, L. Montanaro, „Presence of icaA and icaD Genes and Slime Production in a Collection of Staphylococcal Strains from Catheter-Associated Infections“, *J. Clin. Microbiol.* **2001**, *39*, 2151–2156.

[128] T. Zmantar, B. Kouidhi, H. Miladi, K. Mahdouani, A. Bakhrouf, „A microtiter plate assay for Staphylococcus aureus biofilm quantification at various pH levels and hydrogen peroxide supplementation“, *The New Microbiologica* **2010**, *33*, 137–145.

[129] S. E. Cramton, C. Gerke, N. F. Schnell, W. W. Nichols, F. Götz, „The Intercellular Adhesion (Ica) Locus Is Present in Staphylococcus Aureus and Is Required for Biofilm Formation“, *Infect. Immun.* **1999**, *67*, 5427–5433.

[130] C. R. Arciola, D. Campoccia, P. Speziale, L. Montanaro, J. W. Costerton, „Biofilm formation in Staphylococcus implant infections. A review of molecular mechanisms and implications for biofilm-resistant materials“, *Biomaterials* **2012**, *33*, 5967–5982.

[131] P. Herman-Bausier, C. Formosa-Dague, C. Feuillie, C. Valotteau, Y. F. Dufrêne, „Forces Guiding Staphylococcal Adhesion“, *J. Struct. Biol.*, Molecular Forces to Cellular Function **2017**, *197*, 65–69.

[132] E. Pfender, „Fundamental Studies Associated with the Plasma Spray Process“, *Surf. Coat. Technol.* **1988**, *34*, 1–14.

[133] P. Fauchais, M. Vardelle, A. Vardelle, L. Bianchi, „Plasma Spray: Study of the Coating Generation“, *Ceram. Int.* **1996**, *22*, 295–303.

[134] P. Fauchais, M. Vardelle, A. Vardelle, „Reliability of Plasma-Sprayed Coatings: Monitoring the Plasma Spray Process and Improving the Quality of Coatings“, *J. Phys. D: Appl. Phys.* **2013**, *46*, 224016.

[135] B. R. Gligorijević, M. Vilotijević, M. Šćepanović, D. Vidović, N. A. Radović, „Surface Structural Heterogeneity of High Power Plasma-Sprayed Hydroxyapatite Coatings“, *J. Alloys Compd.* **2016**, *687*, 421–430.

[136] X. Liu, P. K. Chu, C. Ding, „Surface Modification of Titanium, Titanium Alloys, and Related Materials for Biomedical Applications“, *Mater. Sci. Eng. R-Rep.* **2004**, *47*, 49–121.

[137] U. Helmersson, M. Lattemann, J. Bohlmark, A. P. Ehiasarian, J. T. Gudmundsson, „Ionized Physical Vapor Deposition (IPVD): A Review of Technology and Applications“, *Thin Solid Films* **2006**, *513*, 1–24.

[138] D. R. Cooley, A. F. Van Dellen, J. O. Burgess, A. S. Windeler, „The Advantages of Coated Titanium Implants Prepared by Radiofrequency Sputtering from Hydroxyapatite“, *J. Prosthet. Dent.* **1992**, *67*, 93–100.

[139] P. Sigmund, „Theory of Sputtering. I. Sputtering Yield of Amorphous and Polycrystalline Targets“, *Phys. Rev.* **1969**, *184*, 383–416.

[140] A. Rockett, „Physical Vapor Deposition“ in *The Materials Science of Semiconductors*, Springer US, **2008**, pp. 505–572.

[141] W.-J. Chou, G.-P. Yu, J.-H. Huang, „Mechanical Properties of TiN Thin Film Coatings on 304 Stainless Steel Substrates“, *Surf. Coat. Technol.* **2002**, *149*, 7–13.

[142] M. Yamagishi, S. Kuriki, P. K. Song, Y. Shigesato, „Thin Film TiO2 Photocatalyst Deposited by Reactive Magnetron Sputtering“, *Thin Solid Films*, Selected papers from the 4th International Conference on Coatings on Glass **2003**, *442*, 227–231.

[143] A. Kubono, N. Okui, „Polymer Thin Films Prepared by Vapor Deposition“, *Prog. Polym. Sci.* **1994**, *19*, 389–438.

[144] H. Usui, „Preparation of Polymer Thin Films by Physical Vapor Deposition“ in *Functional Polymer Films*, (Eds.: W. Knoll, R. C. Advincula), Wiley-VCH Verlag GmbH & Co. KGaA, **2011**, pp. 287–318.

[145] Y. Zhang, N. W. Franklin, R. J. Chen, H. Dai, „Metal Coating on Suspended Carbon Nanotubes and Its Implication to Metal–tube Interaction“, *Chem. Phys. Lett.* **2000**, *331*, 35–41.

[146] P. Blank, K. Wittmaack, „Energy and Fluence Dependence of the Sputtering Yield of Silicon Bombarded with Argon and Xenon“, *J. Appl. Phys.* **1979**, *50*, 1519–1528.

[147] R. Gago, L. Vázquez, R. Cuerno, M. Varela, C. Ballesteros, J. M. Albella, „Production of Ordered Silicon Nanocrystals by Low-Energy Ion Sputtering“, *Appl. Phys. Lett.* **2001**, *78*, 3316–3318.

[148] A. Eder, G. H. Schmid, H. Mahr, C. Eisenmenger-Sittner, „Aspects of Thin Film Deposition on Granulates by Physical Vapor Deposition“, *Eur. Phys. J. D* **2016**, *70*, 247.

[149] D. D. Hass, Y. Marciano, H. N. G. Wadley, „Physical Vapor Deposition on Cylindrical Substrates“, *Surf. Coat. Technol.* **2004**, *185*, 283–291.

[150] T. Schmitz, F. Warmuth, E. Werner, C. Hertl, J. Groll, U. Gbureck, C. Moseke, „Physical and Chemical Characterization of Ag-Doped Ti Coatings Produced by Magnetron Sputtering of Modular Targets“, *Mater. Sci. Eng. C.* **2014**, *44*, 126–131.

[151] H. Holleck, V. Schier, „Multilayer PVD Coatings for Wear Protection“, *Surf. Coat. Technol.* **1995**, *76*, 328–336.

[152] M. Antonov, I. Hussainova, F. Sergejev, P. Kulu, A. Gregor, „Assessment of Gradient and Nanogradient PVD Coatings Behaviour under Erosive, Abrasive and Impact Wear Conditions“, *Wear* **2009**, *267*, 898–906.

[153] T. Schmitz, C. Hertl, E. Werner, U. Gbureck, J. Groll, C. Moseke, „Oxygen Diffusion Hardening of Tantalum Coatings on Cp-Titanium for Biomedical Applications“, *Surf. Coat. Technol.* **2013**, *216*, 46–51.

[154] R. Olivares-Navarrete, J. J. Olaya, C. Ramírez, S. E. Rodil, „Biocompatibility of Niobium Coatings“, *Coatings* **2011**, *1*, 72–87.

[155] O. O. V. d. Biest, L. J. Vandeperre, „Electrophoretic Deposition of Materials“, *Annu. Rev. Mater. Sci.* **1999**, *29*, 327–352.

[156] L. Besra, M. Liu, „A review on fundamentals and applications of electrophoretic deposition (EPD)“, *Prog. Mater Sci.* **2007**, *52*, 1–61.

[157] Y. Fukada, N. Nagarajan, W. Mekky, Y. Bao, H.-S. Kim, P. S. Nicholson, „Electrophoretic deposition—mechanisms, myths and materials“, *J. Mater. Sci.* **2004**, *39*, 787–801.

[158] T. Ishihara, K. Shimose, T. Kudo, H. Nishiguchi, T. Akbay, Y. Takita, „Preparation of Yttria-Stabilized Zirconia Thin Films on Strontium-Doped LaMnO3 Cathode Substrates via Electrophoretic Deposition for Solid Oxide Fuel Cells“, *J. Am. Ceram. Soc.* **2000**, *83*, 1921–1927.

[159] F. Chen, M. Liu, „Preparation of Yttria-Stabilized Zirconia (YSZ) Films on La0.85Sr0.15MnO3 (LSM) and LSM–YSZ Substrates Using an Electrophoretic Deposition (EPD) Process“, *J. Eur. Ceram. Soc.* **2001**, *21*, 127–134.

[160] S.-J. Ciou, K.-Z. Fung, K.-W. Chiang, „The Mathematical Expression for Kinetics of Electrophoretic Deposition and the Effects of Applied Voltage“, *J. Power Sources* **2007**, *172*, 358–362.

[161] F. Pishbin, A. Simchi, M. Ryan, A. Boccaccini, „A Study of the Electrophoretic Deposition of Bioglass® Suspensions Using the Taguchi Experimental Design Approach“, *J. Eur. Ceram. Soc.* **2010**, *30*, 2963–2970.

[162] A. Chávez-Valdez, A. R. Boccaccini, „Innovations in electrophoretic deposition: Alternating current and pulsed direct current methods“, *Electrochim. Acta* **2012**, *65*, 70–89.

[163] B. Neirinck, J. Fransaer, O. V. der Biest, J. Vleugels, „Aqueous Electrophoretic Deposition in Asymmetric AC Electric Fields (AC–EPD)“, *Electrochem. Commun.* **2009**, *11*, 57–60.

[164] I. Corni, M. P. Ryan, A. R. Boccaccini, „Electrophoretic Deposition: From Traditional Ceramics to Nanotechnology“, *J. Eur. Ceram. Soc.* **2008**, *28*, 1353–1367.

[165] A. R. Boccaccini, S. Keim, R. Ma, Y. Li, I. Zhitomirsky, „Electrophoretic Deposition of Biomaterials“, *J. R. Soc. Interface* **2010**, *7*, S581–S613.

[166] F. Pishbin, V. Mouriño, J. Gilchrist, D. McComb, S. Kreppel, V. Salih, M. Ryan, A. Boccaccini, „Single-Step Electrochemical Deposition of Antimicrobial Orthopaedic Coatings Based on a Bioactive Glass/Chitosan/Nano-Silver Composite System“, *Acta Biomater.* **2013**, *9*, 7469–7479.

[167] S. Singh, G. Singh, N. Bala, „Electrophoretic deposition of hydroxyapatite-iron oxide-chitosan composite coatings on Ti–13Nb–13Zr alloy for biomedical applications“, *Thin Solid Films* **2020**, *697*, 137801.

[168] J. Wang, P. Layrolle, M. Stigter, K. de Groot, „Biomimetic and electrolytic calcium phosphate coatings on titanium alloy: physicochemical characteristics and cell attachment“, *Biomaterials* **2004**, *25*, 583–592.

[169] S. D. Huelin, H. R. Baker, E. F. Merschrod S., K. M. Poduska, „Phase-Selective Electroprecipitation of Calcium Phosphate Thin Films at Physiological Temperatures“, *Cryst. Growth Des.* **2006**, *6*, 2634–2636.

[170] M. Kumar, H. Dasarathy, C. Riley, „Electrodeposition of brushite coatings and their transformation to hydroxyapatite in aqueous solutions“, *J. Biomed. Mater. Res.* **1999**, *45*, 302–310.

[171] I. Stratful, M. D. Scrimshaw, J. N. Lester, „Conditions Influencing the Precipitation of Magnesium Ammonium Phosphate“, *Water Res.* **2001**, *35*, 4191–4199.

[172] F. Abbona, H. E. L. Madsen, R. Boistelle, „The Initial Phases of Calcium and Magnesium Phosphates Precipitated from Solutions of High to Medium Concentrations“, *J. Cryst. Growth* **1986**, *74*, 581–590.

[173] L. Liu, A. Walcarius, „Kinetics of the Electrochemically-Assisted Deposition of Sol–gel Films“, *Phys. Chem. Chem. Phys.* **2017**, *19*, 14972–14983.

[174] B. G. Bøe, R. Ø. Støen, L. B. Solberg, F. P. Reinholt, J. E. Ellingsen, L. Nordsletten, „Coating of titanium with hydroxyapatite leads to decreased bone formation A study in rabbits“, *Bone Jt. Res.* **2012**, *1*, 125–130.

[175] X. Cheng, M. Filiaggi, S. G. Roscoe, „Electrochemically assisted co-precipitation of protein with calcium phosphate coatings on titanium alloy“, *Biomaterials* **2004**, *25*, 5395–5403.

[176] S. Manara, F. Paolucci, B. Palazzo, M. Marcaccio, E. Foresti, G. Tosi, S. Sabbatini, P. Sabatino, G. Altankov, N. Roveri, „Electrochemically-assisted deposition of biomimetic hydroxyapatite–collagen coatings on titanium plate“, *Inorg. Chim. Acta*, Protagonists in Chemistry: Piero Zanello **2008**, *361*, 1634–1645.

[177] M. B. Thomas, N. Metoki, D. Mandler, N. Eliaz, „In Situ Potentiostatic Deposition of Calcium Phosphate with Gentamicin-Loaded Chitosan Nanoparticles on Titanium Alloy Surfaces“, *Electrochim. Acta* **2016**, *222*, 355–360.

[178] R. A. Surmenev, M. A. Surmeneva, A. A. Ivanova, „Significance of calcium phosphate coatings for the enhancement of new bone osteogenesis – A review“, *Acta Biomater.* **2014**, *10*, 557–579.

[179] A. W. G. Nijhuis, S. C. G. Leeuwenburgh, J. A. Jansen, „Wet-Chemical Deposition of Functional Coatings for Bone Implantology“, *Macromol. Biosci.* **2010**, *10*, 1316–1329.

[180] S. Bose, S. Tarafder, „Calcium Phosphate Ceramic Systems in Growth Factor and Drug Delivery for Bone Tissue Engineering: A Review“, *Acta Biomater.* **2012**, *8*, 1401–1421.

[181] G. Jenny, J. Jauernik, S. Bierbaum, M. Bigler, K. W. Grätz, M. Rücker, B. Stadlinger, „A Systematic Review and Meta-Analysis on the Influence of Biological Implant Surface Coatings on Periimplant Bone Formation“, *J. Biomed. Mater. Res. A* **2016**, *104*, 2898–2910.

[182] S. V. Dorozhkin, „Calcium Orthophosphate Coatings, Films and Layers“, *Prog. Biomater.* **2012**, *1*, 1–40.

[183] I. Škugor Rončević, N. Vladislavić, M. Buzuk, M. Buljac, „Electrodeposition of hydroxyapatite coating on Mg alloy modified with organic acid self-assembled monolayers“, *Journal of Chemical Research* **2020**, *44*, 212–220.

[184] S. V. Dorozhkin, „Biphasic, Triphasic and Multiphasic Calcium Orthophosphates“, *Acta Biomater.* **2012**, *8*, 963–977.

[185] S. V. Dorozhkin, „Calcium Orthophosphate-Based Biocomposites and Hybrid Biomaterials“, *J. Mater. Sci.* **2009**, *44*, 2343–2387.

[186] S.-H. Wang, W.-J. Shih, W.-L. Li, M.-H. Hon, M.-C. Wang, „Morphology of Calcium Phosphate Coatings Deposited on a Ti–6Al–4V Substrate by an Electrolytic Method under 80 Torr“, *J. Eur. Ceram. Soc.* **2005**, *25*, 3287–3292.

[187] S. Lin, R. Z. LeGeros, J. P. LeGeros, „Adherent Octacalciumphosphate Coating on Titanium Alloy Using Modulated Electrochemical Deposition Method“, *J. Biomed. Mater. Res. A* **2003**, *66A*, 819–828.

[188] G. Blanda, V. Brucato, F. C. Pavia, S. Greco, S. Piazza, C. Sunseri, R. Inguanta, „Galvanic Deposition and Characterization of Brushite/Hydroxyapatite Coatings on 316L Stainless Steel“, *Mater. Sci. Eng. C.* **2016**, *64*, 93–101.

[189] Y. Sasikumar, A. M. Kumar, R. S. Babu, M. M. Rahman, L. M. Samyn, A. L. F. de Barros, „Biocompatible hydrophilic brushite coatings on AZX310 and AM50 alloys for orthopaedic implants“, *J Mater Sci: Mater Med* **2018**, *29*, 123.

[190] T.-T. Li, L. Ling, M.-C. Lin, H.-K. Peng, H.-T. Ren, C.-W. Lou, J.-H. Lin, „Recent advances in multifunctional hydroxyapatite coating by electrochemical deposition“, *J Mater Sci* **2020**, *55*, 6352–6374.

[191] F. Wenninger, MD thesis, Julius-Maximilians-Universität Würzburg, Medizinische Fakultät, **2013**, 126 pp.

[192] R. Walter, A. Mehjabeen, T. Gordon, M. Kannan in Proceedings of the CHEMECA 2013, Chemeca 2013: Challenging Tomorrow, Brisbane, QLD, Australia, **2013**.

[193] H. Zhao, S. Cai, Z. Ding, M. Zhang, Y. Li, G. Xu, „A simple method for the preparation of magnesium phosphate conversion coatings on a AZ31 magnesium alloy with improved corrosion resistance“, *RSC Adv.* **2015**, *5*, 24586–24590.

[194] M. Meininger, C. Wolf-Brandstetter, J. Zerweck, F. Wenninger, U. Gbureck, J. Groll, C. Moseke, „Electrochemically Assisted Deposition of Strontium Modified Magnesium Phosphate on Titanium Surfaces“, *Mater. Sci. Eng. C.* **2016**, *67*, 65–71.

[195] C. Moseke, K. Wimmer, M. Meininger, J. Zerweck, C. Wolf-Brandstetter, U. Gbureck, A. Ewald, „Osteoclast and osteoblast response to strontium-doped struvite coatings on titanium for improved bone integration“, *Biomedical Engineering / Biomedizinische Technik* **2020**, *-1*, DOI 10.1515/bmt-2019-0265.

[196] Z. Yang, H. Yuan, W. Tong, P. Zou, W. Chen, X. Zhang, „Osteogenesis in extraskeletally implanted porous calcium phosphate ceramics: variability among different kinds of animals“, *Biomaterials* **1996**, *17*, 2131–2137.

[197] G. Daculsi, N. Passuti, S. Martin, C. Deudon, R. Z. Legeros, S. Raher, „Macroporous calcium phosphate ceramic for long bone surgery in humans and dogs. Clinical and histological study“, *J. Biomed. Mater. Res.* **1990**, *24*, 379–396.

[198] H. Daugaard, B. Elmengaard, J. E. Bechtold, T. Jensen, K. Soballe, „The effect on bone growth enhancement of implant coatings with hydroxyapatite and collagen deposited electrochemically and by plasma spray“, *J. Biomed. Mater. Res. A* **2010**, *92A*, 913–921.

[199] J. Wang, J. de Boer, K. de Groot, „Proliferation and differentiation of osteoblast-like MC3T3-E1 cells on biomimetically and electrolytically deposited calcium phosphate coatings“, *J. Biomed. Mater. Res. A* **2009**, *90A*, 664–670.

[200] H. Wang, N. Eliaz, Z. Xiang, H.-P. Hsu, M. Spector, L. W. Hobbs, „Early Bone Apposition in Vivo on Plasma-Sprayed and Electrochemically Deposited Hydroxyapatite Coatings on Titanium Alloy“, *Biomaterials* **2006**, *27*, 4192–4203.

[201] B. G. Bøe, S. M. Röhrl, T. Heier, F. Snorrason, L. Nordsletten, „A prospective randomized study comparing electrochemically deposited hydroxyapatite and plasma sprayed hydroxyapatite on titanium stems: 55 hips followed for 2 years with RSA and DXA“, *Acta Orthop.* **2011**, *82*, 13–19.

[202] B. Flatøy, S. M. Röhrl, B. Bøe, L. Nordsletten, „No medium-term advantage of electrochemical deposition of hydroxyapatite in cementless femoral stems“, *Acta Orthop.* **2016**, *87*, 42–47.

[203] T. A. Gruen, G. M. McNeice, H. C. Amstutz, „"Modes of Failure" of Cemented Stem-Type Femoral Components: A Radiographic Analysis of Loosening.“, *Clin. Orthop.* **1979**, *141*, 17–27.

[204] J. Kwarcinski, P. Boughton, A. Ruys, A. Doolan, J. van Gelder, „Cranioplasty and Craniofacial Reconstruction: A Review of Implant Material, Manufacturing Method and Infection Risk“, *Applied Sciences* **2017**, *7*, 276.

[205] S. D. Elek, P. E. Conen, „The Virulence of Staphylococcus pyogenes for Man. A Study of the Problems of Wound Infection“, *Br. J. Exp. Pathol.* **1957**, *38*, 573–586.

[206] W. Petty, S. Spanier, J. J. Shuster, C. Silverthorne, „The influence of skeletal implants on incidence of infection. Experiments in a canine model.“, *J. Bone Jt. Surg.* **1985**, *67*, 1236–1244.

[207] S. Mistry, S. Roy, N. Jyoti Maitra, R. Roy, S. Datta, A. Chanda, S. Sarkar, „Safety and efficacy of additive and subtractive surface modification of Ti6Al4V endosseous implant in goat bone“, *J. Mech. Behav. Biomed. Mater.* **2016**, *57*, 69–87.

[208] A. Karlov, I. Khlusov, V. Pontak, V. Ignatov, M. Ivin, S. Zinatulina, „Adhesion of Staphylococcus aureus to implants with different physicochemical characteristics“, *Bull. Exp. Biol. Med.* **2002**, *134*, 277–280.

[209] B. Laure, J.-M. Besnier, A.-M. Bergemer-Fouquet, N. Marquet-Van Der Mee, F. Damie, R. Quentin, L. Favard, P. Rosset, „Effect of hydroxyapatite coating and polymethylmethacrylate on stainless steel implant-site infection with Staphylococcus epidermidis in a sheep model“, *J. Biomed. Mater. Res. A* **2008**, *84A*, 92–98.

[210] O. Pieske, L. Pichlmaier, F. Kaltenhauser, N. Schramm, B. Rubenbauer, A. Greiner, S. Piltz, „Hydroxyapatite-Coated Pins Versus Titanium Alloy Pins in External Fixation at the Wrist: A Controlled Cohort Study:“ *The Journal of Trauma: Injury Infection and Critical Care* **2011**, *70*, 845–851.

[211] F. Siedenbiedel, J. C. Tiller, „Antimicrobial Polymers in Solution and on Surfaces: Overview and Functional Principles“, *Polymers* **2012**, *4*, 46–71.

[212] G. Grass, C. Rensing, M. Solioz, „Metallic Copper as an Antimicrobial Surface“, *Appl. Environ. Microbiol.* **2011**, *77*, 1541–1547.

[213] S. Mathews, M. Hans, F. Mücklich, M. Solioz, „Contact Killing of Bacteria on Copper Is Suppressed if Bacterial-Metal Contact Is Prevented and Is Induced on Iron by Copper Ions“, *Appl. Environ. Microbiol.* **2013**, *79*, 2605–2611.

[214] C. Molteni, H. K. Abicht, M. Solioz, „Killing of Bacteria by Copper Surfaces Involves Dissolved Copper“, *Appl. Environ. Microbiol.* **2010**, *76*, 4099–4101.

[215] S. L. Warnes, C. W. Keevil, „Death and genome destruction of methicillin resistant and Methicillin-Sensitive Strains of *Staphylococcus aureus* on wet or dry copper alloy surfaces does not involve Fenton chemistry“, *Appl. Environ. Microbiol.* **2016**, AEM.03861–15.

[216] J. Luo, C. Hein, F. Mücklich, M. Solioz, „Killing of Bacteria by Copper, Cadmium, and Silver Surfaces Reveals Relevant Physicochemical Parameters“, *Biointerphases* **2017**, *12*, 020301.

[217] J. Lin, J. C. Tiller, S. B. Lee, K. Lewis, A. M. Klibanov, „Insights into bactericidal action of surface-attached poly(vinyl-N-hexylpyridinium) chains“, *Biotechnol. Lett.* **2002**, *24*, 801–805.

[218] J. Lin, S. Qiu, K. Lewis, A. M. Klibanov, „Bactericidal Properties of Flat Surfaces and Nanoparticles Derivatized with Alkylated Polyethylenimines“, *Biotechnol. Progr.* **2002**, *18*, 1082–1086.

[219] S. Kang, M. Pinault, L. D. Pfefferle, M. Elimelech, „Single-Walled Carbon Nanotubes Exhibit Strong Antimicrobial Activity“, *Langmuir* **2007**, *23*, 8670–8673.

[220] K. Glinel, A. M. Jonas, T. Jouenne, J. Leprince, L. Galas, W. T. S. Huck, „Antibacterial and Antifouling Polymer Brushes Incorporating Antimicrobial Peptide“, *Bioconjugate Chem.* **2009**, *20*, 71–77.

[221] A. M. Bieser, J. C. Tiller, „Mechanistic Considerations on Contact-Active Antimicrobial Surfaces with Controlled Functional Group Densities“, *Macromol. Biosci.* **2011**, *11*, 526–534.

[222] A. M. Bieser, Y. Thomann, J. C. Tiller, „Contact-Active Antimicrobial and Potentially Self-Polishing Coatings Based on Cellulose“, *Macromol. Biosci.* **2011**, *11*, 111–121.

[223] J. A. Lemire, J. J. Harrison, R. J. Turner, „Antimicrobial activity of metals: mechanisms, molecular targets and applications“, *Nat. Rev. Microbiol.* **2013**, *11*, 371–384.

[224] C. Andreini, I. Bertini, A. Rosato, „A hint to search for metalloproteins in gene banks“, *Bioinformatics* **2004**, *20*, 1373–1380.

[225] K. J. Waldron, N. J. Robinson, „How do bacterial cells ensure that metalloproteins get the correct metal?“, *Nat. Rev. Microbiol.* **2009**, *7*, 25–35.

[226] J. J. Harrison, H. Ceri, C. A. Stremick, R. J. Turner, „Biofilm susceptibility to metal toxicity“, *Environ. Microbiol.* **2004**, *6*, 1220–1227.

[227] D. H. Nies, „Microbial heavy-metal resistance“, *Appl. Microbiol. Biotechnol.* **1999**, *51*, 730–750.

[228] Y. Kaneko, M. Thoendel, O. Olakanmi, B. E. Britigan, P. K. Singh, „The transition metal gallium disrupts *Pseudomonas aeruginosa* iron metabolism and has antimicrobial and antibiofilm activity“, *J. Clin. Investig.* **2007**, *117*, 877–888.

[229] J. B. Wright, K. Lam, R. E. Burrell, „Wound management in an era of increasing bacterial antibiotic resistance: A role for topical silver treatment“, *Am. J. Infect. Control* **1998**, *26*, 572–577.

[230] A. Mikolay, S. Huggett, L. Tikana, G. Grass, J. Braun, D. H. Nies, „Survival of bacteria on metallic copper surfaces in a hospital trial“, *Appl. Microbiol. Biotechnol.* **2010**, *87*, 1875–1879.

[231] E. Banin, A. Lozinski, K. M. Brady, E. Berenshtein, P. W. Butterfield, M. Moshe, M. Chevion, E. P. Greenberg, E. Banin, „The potential of desferrioxamine-gallium as an anti-Pseudomonas therapeutic agent“, *PNAS* **2008**, *105*, 16761–16766.

[232] L. A. Finney, T. V. O'Halloran, „Transition Metal Speciation in the Cell: Insights from the Chemistry of Metal Ion Receptors“, *Science* **2003**, *300*, 931–936.

[233] M. Elias, A. Wellner, K. Goldin-Azulay, E. Chabriere, J. A. Vorholt, T. J. Erb, D. S. Tawfik, „The molecular basis of phosphate discrimination in arsenate-rich environments“, *Nature* **2012**, *491*, 134–137.

[234] T. W. Clarkson, „Molecular and Ionic Mimicry of Toxic Metals“, *Annu. Rev. Pharmacol. Toxicol.* **1993**, *33*, 545–571.

[235] K. W. Jennette, „The role of metals in carcinogenesis: biochemistry and metabolism.“, *Environ. Health Perspect.* **1981**, *40*, 233–252.

[236] M. L. Workentine, J. J. Harrison, P. U. Stenroos, H. Ceri, R. J. Turner, „Pseudomonas fluorescens' view of the periodic table“, *Environ. Microbiol.* **2008**, *10*, 238–250.

[237] J. J. Harrison, H. Ceri, R. J. Turner, „Multimetal resistance and tolerance in microbial biofilms“, *Nat. Rev. Microbiol.* **2007**, *5*, 928–938.

[238] D. H. Nies, „Efflux-mediated heavy metal resistance in prokaryotes“, *FEMS Microbiology Reviews* **2003**, *27*, 313–339.

[239] J. M. Pérez, I. L. Calderón, F. A. Arenas, D. E. Fuentes, G. A. Pradenas, E. L. Fuentes, J. M. Sandoval, M. E. Castro, A. O. Elías, C. C. Vásquez, „Bacterial Toxicity of Potassium Tellurite: Unveiling an Ancient Enigma“, *PLoS One* **2007**, *2*, e211.

[240] G. M. Teitzel, A. Geddie, S. K. D. Long, M. J. Kirisits, M. Whiteley, M. R. Parsek, „Survival and Growth in the Presence of Elevated Copper: Transcriptional Profiling of Copper-Stressed Pseudomonas aeruginosa“, *J. Bacteriol.* **2006**, *188*, 7242–7256.

[241] Y. H. Jin, P. E. Dunlap, S. J. McBride, H. Al-Refai, P. R. Bushel, J. H. Freedman, „Global Transcriptome and Deletome Profiles of Yeast Exposed to Transition Metals“, *PLOS Genetics* **2008**, *4*, e1000053.

[242] J. A. Imlay, „Pathways of Oxidative Damage“, *Annu. Rev. Microbiol.* **2003**, *57*, 395–418.

[243] O. Gordon, T. V. Slenters, P. S. Brunetto, A. E. Villaruz, D. E. Sturdevant, M. Otto, R. Landmann, K. M. Fromm, „Silver Coordination Polymers for Prevention of Implant Infection: Thiol Interaction, Impact on Respiratory Chain Enzymes, and Hydroxyl Radical Induction“, *Antimicrob. Agents Chemother.* **2010**, *54*, 4208–4218.

[244] C.-N. Lok, C.-M. Ho, R. Chen, Q.-Y. He, W.-Y. Yu, H. Sun, P. K.-H. Tam, J.-F. Chiu, C.-M. Che, „Proteomic Analysis of the Mode of Antibacterial Action of Silver Nanoparticles“, *J. Proteome Res.* **2006**, *5*, 916–924.

[245] P. D. Bragg, D. J. Rainnie, „The effect of silver ions on the respiratory chain of Escherichia coli“, *Can. J. Microbiol.* **1974**, *20*, 883–889.

[246] P. Dibrov, J. Dzioba, K. K. Gosink, C. C. Häse, „Chemiosmotic Mechanism of Antimicrobial Activity of Ag+ in Vibrio cholerae“, *Antimicrob. Agents Chemother.* **2002**, *46*, 2668–2670.

[247] S. Chernousova, M. Epple, „Silver as Antibacterial Agent: Ion, Nanoparticle, and Metal“, *Angew. Chem. Int. Ed.* **2013**, *52*, 1636–1653.

[248] N. M. Bernthal, A. I. Stavrakis, F. Billi, J. S. Cho, T. J. Kremen, S. I. Simon, A. L. Cheung, G. A. Finerman, J. R. Lieberman, J. S. Adams, L. S. Miller, „A Mouse Model of Post-Arthroplasty Staphylococcus aureus Joint Infection to Evaluate In Vivo the Efficacy of Antimicrobial Implant Coatings“, *PLoS ONE* **2010**, *5*, e12580.

[249] S. Geißler, H. Tiainen, H. J. Haugen, „Effect of cathodic polarization on coating doxycycline on titanium surfaces“, *Mater. Sci. Eng. C.* **2016**, *63*, 359–366.

[250] M. Badar, M. I. Rahim, M. Kieke, T. Ebel, M. Rohde, H. Hauser, P. Behrens, P. P. Mueller, „Controlled drug release from antibiotic-loaded layered double hydroxide (LDH)-coatings on porous titanium implants in a mouse model“, *J. Biomed. Mater. Res. A* **2015**, *103*, 2141–2149.

[251] X. Shi, H. Wu, Y. Li, X. Wei, Y. Du, „Electrical signals guided entrapment and controlled release of antibiotics on titanium surface“, *J. Biomed. Mater. Res. A* **2013**, *101A*, 1373–1378.

[252] C.-J. Pan, Y.-X. Dong, Y.-Y. Zhang, Y.-D. Nie, C.-H. Zhao, Y.-L. Wang, „Enhancing the antibacterial activity of biomimetic HA coatings by incorporation of norvancomycin“, *J. Orthop. Sci.* **2011**, *16*, 105–113.

[253] V. Alt, A. Bitschnau, J. Österling, A. Sewing, C. Meyer, R. Kraus, S. A. Meissner, S. Wenisch, E. Domann, R. Schnettler, „The effects of combined gentamicin–hydroxyapatite coating for cementless joint prostheses on the reduction of infection rates in a rabbit infection prophylaxis model“, *Biomaterials* **2006**, *27*, 4627–4634.

[254] N. J. Hickok, I. M. Shapiro, „Immobilized antibiotics to prevent orthopaedic implant infections“, *Adv. Drug Delivery Rev.*, Targeted delivery of therapeutics to bone and connective tissues **2012**, *64*, 1165–1176.

[255] Y. Ando, H. Miyamoto, I. Noda, N. Sakurai, T. Akiyama, Y. Yonekura, T. Shimazaki, M. Miyazaki, M. Mawatari, T. Hotokebuchi, „Calcium phosphate coating containing silver shows high antibacterial activity and low cytotoxicity and inhibits bacterial adhesion“, *Mater. Sci. Eng. C.* **2010**, *30*, 175–180.

[256] X. Bai, S. Sandukas, M. Appleford, J. L. Ong, A. Rabiei, „Antibacterial effect and cytotoxicity of Ag-doped functionally graded hydroxyapatite coatings“, *J. Biomed. Mater. Res. B.* **2011**, *100B*, 553–561.

[257] X. Chatzistavrou, J. C. Fenno, D. Faulk, S. Badylak, T. Kasuga, A. R. Boccaccini, P. Papagerakis, „Fabrication and characterization of bioactive and antibacterial composites for dental applications“, *Acta Biomater.* **2014**, *10*, 3723–3732.

[258] S. Ferraris, S. Spriano, „Antibacterial titanium surfaces for medical implants“, *Mater. Sci. Eng. C.* **2016**, *61*, 965–978.

[259] C. Wolf-Brandstetter, R. Beutner, R. Hess, S. Bierbaum, K. Wagner, D. Scharnweber, U. Gbureck, C. Moseke, „Multifunctional calcium phosphate based coatings on titanium implants with integrated trace elements“, *Biomed. Mater.* **2020**, *15*, 025006.

[260] C.-M. Tîlmaciu, M. Mathieu, J.-P. Lavigne, K. Toupet, G. Guerrero, A. Ponche, J. Amalric, D. Noël, P. H. Mutin, „In vitro and in vivo characterization of antibacterial activity and biocompatibility: A study on silver-containing phosphonate monolayers on titanium“, *Acta Biomater.* **2015**, *15*, 266–277.

[261] E. Unosson, D. Rodriguez, K. Welch, H. Engqvist, „Reactive combinatorial synthesis and characterization of a gradient Ag–Ti oxide thin film with antibacterial properties“, *Acta Biomater.* **2015**, *11*, 503–510.

[262] G. Gosheger, J. Hardes, H. Ahrens, A. Streitburger, H. Buerger, M. Erren, A. Gunsel, F. H. Kemper, W. Winkelmann, C. von Eiff, „Silver-coated megaendoprostheses in a rabbit model–an analysis of the infection rate and toxicological side effects“, *Biomaterials* **2004**, *25*, 5547–5556.

[263] J. Hardes, H. Ahrens, C. Gebert, A. Streitbuerger, H. Buerger, M. Erren, A. Gunsel, C. Wedemeyer, G. Saxler, W. Winkelmann, G. Gosheger, „Lack of toxicological side-effects in silver-coated megaprostheses in humans“, *Biomaterials* **2007**, *28*, 2869–2875.

[264] J. Hardes, C. von Eiff, A. Streitbuerger, M. Balke, T. Budny, M. P. Henrichs, G. Hauschild, H. Ahrens, „Reduction of periprosthetic infection with silver-coated megaprostheses in patients with bone sarcoma“, *J. Surg. Oncol.* **2010**, *101*, 389–395.

[265] H. Wafa, R. J. Grimer, K. Reddy, L. Jeys, A. Abudu, S. R. Carter, R. M. Tillman, „Retrospective evaluation of the incidence of early periprosthetic infection with silver-treated endoprostheses in high-risk patients case-control study“, *Bone Jt. J.* **2015**, *97-B*, 252–257.

[266] T. Schmidt-Braekling, A. Streitbuerger, G. Gosheger, F. Boettner, M. Nottrott, H. Ahrens, R. Dieckmann, W. Guder, D. Andreou, G. Hauschild, B. Moellenbeck, W. Waldstein, J. Hardes, „Silver-coated megaprostheses: review of the literature“, *Eur. J. Orthop. Surg. Traumatol.* **2017**, *27*, 483–489.

[267] J. Hardes, A. Streitburger, H. Ahrens, T. Nusselt, C. Gebert, W. Winkelmann, A. Battmann, G. Gosheger, „The Influence of Elementary Silver Versus Titanium on Osteoblasts Behaviour In Vitro Using Human Osteosarcoma Cell Lines“, *Sarcoma* **2007**, *2007*, 1–5.

[268] G. Hauschild, J. Hardes, G. Gosheger, S. Stoeppeler, H. Ahrens, F. Blaske, C. Wehe, U. Karst, S. Höll, „Evaluation of Osseous Integration of PVD-Silver-Coated Hip Prostheses in a Canine Model“, *BioMed Res. Int.* **2015**, DOI 10.1155/2015/292406.

[269] A. Shivaram, S. Bose, A. Bandyopadhyay, „Understanding long-term silver release from surface modified porous titanium implants“, *Acta Biomater.* **2017**, *58*, 550–560.

[270] S. Sütterlin, M. Dahlö, C. Tellgren-Roth, W. Schaal, Å. Melhus, „High Frequency of Silver Resistance Genes in Invasive Isolates of Enterobacter and Klebsiella Species“, *J. Hosp. Infect.* **2017**, *96*, 256–261.

[271] I. Burghardt, F. Lüthen, C. Prinz, B. Kreikemeyer, C. Zietz, H.-G. Neumann, J. Rychly, „A dual function of copper in designing regenerative implants“, *Biomaterials* **2015**, *44*, 36–44.

[272] D.-J. Lin, M.-T. Tsai, T.-M. Shieh, H.-L. Huang, J.-T. Hsu, Y.-C. Ko, L.-J. Fuh, „In vitro antibacterial activity and cytocompatibility of bismuth doped micro-arc oxidized titanium“, *J. Biomater. Appl.* **2013**, *27*, 553–563.

[273] T. Shirai, H. Tsuchiya, H. Nishida, N. Yamamoto, K. Watanabe, J. Nakase, R. Terauchi, Y. Arai, H. Fujiwara, T. Kubo, „Antimicrobial megaprostheses supported with iodine“, *J. Biomater. Appl.* **2014**, 0885328214539365.

[274] X. Ge, Y. Leng, C. Bao, S. L. Xu, R. Wang, F. Ren, „Antibacterial coatings of fluoridated hydroxyapatite for percutaneous implants“, *J. Biomed. Mater. Res. A* **2010**, *95A*, 588–599.

[275] D. Scharnweber, M. Flössel, R. Born, H. Worch, „Adjusting the Chlorhexidine Content of Calcium Phosphate Coatings by Electrochemically Assisted Co-Deposition from Aqueous Solutions“, *J. Mater. Sci.: Mater. Med.* **2007**, *18*, 391–397.

[276] J. F. Siqueira Jr, H. P. Lopes, „Mechanisms of Antimicrobial Activity of Calcium Hydroxide: A Critical Review“, *Int. Endod. J.* **1999**, *32*, 361–369.

[277] C. A. Klein-Júnior, E. Reston, A. M. Plepis, V. C. Martins, I. C. Pötter, F. Lundy, G. S. Hentschke, V. S. Hentschke, I. E. Karim, „Development and evaluation of calcium hydroxide-coated, pericardium-based biomembranes for direct pulp capping“, *J Invest Clin Dent.* **2019**, *10*, e12380.

[278] B. Athanassiadis, P. Abbott, N. George, L. Walsh, „In Vitro Study of the Inactivation by Dentine of Some Endodontic Medicaments and Their Bases“, *Aust. Dent. J.* **2010**, *55*, 298–305.

[279] B. Athanassiadis, P. Abbott, L. Walsh, „The Use of Calcium Hydroxide, Antibiotics and Biocides as Antimicrobial Medicaments in Endodontics“, *Aust. Dent. J.* **2007**, *52*, S64–S82.

[280] Z. Ahangari, M. M. Bidabadi, M. Asnaashari, A. Rahmati, F. S. Tabatabaei, „Comparison of the Antimicrobial Efficacy of Calcium Hydroxide and Photodynamic Therapy Against Enterococcus Faecalis and Candida Albicans in Teeth With Periapical Lesions; An In Vivo Study“, *J. Lasers Med. Sci.* **2017**, *8*, 72–78.

[281] R. Weiger, R. Rosendahl, C. Löst, „Influence of calcium hydroxide intracanal dressings on the prognosis of teeth with endodontically induced periapical lesions“, *Int. Endod. J.* **2000**, *33*, 219–226.

[282] A. Byström, R. Claesson, G. Sundqvist, „The antibacterial effect of camphorated paramonochlorophenol, camphorated phenol and calcium hydroxide in the treatment of infected root canals“, *Dent. Traumatol.* **1985**, *1*, 170–175.

[283] K. E. Safavi, F. C. Nichols, „Effect of Calcium Hydroxide on Bacterial Lipopolysaccharide“, *J. Endod.* **1993**, *19*, 76–78.

[284] C. R. Barthel, L. G. Levin, H. M. Reisner, M. Trope, „TNF-α release in monocytes after exposure to calcium hydroxide treated *Escherichia coli* LPS“, *Int. Endod. J.* **1997**, *30*, 155–159.

[285] Y. Xie, L. Yang, „Calcium and Magnesium Ions Are Membrane-Active against Stationary-Phase *Staphylococcus Aureus* with High Specificity“, *Sci. Rep.* **2016**, *6*, srep20628.

[286] C. Estrela, G. B. Sydney, L. L. Bammann, O. Felippe Jr, „Mechanism of Action of Calcium and Hydroxyl Ions of Calcium Hydroxide on Tissue and Bacteria“, *Braz. Dent. J.* **1995**, *6*, 85–90.

[287] P. P. Wright, L. J. Walsh, „Optimizing Antimicrobial Agents in Endodontics“ in *Antibacterial Agents*, **2017**.

[288] H. Cao, H. Qin, Y. Zhao, G. Jin, T. Lu, F. Meng, X. Zhang, X. Liu, „Nano-Thick Calcium Oxide Armed Titanium: Boosts Bone Cells against Methicillin-Resistant Staphylococcus Aureus“, *Sci. Rep.* **2016**, *6*, srep21761.

[289] Y. Shen, W. Liu, C. Wen, H. Pan, T. Wang, B. W. Darvell, W. W. Lu, W. Huang, „Bone Regeneration: Importance of Local pH—strontium-Doped Borosilicate Scaffold“, *J. Mater. Chem.* **2012**, *22*, 8662–8670.

[290] C. Nathan, „Neutrophils and Immunity: Challenges and Opportunities“, *Nat. Rev. Immunol.* **2006**, *6*, 173–182.

[291] B. D. Corbin, E. H. Seeley, A. Raab, J. Feldmann, M. R. Miller, V. J. Torres, K. L. Anderson, B. M. Dattilo, P. M. Dunman, R. Gerads, R. M. Caprioli, W. Nacken, W. J. Chazin, E. P. Skaar, „Metal Chelation and Inhibition of Bacterial Growth in Tissue Abscesses“, *Science* **2008**, *319*, 962–965.

[292] W. Razzell, I. R. Evans, P. Martin, W. Wood, „Calcium Flashes Orchestrate the Wound Inflammatory Response through DUOX Activation and Hydrogen Peroxide Release“, *Curr. Biol.* **2013**, *23*, 424–429.

[293] W. Braun, R. Thull, „Elektrochemische Abscheidung von $Ca(OH)_2$ auf Titan zur Unterstützung der Osteointegration“, *BIOmaterialien* **2005**, *6*, DOI 10.1515/BIOMAT.2005.6.4.269.

[294] A. Ewald, S. K. Glückermann, R. Thull, U. Gbureck, „Antimicrobial titanium/silver PVD coatings on titanium“, *Biomed. Eng. Online* **2006**, *5*, 22.

[295] O. Braissant, P. Chavanne, M. de Wild, U. Pieles, S. Stevanovic, R. Schumacher, L. Straumann, D. Wirz, P. Gruner, A. Bachmann, G. Bonkat, „Novel microcalorimetric assay for antibacterial activity of implant coatings: The cases of silver-doped hydroxyapatite and calcium hydroxide“, *J. Biomed. Mater. Res. B.* **2015**, *103*, 1161–1167.

[296] M. Hipp, MD thesis, Julius-Maximilians-Universität Würzburg, Würzburg, **2010**.

[297] M. Meininger, S. Meininger, J. Groll, U. Gbureck, C. Moseke, „Silver and copper addition enhances the antimicrobial activity of calcium hydroxide coatings on titanium“, *Journal of Materials Science: Materials in Medicine* **2018**, *29*, 61.

[298] D. C. Harris, *Lehrbuch der quantitativen Analyse*, 8th ed., (Eds.: G. Werner, T. Werner), Springer Spektrum, Berlin, **2014**, 977 pp.

[299] T. Kokubo, „Apatite formation on surfaces of ceramics, metals and polymers in body environment“, *Acta Mater.* **1998**, *46*, 2519–2527.

[300] C. Zhao, X. Zhu, K. Liang, J. Ding, Z. Xiang, H. Fan, X. Zhang, „Osteoinduction of porous titanium: A comparative study between acid-alkali and chemical-thermal treatments“, *J. Biomed. Mater. Res. B.* **2010**, *95B*, 387–396.

[301] T.-D. T. Nguyen, I.-S. Park, M.-H. Lee, T.-S. Bae, „Enhanced biocompatibility of a pre-calcified nanotubular TiO2 layer on Ti–6Al–7Nb alloy“, *Surf. Coat. Technol.* **2013**, *236*, 127–134.

[302] K. Molt, U. Telgheder, DIN/ISO Compliant Calibrations, q&more, **2013**, http://q-more.chemeurope.com/q-more-articles/17/din-iso-compliant-calibrations.html (visited on 2017-10-10).

[303] J. Schindelin, I. Arganda-Carreras, E. Frise, V. Kaynig, M. Longair, T. Pietzsch, S. Preibisch, C. Rueden, S. Saalfeld, B. Schmid, J.-Y. Tinevez, D. J. White, V. Hartenstein, K. Eliceiri, P. Tomancak, A. Cardona, „Fiji: An Open-Source Platform for Biological-Image Analysis“, *Nat. Methods* **2012**, *9*, 676–682.

[304] B. Aigouy, V. Mirouse, „ScientiFig: A Tool to Build Publication-Ready Scientific Figures“, *Nat. Methods* **2013**, *10*, 1048–1048.

[305] M. Linkert, C. T. Rueden, C. Allan, J.-M. Burel, W. Moore, A. Patterson, B. Loranger, J. Moore, C. Neves, D. MacDonald, A. Tarkowska, C. Sticco, E. Hill, M. Rossner, K. W. Eliceiri, J. R. Swedlow, „Metadata Matters: Access to Image Data in the Real World“, *J. Cell Biol.* **2010**, *189*, 777–782.

[306] R. Shacham, D. Avnir, D. Mandler, „Electrodeposition of Methylated Sol-Gel Films on Conducting Surfaces“, *Adv. Mater.* **1999**, *11*, 384–388.

[307] D. Wei, Q. Du, S. Guo, D. Jia, Y. Wang, B. Li, Y. Zhou, „Structures, bonding strength and in vitro bioactivity and cytotoxicity of electrochemically deposited bioactive nano-brushite coating/TiO2 nanotubes composited films on titanium“, *Surface and Coatings Technology* **2018**, *340*, 93–102.

[308] V. Khalili, H. Naji, „Developing a mechanochemical surface pretreatment to increase the adhesion strength of hydroxyapatite electrophoretic coating on the NiTi alloy as a bone implant“, *Surface and Coatings Technology* **2020**, *397*, 125985.

[309] N. Eliaz, N. Metoki, „Calcium Phosphate Bioceramics: A Review of Their History, Structure, Properties, Coating Technologies and Biomedical Applications“, *Materials* **2017**, *10*, 334.

[310] I. Izquierdo-Barba, J. M. García-Martín, R. Álvarez, A. Palmero, J. Esteban, C. Pérez-Jorge, D. Arcos, M. Vallet-Regí, „Nanocolumnar coatings with selective behavior towards osteoblast and Staphylococcus aureus proliferation“, *Acta Biomater.* **2015**, *15*, 20–28.

[311] H. J. Rønold, S. P. Lyngstadaas, J. E. Ellingsen, „A study on the effect of dual blasting with TiO2 on titanium implant surfaces on functional attachment in bone“, *J. Biomed. Mater. Res. A* **2003**, *67A*, 524–530.

[312] K. Liu, H. Zhang, M. Lu, L. Liu, Y. Yan, Z. Chu, Y. Ge, T. Wang, C. Tang, „Enhanced bioactive and osteogenic activities of titanium by modification with phytic acid and calcium hydroxide“, *Applied Surface Science* **2019**, *478*, 162–175.

[313] N. Eliaz, S. Shmueli, I. Shur, D. Benayahu, D. Aronov, G. Rosenman, „The effect of surface treatment on the surface texture and contact angle of electrochemically deposited hydroxyapatite coating and on its interaction with bone-forming cells“, *Acta Biomater.* **2009**, *5*, 3178–3191.

[314] L. G. Harris, D. O. Meredith, L. Eschbach, R. G. Richards, „Staphylococcus aureus adhesion to standard micro-rough and electropolished implant materials“, *J. Mater. Sci.: Mater. Med.* **2007**, *18*, 1151–1156.

[315] L. G. Harris, R. G. Richards, „Staphylococcus aureus adhesion to different treated titanium surfaces“, *J. Mater. Sci.: Mater. Med.* **2004**, *15*, 311–314.

[316] H. J. Rønold, J. E. Ellingsen, „The use of a coin shaped implant for direct in situ measurement of attachment strength for osseointegrating biomaterial surfaces“, *Biomaterials* **2002**, *23*, 2201–2209.

[317] O. Veiseh, J. C. Doloff, M. Ma, A. J. Vegas, H. H. Tam, A. R. Bader, J. Li, E. Langan, J. Wyckoff, W. S. Loo, S. Jhunjhunwala, A. Chiu, S. Siebert, K. Tang, J. Hollister-Lock, S. Aresta-Dasilva, M. Bochenek, J. Mendoza-Elias, Y. Wang, M. Qi, D. M. Lavin, M. Chen, N. Dholakia, R. Thakrar, I. Lacík, G. C. Weir, J. Oberholzer, D. L. Greiner, R. Langer, D. G. Anderson, „Size- and shape-dependent foreign body immune response to materials implanted in rodents and non-human primates“, *Nat. Mater.* **2015**, *14*, 643–651.

[318] Q. Yu, Z. Wu, H. Chen, „Dual-function antibacterial surfaces for biomedical applications“, *Acta Biomater.* **2015**, *16*, 1–13.

[319] M. Zaborowska, K. Welch, R. Brånemark, P. Khalilpour, H. Engqvist, P. Thomsen, M. Trobos, „Bacteria-material surface interactions: methodological development for the assessment of implant surface induced antibacterial effects“, *J. Biomed. Mater. Res. B.* **2015**, *103*, 179–187.

[320] R. Kumar, H. Münstedt, „Silver ion release from antimicrobial polyamide/silver composites“, *Biomaterials* **2005**, *26*, 2081–2088.

[321] *CRC handbook of chemistry and physics*, 79th ed., (Ed.: D. R. Lide), Chemical Rubber Company (Cleveland, Ohio), CRC Press, Boca Raton, **1998**.

[322] S. Moses, R. K. Witt, „Evaluation of adhesion by ultrasonic vibrations“, *Ind. Eng. Chem.* **1949**, *41*, 2334–2338.

[323] K. Ramanathan, R. Stallings, J. Newsome, „An ultrasonic technique for the measurement of adhesion of asphalt to aggregate“, *J. Adhes. Sci. Technol.* **1991**, *5*, 181–190.

[324] L. Mei, X. He, Y. Li, Q. Peng, R. Wang, J. Xu, „Enhancement of composite-metal interfacial adhesion strength by dendrimer“, *Surf. Interface Anal.* **2011**, *43*, 726–733.

[325] J. Forsgren, F. Svahn, T. Jarmar, H. Engqvist, „Formation and adhesion of biomimetic hydroxyapatite deposited on titanium substrates“, *Acta Biomater.* **2007**, *3*, 980–984.

[326] S. Bull, D. Rickerby, A. Matthews, A. Leyland, A. Pace, J. Valli, „The use of scratch adhesion testing for the determination of interfacial adhesion: The importance of frictional drag“, *Surf. Coat. Technol.* **1988**, *36*, 503–517.

[327] A. Rakngarm, Y. Mutoh, „Electrochemical depositions of calcium phosphate film on commercial pure titanium and Ti-6Al-4V in two types of electrolyte at room temperature“, *Mater. Sci. Eng. C.* **2009**, *29*, 275–283.

[328] A. Perry, „Scratch adhesion testing of hard coatings“, *Thin Solid Films* **1983**, *107*, 167–180.

[329] Natriumhydroxid CAS 1310-73-2 | 106469, http://www.merckmillipore.com/DE/de/product/Sodium-hydroxide,MDA_CHEM-106469 (visited on 2017-10-12).

[330] Kaliumhydroxid CAS 1310-58-3 | 105033, http://www.merckmillipore.com/DE/de/product/Potassium-hydroxide,MDA_CHEM-105033 (visited on 2017-10-12).

[331] Calciumhydroxid CAS 1305-62-0 | 102047, http://www.merckmillipore.com/DE/de/product/Calcium-hydroxide,MDA_CHEM-102047 (visited on 2017-10-12).

[332] U. Gbureck, O. Knappe, N. Hofmann, J. E. Barralet, „Antimicrobial properties of nanocrystalline tetracalcium phosphate cements“, *J. Biomed. Mater. Res. B.* **2007**, *83B*, 132–137.

[333] A. Steinbüchel, F. B. Oppermann-Sanio, C. Ewering, M. Pötter, *Mikrobiologisches Praktikum, Versuche und Theorie*, 2nd ed., Springer Spektrum, Berlin, Heidelberg, **2013**.

[334] A. Ben-David, C. E. Davidson, „Estimation method for serial dilution experiments“, *J. Microbiol. Methods* **2014**, *107*, 214–221.

[335] M. M. Baum, A. Kainović, T. O'Keeffe, R. Pandita, K. McDonald, S. Wu, P. Webster, „Characterization of structures in biofilms formed by a Pseudomonas fluorescens isolated from soil“, *Bmc Microbiol.* **2009**, *9*, 103.

[336] H. Zipper, H. Brunner, J. Bernhagen, F. Vitzthum, „Investigations on DNA intercalation and surface binding by SYBR Green I, its structure determination and methodological implications“, *Nucleic Acids Res.* **2004**, *32*, e103–e103.

[337] J. M. Schierholz, J. Beuth, „Implant Infections: A Haven for Opportunistic Bacteria“, *J. Hosp. Infect.* **2001**, *49*, 87–93.

[338] E. Anitua, R. Tejero, M. Á. Pacha-Olivenza, M. C. Fernández-Calderón, M. Delgado-Rastrollo, M. M. Zalduendo, M. Troya, C. Pérez-Giraldo, M. L. González-Martín, „Balancing microbial and mammalian cell functions on calcium ion-modified implant surfaces“, *J. Biomed. Mater. Res. B.* **2018**, 421–432.

[339] J. D. Tavitian, S. M. Ong, N. A. Taub, G. J. S. Taylor, „Body-exhaust suit versus occlusive clothing“, *Bone Jt. J.* **2003**, *85-B*, 490–494.

[340] O. M. Lidwell, „Air, antibiotics and sepsis in replacement joints“, *J. Hosp. Infect.*, Infection Control in Orthopaedic Surgery **1988**, *11*, 18–40.

[341] L. Drago, S. Agrappi, M. Bortolin, M. Toscano, C. Romanò, E. De Vecchi, „How to Study Biofilms after Microbial Colonization of Materials Used in Orthopaedic Implants“, *Int. J. Mol. Sci.* **2016**, *17*, 293.

[342] A. Ewald, D. Hösel, S. Patel, L. M. Grover, J. E. Barralet, U. Gbureck, „Silver-doped calcium phosphate cements with antimicrobial activity“, *Acta Biomater.* **2011**, *7*, 4064–4070.

[343] G. Blanda, V. Brucato, F. C. Pavia, S. Greco, S. Piazza, C. Sunseri, R. Inguanta, „In Vitro Corrosion and Biocompatibility of Brushite/Hydroxyapatite Coatings Obtained by Galvanic Deposition on 316LSS“, *J. Electrochem. Soc.* **2018**, *165*, G1.

[344] A. Adhilakshmi, K. Ravichandran, T. Sankara Narayanan, „Cathodic electrodeposition of zinc–zinc phosphate–calcium phosphate composite coatings on pure iron for biodegradable implant applications“, *New J. Chem.* **2020**, *44*, 6475–6489.

[345] E. Sassoni, G. Masi, M. C. Bignozzi, E. Franzoni, „Electrodeposition of Hydroxyapatite Coatings for Marble Protection: Preliminary Results“, *Coatings* **2019**, *9*, 207.

[346] F. Olivier, Q. Picard, S. Delpeux-Ouldriane, J. Chancolon, F. Warmont, V. Sarou-Kanian, F. Fayon, S. Bonnamy, „Influence of electrochemical parameters on the characteristics of sono-electrodeposited calcium phosphate-coated carbon fiber cloth“, *Surf. Coat. Technol.* **2020**, *389*, 125507.

[347] N. López-Valverde, J. Flores-Fraile, J. M. Ramírez, B. Macedo de Sousa, S. Herrero-Hernández, A. López-Valverde, „Bioactive Surfaces vs. Conventional Surfaces in Titanium Dental Implants: A Comparative Systematic Review“, *J. Clin. Med.* **2020**, *9*, 2047.

[348] A. Jacobs, G. Renaudin, C. Forestier, J.-M. Nedelec, S. Descamps, „Biological properties of copper-doped biomaterials for orthopedic applications: A review of antibacterial, angiogenic and osteogenic aspects“, *Acta Biomater.* **2020**, *117*, 21–39.

Danksagung

Herrn Prof. Dr. Jürgen Groll danke ich für die Möglichkeit am Lehrstuhl für Funktionswerkstoffe der Medizin und Zahnheilkunde meine Doktorarbeit durchführen zu können, sowie für die Begutachtung meiner Arbeit. Bei meinem Zweitgutachter Prof. Dr. Matthias Lehmann möchte ich mich ganz herzlich bedanken, dass er sich die Zeit genommen hat meine Arbeit zu begutachten. Besonders bedanke ich mich bei meinem Doktorvater Prof. Dr. Uwe Gbureck und Dr. Claus Moseke für die hervorragende Betreuung während meiner Doktorarbeit. Danke für Motivation, Ideen und fachliche Diskussionen.

Vielen Dank Prof. Dr. Rudert und Dr. Sebastian Bölch vom König-Ludwig Haus für Inspirationen und Diskussionen aus der klinischen Praxis.

Für die Unterstützung bei allen Fragen rund ums Labor bedanke ich mich herzlich bei Isabell Biermann, für alles rund um Organisation ebenso herzlich bei Dr. Jörg Teßmar. Dr. Andrea Ewald möchte ich für die Diskussionen über meine biologischen Experimente danken. Vielen Dank an Maria Aniolek und Simone Werner für die große Unterstützung während meiner mikro- und zellbiologischen Experimente.

Außerdem bedanke ich mich bei Dr. Claus Moseke, Judith Friedlein, Dr. Tomasz Jüngst und Philipp Stahlhut für die Unterstützung am Rasterelektronenmikroskop. Für die Finanzierung des Rasterelektronenmikroskops geht mein Dank an die Deutschen Forschungsgemeinschaft (INST 105022/58-1 FUGG). Vielen Dank an Stefanie Hauck für die Unterstützung bei den Messungen am Atomic Force Microscope. Harald Hümpfer und Anton Hofmann standen mir immer mit Material, guten Ideen und Reparaturen zur Seite. Vielen Dank!

Vielen Dank auch an die zahlreichen Mitstreitenden bei den Türöffner-Tagen der Sendung mit der Maus des WDR und die Möglichkeit diese durchzuführen. Als eingefleischter Maus-Fan hat es mich gefreut, den Kindern die Bedeutung unserer Forschung und den Spaß daran näher bringen zu können.

Für das gute Arbeitsklima möchte ich mich bei allen FMZ-Kollegen und Kolleginnen bedanken. Danke für Unterstützung und viele hilfreiche Diskussionen wissenschaftlicher und unwissenschaftlicher Natur. Besonderer Dank gilt meinen Bürokollegen Dr. Theresa Brückner und Dr. Gernot Hochleitner.

Ich bedanke mich bei meiner Theater Dreieck Familie und der Taekwondo-Abteilung der Turngemeinde Würzburg von 1848 e.V. für die angenehme Freizeitgestaltung :).

Mama, Papa, Bine, Philipp, Lars, Lea, Conny, Michael, Susi, Matthias und Theresa: In der Kürze liegt die Würze: Danke!